High Frequency Acoustic Propagation and Modeling in Stratified Estuaries

by

Nicholas Swanda
B.S. 2008, Nuclear Engineering, Rensselaer Polytechnic Institute

Submitted to the Department of Mechanical Engineering and the Joint Program in Applied Ocean Science and Engineering on August 5th, 2022 in partial fulfillment of the requirements for the degree of Master of Science

at the

Massachusetts Institute of Technology

and the

Woods Hole Oceanographic Institution

September 2022

Author . . . .
Department of Mechanical Engineering, MIT
Applied Ocean Science & Engineering, WHOI
August 5th, 2022

Certified by . . . .
Andone C. Lavery
Department Chair of Applied Ocean Physics & Engineering, WHOI
Thesis Supervisor

Accepted by . . . .
Nicolas Hadjiconstantinou
Professor of Mechanical Engineering, MIT
Chair, Department Committee on Graduate Students

Accepted by . . . .
David Ralston
Associate Scientist with Tenure, Applied Ocean Physics & Engineering, WHOI
Chair, Joint Committee for Applied Ocean Science & Engineering

High Frequency Acoustic Propagation and Modeling in Stratified Estuaries

by

Nicholas Swanda

Submitted to the Department of Mechanical Engineering and the Joint Program in Applied Ocean Science and Engineering on August 5th, 2022 in partial fulfillment of the requirements for the degree of Master of Science

Abstract

Acoustic propagation measurements are made in a highly variable and stratified estuary using high frequency transducers (120kHz) on tripods placed across the main channel of the river flow. The measurements are taken in the Connecticut River across several tidal cycles, when the flood tide causes a wedge of seawater to press up the river bed, beneath the fresh water, and then be eroded and pushed back out during the ebb. BELLHOP, implemented via Matlab, is a beam/ray tracing method and is used to model the acoustic propagation in this environment using collected temperature, salinity, and depth data. Multiple modeling comparisons are done over the period of three full tidal cycles, totaling a thousand separate modeling runs and compiled into a time series. Arrival times measurements from the transducer system were able to be accurately modeled, validating BELLHOP as a useful tool in modeling this very dynamic and challenging acoustic environment.

Thesis Supervisor: Andone Lavery
Title: Department Chair of Applied Ocean Physics & Engineering
Woods Hole Oceanographic Institution

Acknowledgments

I want to thank Dr. Andone Lavery, my adviser, for her unwavering support, compassion, and understanding throughout the study. I would not have been able to make it through this program without her guidance and care, for which I will be forever grateful. It was a pleasure and privilege to get to work with her and to see her passion for both the scientific field and the people she works with.

Thank you to Kat, Craig, Pete, and Greg from MIT, WHOI, and the Navy for their companionship and support as we negotiated the joint program and our classes together, with the extra stress of Covid. I wish you all the best in your future endeavors.

This thesis would not have been possible with the data collected by Dr. Andone Lavery, Jonathan Fincke and others, originally funded by the Office of Naval Research (through ONR Grant #N00014-11-10058).

Contents

List of Figures

List of Tables

1 Introduction

Acoustic propagation through the environment can be quite complex, and modeling it can prove quite challenging. This is especially true in shallower water or in areas of high variability. However, there is a lot going on in these areas, so understanding how sound propagates and being able to model it are both vital. One basic example is utilizing acoustics to map or identify items; this may appear straightforward, but understanding the environment might limit efficacy and determine equipment selection. It is beneficial in trying to design a modem system for underwater communication, as analyzed by Freeman and colleagues, attempting to use high frequency directional transducers for high data rates.[1] Another example is to consider an autonomous or remote underwater vehicle that require acoustic communications. We don't want to suddenly lose communication especially but could even at short ranges based on the environment and must account for changing conditions. This is doubly true in the case of military operations where there might be a need for covertness, as studied by Walree and others.[2] The capacity to continue communications and avoid interception can be greatly enhanced if the environment is understood and modelled so that it can be utilized.

This study looks at high frequency (120 kHz) acoustic propagation over short ranges in a high variability estuary that varies significantly with the tidal cycle. A large wedge of salty seawater pushes in during flood tides and washes out during ebb tides, creating a dynamic and challenging environment. A section of the Connecticut River roughly 4 km from the river's mouth where it joins the Long Island Sound, served as the testing ground. The environment should ideally be modeled to aid in and facilitate other research and applications because studies and field measurements can be expensive. This work makes an effort to simulate the environment of a prior data set using a very complicated and dynamic estuary. BELLHOP, written by M. Porter a ray/beam tracing algorithm that is a part of the acoustic toolbox, is used to represent acoustic propagation

---

[1] Freeman *et al.*, "High-frequency, highly directional short-range underwater acoustic communications".

[2] Walree *et al.*, "UUV Covert Acoustic Communications".

in the environment.[3] It has been used successfully by others such Zeh and colleagues in modeling the Arctic fjord, another challenging environment.[4] It is freely available and can be downloaded at `http://oalib.hlsresearch.com/Rays/`.[5] The code can be compiled in FORTRAN. There are also Matlab and Python code that will allow BELLHOP to be used. The Matlab version was used for this project. It is always a question of how many variables and how much data our model needs to account for in order to provide an accurate solution or representation.

---

[3] *Acoustic Toolbox*.

[4] Zeh *et al.*, "Model-data comparison of sound propagation in a glacierized fjord with a simulated brash ice surface".

[5] *Acoustic Toolbox*.

2 Methods

This section discusses the location of and equipment setup where the data was collected. It addresses the data from this study that was available. The discourse is followed by a summary of the modeling done, and the methods used to implement BELLHOP.

2.1 Background Theory and Ray Tracing

Acoustics modeling has been done with the aid of Ray/Beam tracing since the 1960s.[1] Normal modes is an alternate modeling method that has been developed, however it is computationally expensive at higher frequencies. Ray tracing has some drawbacks and has fallen somewhat out of favor for modal methods. Ray tracing does have some problems at low frequency with inaccuracies, when the wave length is with in an order of magnitude of the water depth. However, for this study it is an excellent candidate since it utilizes high frequencies of 120 kHz. Ray tracing is more efficient and quicker than other techniques, especially at high frequencies. Additionally, ray tracing is considerably more logical and enables one to visualize the issue as well as comprehend practically how the sound is moving through the water. Furthermore, modern code such as BELLHOP has adopted finite elements approach with geometric beams for the rays, which has shown to be very accurate.[2]

Sound will bend as it moves through the water depending on the water properties as given by Snell's Law. As we have a changing sound speed profile for given depths, we can describe this with:

$$k(z_1)cos(\theta(z_1)) = k(z_2)cos(\theta(z_2)) \tag{2.1}$$

Where $k(z_i)$ is the wave number at depth z_i and θ is the angle of the ray in the respective layers. This relates back to the speed of sound, c, in a medium, where f is the frequency

---

[1] Jensen *et al.*, *Computational Ocean Acoustics*.

[2] Porter *et al.*, *Finite-Element Ray Tracing*.

and λ is the wavelength. Also the wave number, k, is related to the wavelength. Given by the following two equations:

$$c = f\lambda \tag{2.2}$$

$$k = 2\pi/\lambda \tag{2.3}$$

The basis of ray tracing is having a starting fan of beams and trace their path as they move through the water. This is easier to represent in cylindrical coordinates, where $[r(s), z(s)]$ is a ray's trajectory and s is the distance along the arc with $[\xi(s), \zeta(s)]$ representing the tangent.$[\xi(s), \zeta(s)]$ are described by the following equations and well visualized in figure 2.1:[3]

$$\frac{dr}{ds} = c\xi(s), \quad \frac{d\xi}{ds} = -\frac{1}{c^2}\frac{dc}{dr} \tag{2.4}$$

$$\frac{dz}{ds} = c\zeta(s), \quad \frac{d\zeta}{ds} = -\frac{1}{c^2}\frac{dc}{dz} \tag{2.5}$$

The initial conditions of the source and beam angle are given by:

$$r = r_0, \quad \xi = \frac{cos\theta_0}{c(0)} \tag{2.6}$$

$$z = z_0, \quad \zeta = \frac{sin\theta_0}{c(0)} \tag{2.7}$$

Travel time, τ, along the ray can be written as:

$$\frac{d\tau}{ds} = \frac{1}{c} \tag{2.8}$$

$$\tau(s) = \tau(o) + \int_0^s \frac{1}{c(s')}ds' \tag{2.9}$$

The direction of travel of an individual ray is explained here. BELLHOP, however, does Gaussian and geometric beam tracing.[4] This basically fills up the gaps between the individual beams as they expand out from the source. This is depicted in the Figure 2.2 from Porter and Lui.[5] The pressure, P, and amplitude, A, fields can be calculated with:[6]

---

[3] Jensen *et al.*, *Computational Ocean Acoustics*.

[4] Porter, *The BELLHOP Manual and User's Guide*.

[5] Porter *et al.*, *Finite-Element Ray Tracing*.

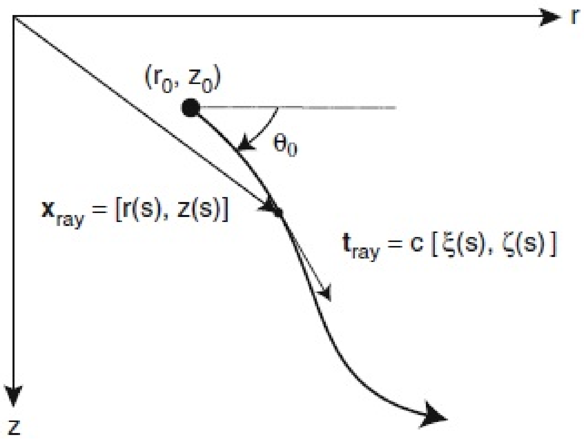

Figure 2.1: Schematic of ray in cylindrical coordinates. Image from Jensen and authors, *Computational Ocean Acoustics*.

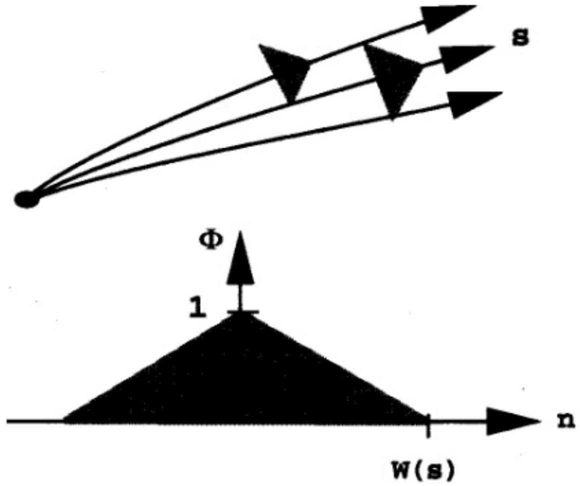

Figure 2.2: Geometric hat beam made to perfectly fit the space between the rays as they spread. Image from Porter and Lui.

$$P(s,n) = A(s)\phi(s,n)e^{i\omega\tau(s)} \tag{2.10}$$

$$A(s) = \frac{1}{(2\pi)^{1/4}}\sqrt{\frac{\delta\theta_0}{r}\frac{c(s)}{c(0)}\frac{2cos\theta_0}{W(s)}} \tag{2.11}$$

where, ω is the angular frequency and the beam width is $W(s)$, and ϕ can either be a geometric hat shaped or a Gaussian shape given by:

$$W(s) = \mid q(s)\delta\theta_0 \mid \tag{2.12}$$

$$\phi(s,n) = \begin{cases} \frac{W(s)-n}{W(s)}, & for\ n \leq W(s) \\ 0, & else \end{cases} \quad (Hat) \tag{2.13}$$

$$\phi(s,n) = e^{-(\frac{n}{W(s)})^2} \quad (Gaussian) \tag{2.14}$$

The pressure field of numerous rays, N, can be summed for specific ranges and depths with their amplitudes combined. From this, we can determine the transmission loss (TL) as a function of depth and range.

$$TL(r,z) = -20log_{10}\frac{\sum_i^N \mid A(r,z)_i \mid^2}{A_{ref}} \tag{2.15}$$

BELLHOP includes a number of built-in functionalities. BELLHOP uses finite element Gaussian ray tracing in a user-defined environment. The primary two used were *plotshd* and an edited version of *plotarr*. The *plotshd* function plots the TL in a color map. This shows both the transmission loss as well as visualising the rays. The *plotarr* function is able to calculate arrival times of the different rays for either specific depths or ranges.

2.2 Site and Instrumentation

The Connecticut River is an energetic estuary who's water column varies significantly with the tidal cycle. This water column is highly stratified between the ocean salt water from the Long Island Sound and the fresh water of the CT River. This is caused by the flood tide, which drives a salt wedge up the river starting at the river floor gradually filling up the water column close to the surface. The freshwater then pushes back out towards the sound during the ebb, while the salt wedge remains practically immobile and is steadily eroded by the freshwater until the water column is mostly freshwater. This

---

[6] Jensen *et al.*, Computational Ocean Acoustics.

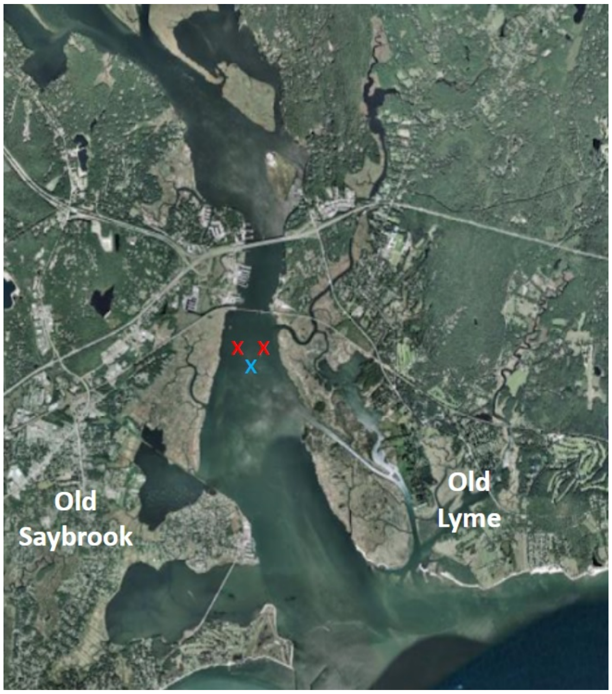

Figure 2.3: Google Earth image of Connecticut River estuary. Red *X*'s denote the scintillation system across the river. The blue *X* is the location of the backscatter array. Image by A. Lavery of WHOI.

also generates high shear instabilities along the boundary of the salt wedge, discussed by Fincke.[7]

This study had two different instrument suites set up along the river floor. One was a scintillation detector system, comprised of two tripods set across the river floor, each having four directional high frequency transducers. The other was a backscatter array, located about 20 meters south of the scintillation system. The back scatter array had six upward-looking broadband transducers along with an upward-looking acoustic Doppler velocity profiler (ADCP). The backscatter system is described in more detail in the paper by Fincke.[8] In this study it was only used as a nearby measurement of water depth. In addition, workers onboard the R/V Connecticut to deploy a conductivity, temperature, and depth (CTD) sensor. The R/V Connecticut was roughly 50 meters away towards the west.

---

[7] Fincke, "Quantification of the spatial and temporal evolution of stratifed shear instabilities at high Reynolds number using quantitative acoustic scattering techniques".

[8] Ibid.

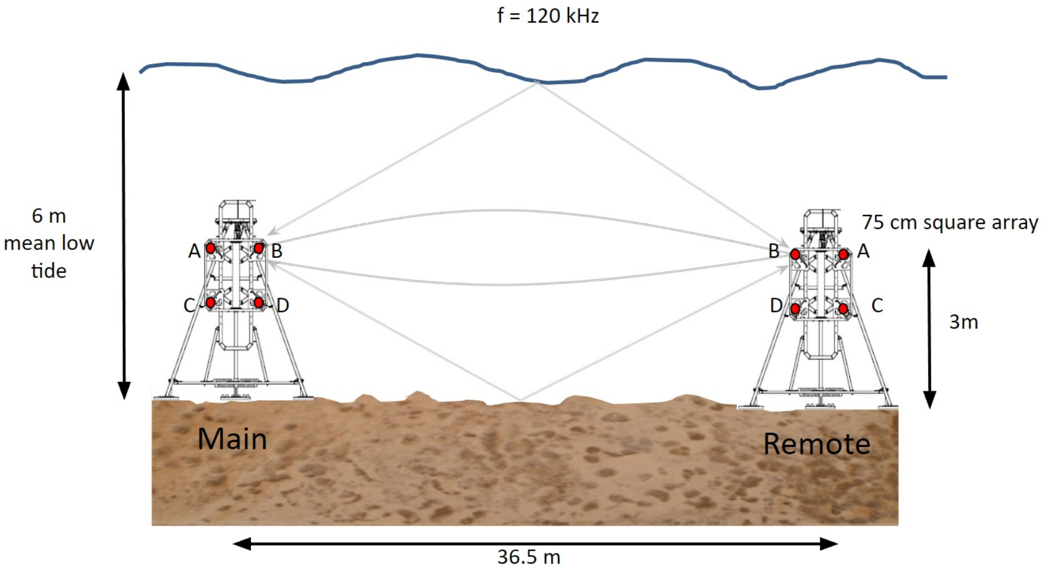

Figure 2.4: Depiction of the Main and Remote tripods of the scintillation system. Image by A. Lavery of WHOI.

2.2.1 Scintillation System

The scintillation system was made up of two tripods. Each had four two-way directional transducers set to 120 kHz. The four transducers were arranged in a square array 75 cm apart and coded as channels A through D. The channels used short 8-cycle sine waves to allow each channel to be distinguished from each other. The A and B channels were located 3 m above the bottom of the river, and channels C and D were 75 cm lower at 2.25 m above the bottom. The direction beamwidth can be seen in Figure 2.5 and the values used are presented in Table 2.1. The tripods were positioned across the river perpendicular to the flow. The main tripod, denoted as M, was on the west side of the channel (Old Saybrook) at Lat/Long 41, 18.503906 N / 72,20.070313 W. The remote tripod, denoted as R, on the east side (Old Lyme) was at Lat/Long 41,18.499023 N / 72,20.995117 W. They were dropped in the sea and aligned by divers after being separated 36.5 meters apart. This can be seen in Figure 2.4.

Each transducer was cabled to the vessel independently. This allowed for real time data acquisition. However, based on the amount of cabling and current, some instruments stopped working over the course of the duration of the study. In this section, we will focus mainly on the A transducers, A_M to A_R, as that is the data available. Figure 2.6 shows one of the scintillation system tripods. It should also be mentioned that be-

Beamwidth Values	
Beamwidth	**Degrees**
`-3dB`	`±5.5°`
`-6dB`	`±8°`
`Full main beam`	`±11°`

Table 2.1: Table showing the beam widths values for transducers used as seen in figure 2.5.

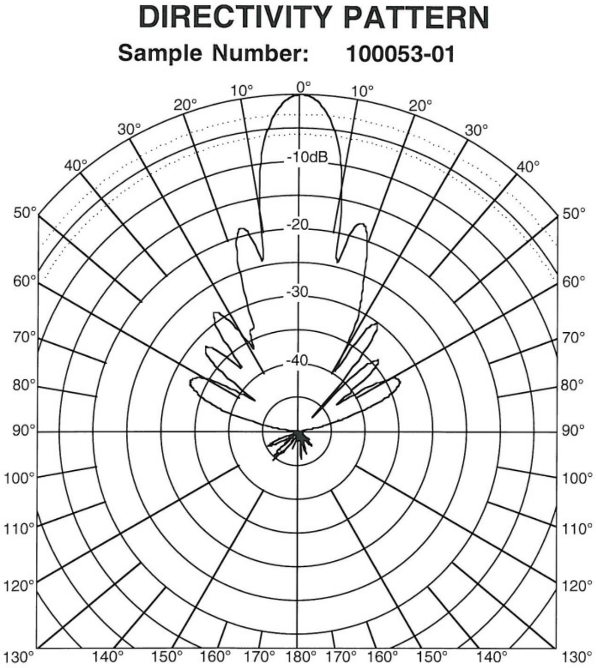

Figure 2.5: Directional beam pattern for transducers in the scintillation system.

Figure 2.6: Photo of the square 75 cm array on one of the tripods of the scintillation system. Image by A. Lavery of WHOI.

cause of its deployment in the Connecticut River, this system required permits and the installation of floats and buoys to inform mariners of its presence.

2.3 Data Available

This investigation conducted in the Connecticut River yielded a vast amount of data. However, this study was conducted in 2012, which was about ten years ago at the time of writing of this thesis. This raises some concerns because some initial data was collected using proprietary code that was not available. Furthermore, there are some concerns with the data being older and not being collected firsthand, which leads to some assumptions being made.

The main data set that is attempted to be modeled and explained in this paper is the arrival times of the scintillation system described above. The primary data set examined is the A_M to A_R transducer arrival time. This consisted of a Matlab Fig file. Dr. A. Lavery

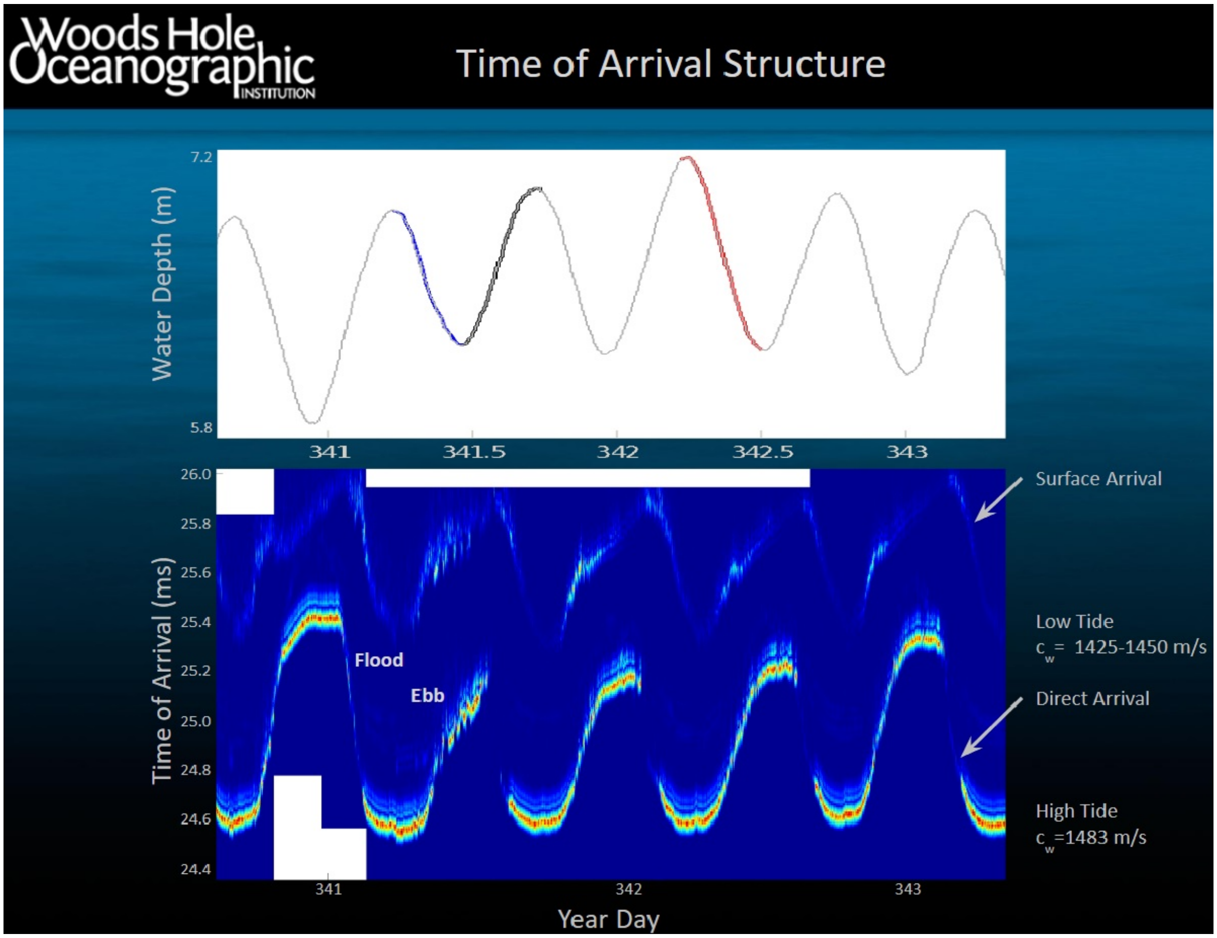

Figure 2.7: Time of Arrival Structure over multiple day tidal cycles in the CT River recorded by the scintillation system. Water depth is measured in meters, located above for comparison. Image by A. Lavery of WHOI.

also offered a saved version of the figure with depths and labeling seen below in figure 2.7.[9]

CTD casts were also conducted as described in section 2.2. This had salinity, temperature, depth saved in a .mat data file. The CTD casts were done by hand off of the R/V Connecticut. Figure 2.8 shows the plotted temperature, salinity, and sound speed over time and water depths. The sound speed has a quantitative relationship with the temperature, salinity, and water depth. There are many empirical formulas for sound speed. Medwin's formula was utilized in the computations given by the equation below:[10]

$$C = 1449.2 + 4.6T - 0.055T^2 + 0.00029T^3 + (1.34 - 0.01T)(S - 35) + 0.016D \quad (2.16)$$

---

[9] Lavery, "High-Frequency Acoustic Propagation in a Shallow, Energetic, Salt-Wedge Estuary".

[10] Menn, *Instrumentation and Metrology in Oceanography*.

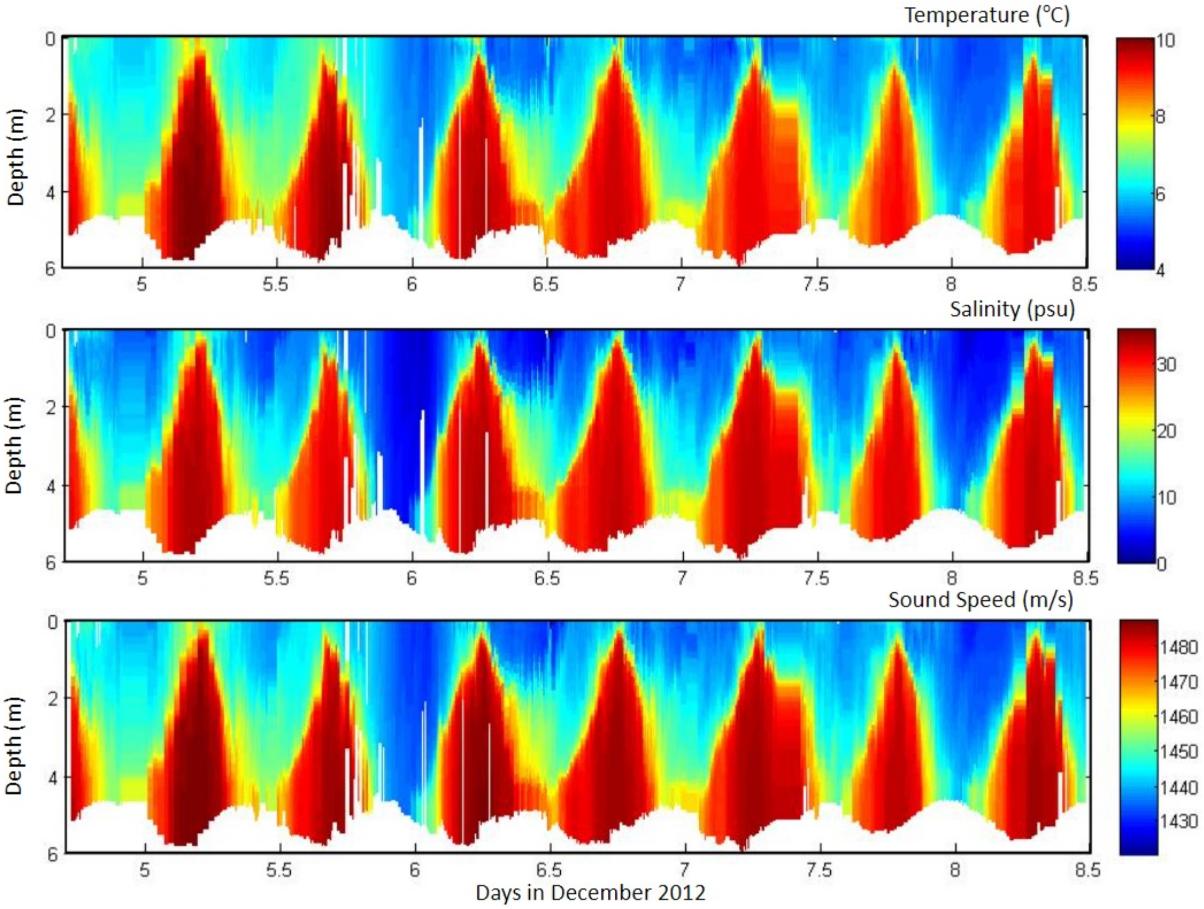

Figure 2.8: Temperature, Salinity and Sound Speed as functions of time and depth, from CTD casts done off of the R/V Connecticut.

Here, the speed of sound in seawater, C, is a function of the temperature, T, salinity, S, and depth, D. It is valid from 0 to 35 °C, 0-40 *PSU*, 0 - 1000 m.[11]

Additionally, there is depth data from the upward looking backscatter array discussed in section 2.2. We have depth data from the system for December 5th and 6th. Furthermore, tidal data from the nearest National Oceanic and Atmospheric Administration (NOAA) buoy, which is immediately to the north of the bridge, was obtained from the NOAA website (buoy ID 8461490 New London, CT).[12] The tide data was then fitted to the backscatter array depths. This allowed for this source of depth data to be extended past Dec 6th. It should be noted that these depths are significantly deeper than the CTD depths from the casts off the R/V Connecticut. This is discussed in detail later.

---

[11] Menn, *Instrumentation and Metrology in Oceanography*.

[12] *NOAA Tides and Currents*.

2.4 Modeling

2.4.1 Environment: Depth and SSP

The depth and sound speed profile (SSP) for the region where the scintillation system measured are the two parameters that most impact the results of the modeling. We don't have any direct measurements of these two things at the area where arrival time measurements were taken. We have depths from the CTDs themselves done roughly 50m away on the R/V Connecticut, tides from the NOAA buoy located at 41°22.3 N, 72°5.7 W, and depths from the backscatter system. All of this helps us to limit and constrain the depths we would expect for the area of the estuary that the scintillation system covered.

Because the CTD casts were done closer to the shore, where the water is shallower, the depths from CTD casts across the period of time the modeling was performed are predicted to be on the shallower end. Additionally, we have the NOAA tides from a buoy just to the north of the bridge. This along with the water depth fluctuation seen in the original figure 2.7 were used to create a smoother depth profile over time. In this same figure 2.7, we can also see that we have a minimum time delay between the arrival of the direct path signal and the surface reflection. We can use this to help bound the minimum amount of water that must be above the transducer to achieve this time delay. If we assume a sound speed, C, and a known time delay, then the extra distance in the travel path between the two arrival paths is just:

$$\Delta x = c * \mathit{time\ delay} \tag{2.17}$$

We can calculate what this minimum water height, *z*, must be above our transducer just using geometry and Pythagorean theorem to determine the water height above at a range, *r* between our transducer to receiver and depicted in Figure 2.9.

$$z = \sqrt{((\Delta x + r)/2)^2 - (r/2)^2} \tag{2.18}$$

Table 2.2 shows calculated values for the height of water that must be above our transducer to have different delays in arrival times between a direct path signal and a surface reflection. Figure 2.7 shows a minimum time delay of 0.2 msec between the direct path signal and the upper surface reflection. Using this value of the time delay from Table 2.2 this is 2.3 m above the transducer, which is at a depth of 3 m. As a result, a minimum water height of roughly 5.3 meters for there to be a surface reflection at low tide. This

Required Water Height above Transducers 36.5 m Apart, z		
Time Delay, $\triangle x$	**SS=1425m/s**	**SS=1480m/s**
0.2msec	2.29meters	2.33meters
0.3msec	2.80meters	2.86meters
0.4msec	3.24meters	3.30meters
0.6msec	3.97meters	4.05meters

Table 2.2: Table showing the required water height above the transducer for different time delays between surface reflection and direct path arrival times at different sound speeds, assuming straight line rays.

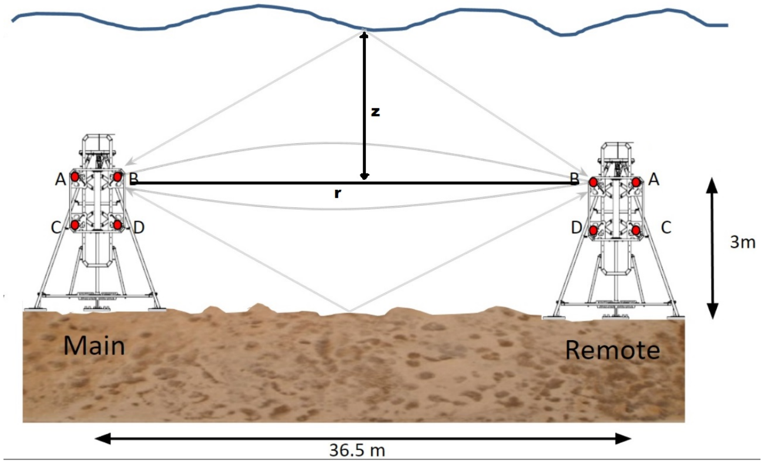

Figure 2.9: Geometry for required water height above transducers for surface bounce.

is accomplished by adding 60cm to the CTD depths in order to constrain the depth problem on the shallow end. We then have the backscatter system depths for the 5th and 6th of December. These were used along with the tides from the same buoy to fit a depth profile on the deeper range. Figure 2.10 shows the different depth data along with the two fitted depth profiles that were used that bound the possible depths at the scintillation system.

There are portions of times the CTD data is missing for the SSP to go along with the certain depths and times. This was handled in a few ways. The first issue was that portions of data contained shallow gaps, such as, i.e. NaN. The data was pulled from the immediate previous time in the series at the same depth if data was missing. The second issue is that due to the shallow nature of the depth profile where the CTD's casts were conducted, there was no CTD data at deeper depths. This was handled in a few ways. The SSP was mostly extended deeper, assuming isovelocity in the sense that at these deeper depths it is likely all seawater at basically the same salinity and

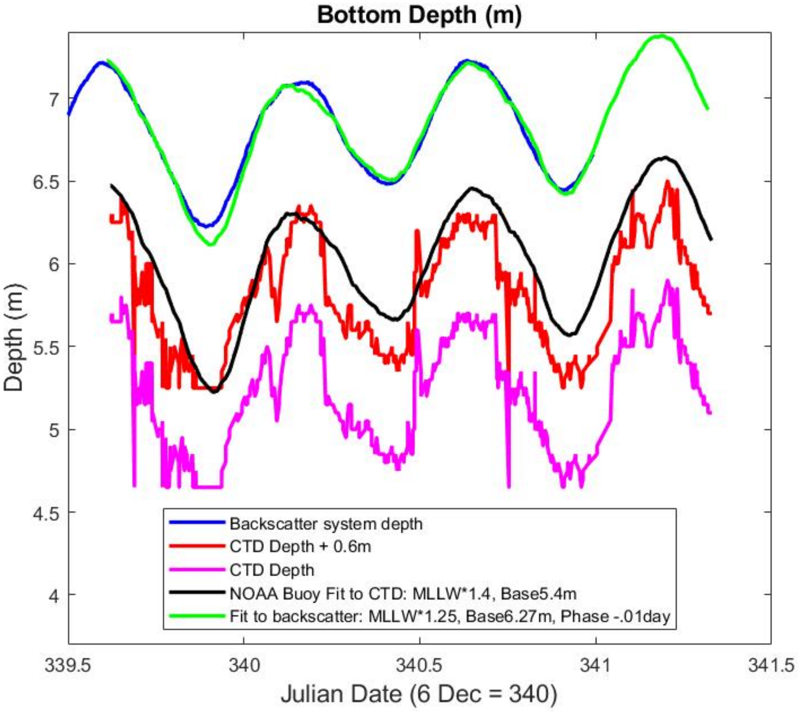

Figure 2.10: Water depth profiles over time, including raw data and fitted curves using tides from nearby NOAA buoy.

temperatures. However, due to the difference in depths from the CTD casts and the back scatter system, this left a large amount of the depth band being assumed to be isovelocity for this deeper depth profile. To examine what the SSP could have been in this deeper case, the SSP was stretched' by 10%. To do this all the 5 cm CTD depth increments were changed to 5.5 cm spacing in the SSP profile creating a new SSP that was now stretched by 10%. Any deeper depth beyond this point was reached using the same isovelocity extension of the SSP. In the case of the deeper depth, profile modeling was performed using both the isovelocity extension of the SSP for the deeper depths and the stretching of the SSP by 10% using the 5.5 cm spacing.

Additional Assumptions

Besides the water depth and SSP, other assumptions that were made in the modeling are:

Smooth flat bottom: The site location for the scintillation system was chosen in that it is relatively flat and level over the distance the system spans.

Sandy bottom: The bottom was assumed to be a sandy bottom based on questioning WHOI scientists who have done data collection in the past having seen those results. The bottom parameters are with a sound speed of 1600 m/s with a density of 1.8 g/cm^3.

CTD data: The CTD data is accurate, well calibrated.

Range independent SSP: The SSP is assumed to be homogeneous across the region between the tripods.

Surface: The surface is also modeled as smooth without waves and modeled as a pressure release boundary.

2.4.2 Arrival Times

BELLHOP does have a built-in function that produces arrival times. This function, *plotarr*, allows for arrival times at a specific range from the source. However, the output is not exactly immediately useful. It generates a 3-dimensional steam plot that has arrival time and depth both as axis, with the 3rd axis being the relative strength of that impulse. The relative strength of that input is not particularly useful, and working with this 3-D plot adds more time and memory to compute. Additionally, this built-in *plotarr* function plots two other plots that are also not needed. The *plotarr* was edited to remove the 2 additional plots and also to change the 3-D stem plot to a 2-D arrival time vs depth plot. This edited version of the function can be found in the Appendix. From

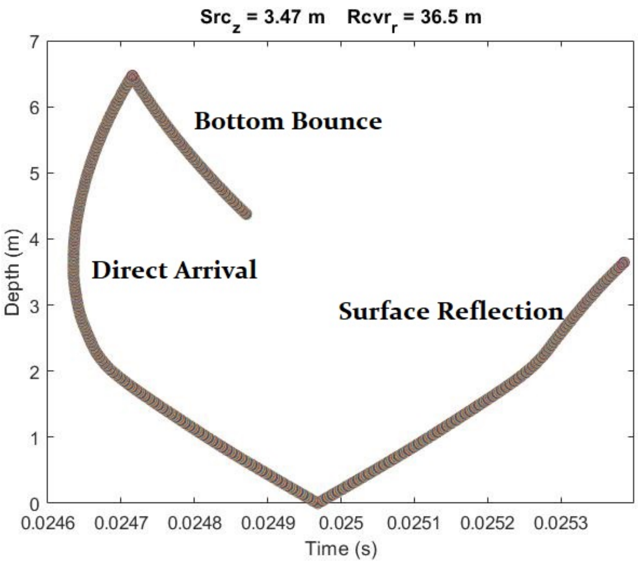

Figure 2.11: Example of one of the 2-D plot of arrival times vs depth at a specific range from the source.

here we are left with a with a simple scatter plot of the arrival time. However, as can be seen in the Figure 2.11 of one such plot, this is made up of many plots on the same plot. This makes extracting the data out a little more complicated. Furthermore, these plots make it simple to visualize where the arrival of the ray came from and other information, such as the source of the arrival if it is a surface or bottom reflection. Moreover, if there is no surface reflection, we may determine whether there was insufficient water depth for the reflection to reach the surface and return to the receiver depth. It should be noted that the depths on all of these plots are inverted from the majority of other plots, with the surface at 0 meters at the bottom and rising.

Based on the characteristics of our transducers they have a surface area. So again Matlab was used to take the 2-D arrival time vs depth plots, and a depth band was set to scan through all the plots and all those arrival times for that single run were saved into another array. Due to the transducers having roughly a diameter of 10cm, a band of 5cm was set to either side of the receiver depth to capture this in the modeling. This Matlab script which scans, saves, and plots the arrival times for each run can also be found in the Appendix. It should be noted that this method of scanning through the plots did work for the 3-D stem plots as well; however, it was significantly slower. Multiple runs to determine the arrival timings at our receiver transducer are completed over time, we can aggregate the results to evaluate how well BELLHOP was able to predict what was recorded with the scintillation system.

Another factor to bear in mind while running these arrival time modeling runs is that BELLHOP is substantially slower and must output far larger files than the transmission loss and ray modeling outlined before. Each arrival time working file, the *.aar* file type that bellhop generates, would be anywhere from 200 MB to almost 1 GB in size, even though the individual arrival time vs depth plots were only about 300 KB in the end. This amount of data could result in doing a full run of arrival times of 1000 casts taking a day to complete, with the *.aar* files needing to be deleted either automatically as part of the script or manually after portions of the run where completed. However, the findings of this method allow for easy comparison to the gathered arrival times from the actual scintillation system and can always be shown on top of the scintillation data figure as seen in the results section. Although the documentation claims that the FORTRAN version of BELLHOP is faster, Matlab was used for this investigation due to its simplicity of use and data comparison.

3 Results & Discussion

In this section, we evaluate the data and examine what transpires during the tidal cycle in this estuary with a highly dynamic stratified structure. We also compare how successfully we modelled this dynamic environment in BELLHOP. The first three tidal cycles were chosen to be modeled in this work. This was done since the first three have drastically varied arrival time structures. The remaining ones seen in Figure 2.7 seem to closely resemble that of the 3rd tidal cycle.

3.1 General Comparison and Sound Speed Profiles

Figures 3.1 and Figure 2.8 shows the relationship between the tides and the structure of the water column and the SSP with the resulting arrival times for the scintillation system. As discussed in the previous section, the flood tide causes seawater to push up the river bed underneath the fresh water. This salt wedge slowly gets bigger and increases in depth until most of the water column is seawater and just the small 1 meter layer of fresh water remains on top. Figure 3.2 shows over 200 SSP's over the course of the first tidal cycle. This image helps to visualize the salt wedge with the fresh water sitting on top.

This process lags behind the tides slightly because it takes time for the salt wedge to push up the estuary before being pushed/eroded back out with the ebb. This structure delay can be noticed in figure 3.1 which demonstrates how the arrival times structure lags behind the tides. Figures 3.3 to 3.5 show SSP's near the min and max, as well as the max rate of change portions of the arrival time structure. The minimum arrival times happen when the salt wedge takes up most of the water column and consequently swift arrivals. The opposite is true for near the peaks of the arrival times, with the water column being mostly freshwater. We can see, however, that there are some differences between the tidal cycles here. The first and third tidal cycles were able to force out the majority of the seawater, while the second tidal cycle had a significantly weaker ebb, causing a more of the salt wedge near the river bed to remain than the

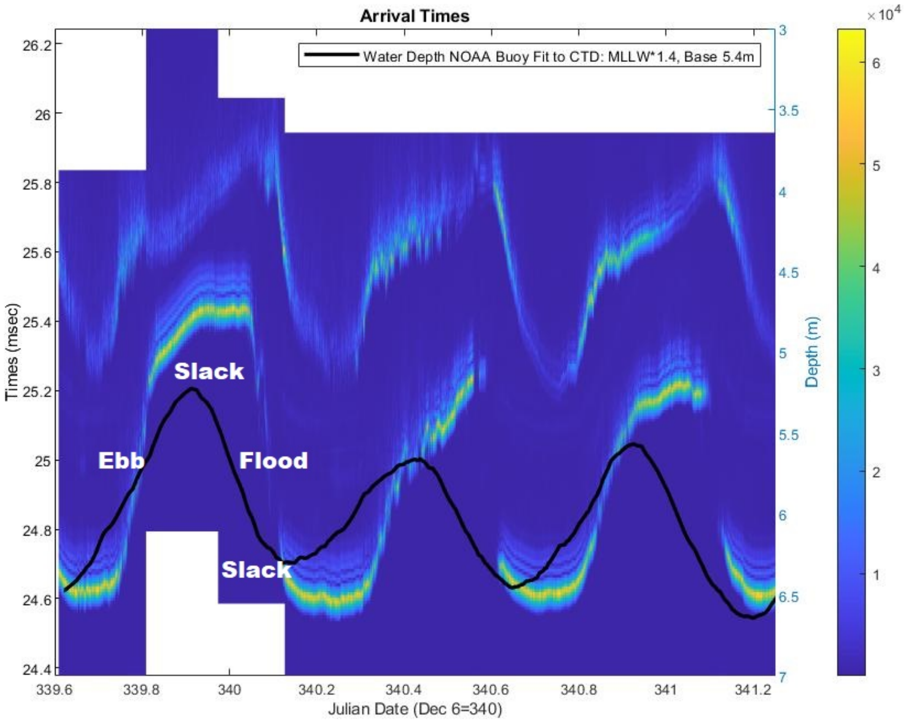

Figure 3.1: Arrival time structure with color bar showing received intensity on transducer A_R, plotted against a projected water depth for 3 tidal cycles.

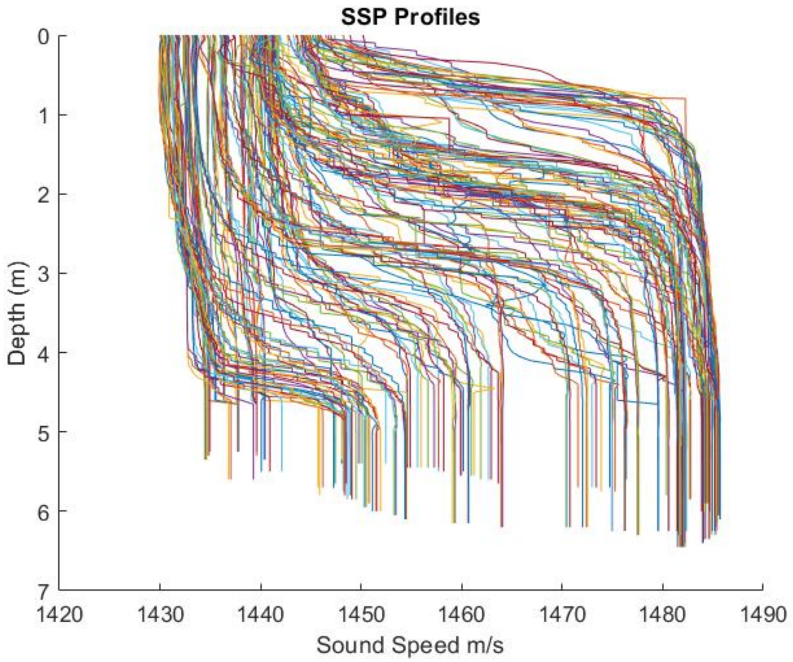

Figure 3.2: Sound speed profiles over a full tidal cycle covering Julian date 339.6 to 340.2.

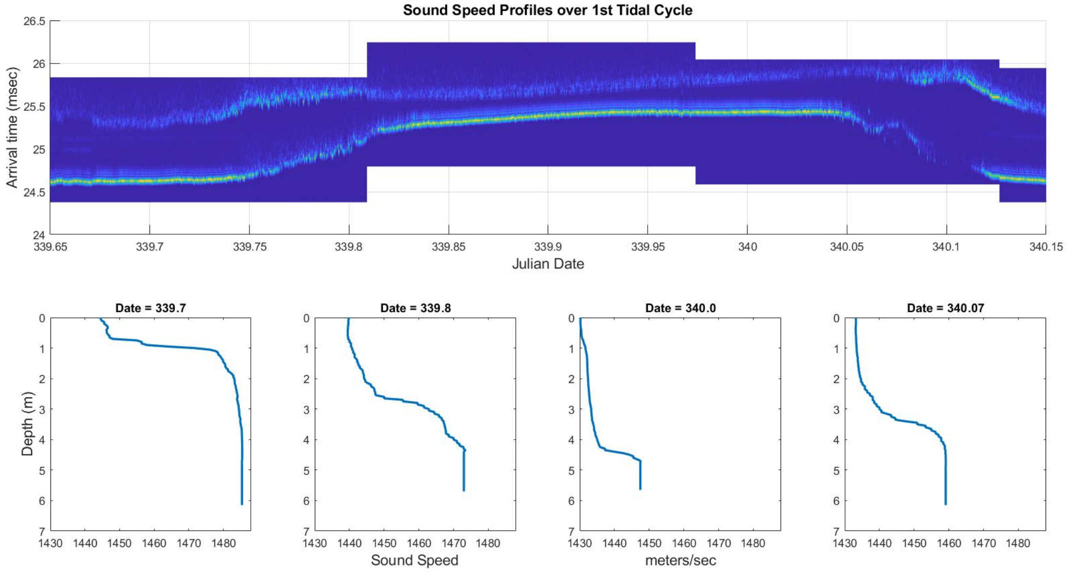

Figure 3.3: Arrival Time structure over the 1st tidal cycle, showing different SSP's over the course of its duration.

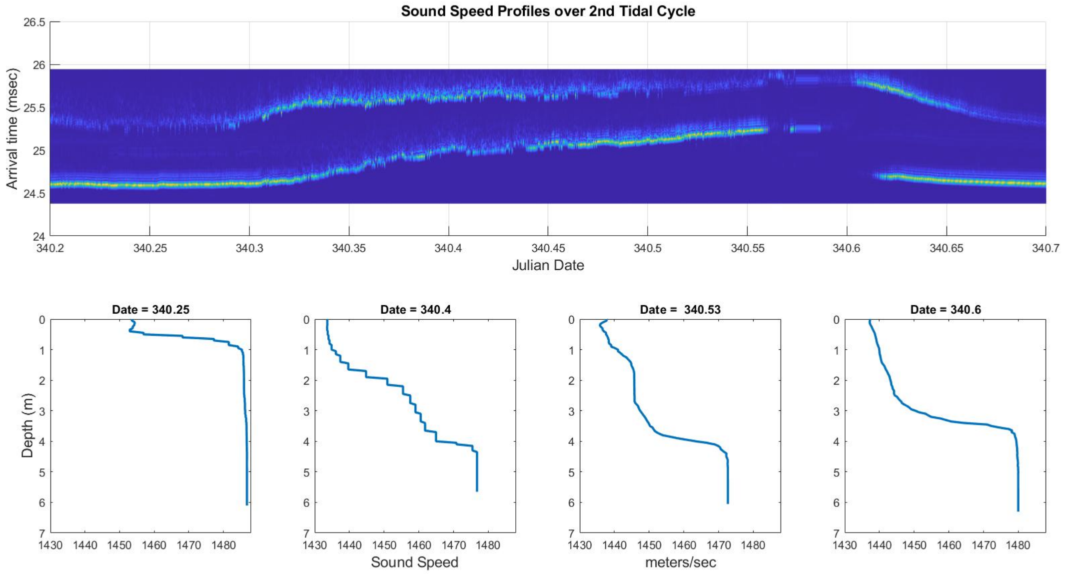

Figure 3.4: Arrival Time structure over the 2nd tidal cycle, showing different SSP's over the course of its duration.

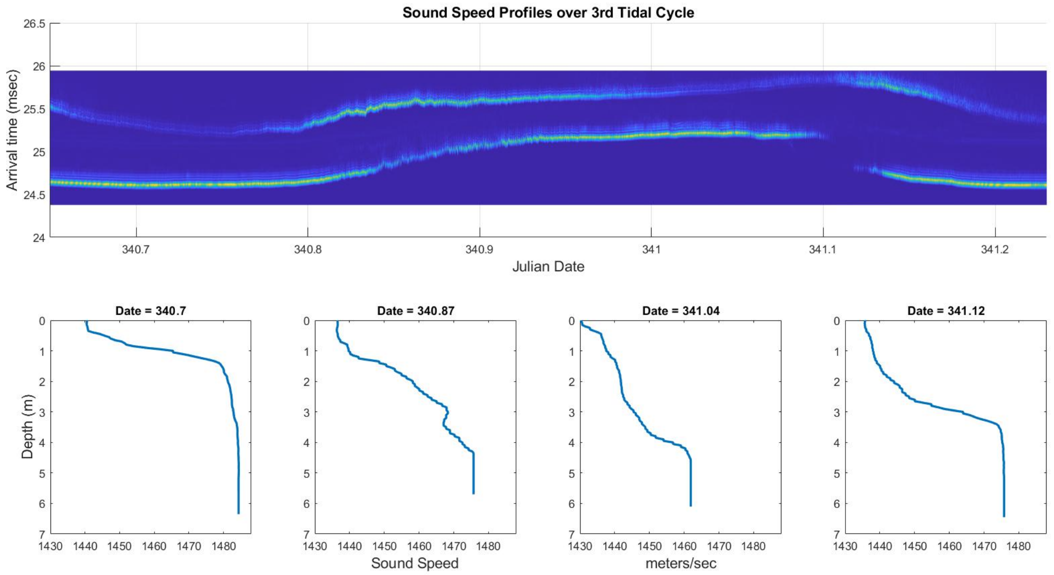

Figure 3.5: Arrival Time structure over the 3^{rd} tidal cycle, showing different SSP's over the course of its duration.

other two. As a result, the arrival structure is considerably less defined during the peak and is unable to smooth out before it begins to descend and decrease again. There is a noticeable difference between the increase in arrival time after the ebb and the decrease in quick arrival times during a flood. The distinction is in the shape of the salt wedge. As described previously by Fincke,[1] the ebb tide is slowly eroded away, making a much more linear SSP. In the case of a flood, the salt wedge maintains the water column relatively stratified, with fresh water just sitting on top of the SSP and gradually rising up, filling the water column with a much more discrete jump in SSP. Figures 3.6 and 3.7 shows the echo sounding returns from the upward looking ADCP on the backscatter array. The surface is seen here as the black return. We can also see the variability and get a decent idea of how stratified the water column has become over time. In Figure 3.6, over the first hour, we can see that the water column has very minimal variability, with most of the water being all fresh water, although we do start to see the salt wedge near the bottom. We can see that this continues and the variability does increase during the flood to about the 3 to 4 hour point were the variability start to go down and you can see a more defined stratified layer during the slack following the flood. Figure 3.7 shows that as the ebb begins, the stratification begins to reduce as the water begins to

---

[1] Fincke, "Quantification of the spatial and temporal evolution of stratifed shear instabilities at high Reynolds number using quantitative acoustic scattering techniques".

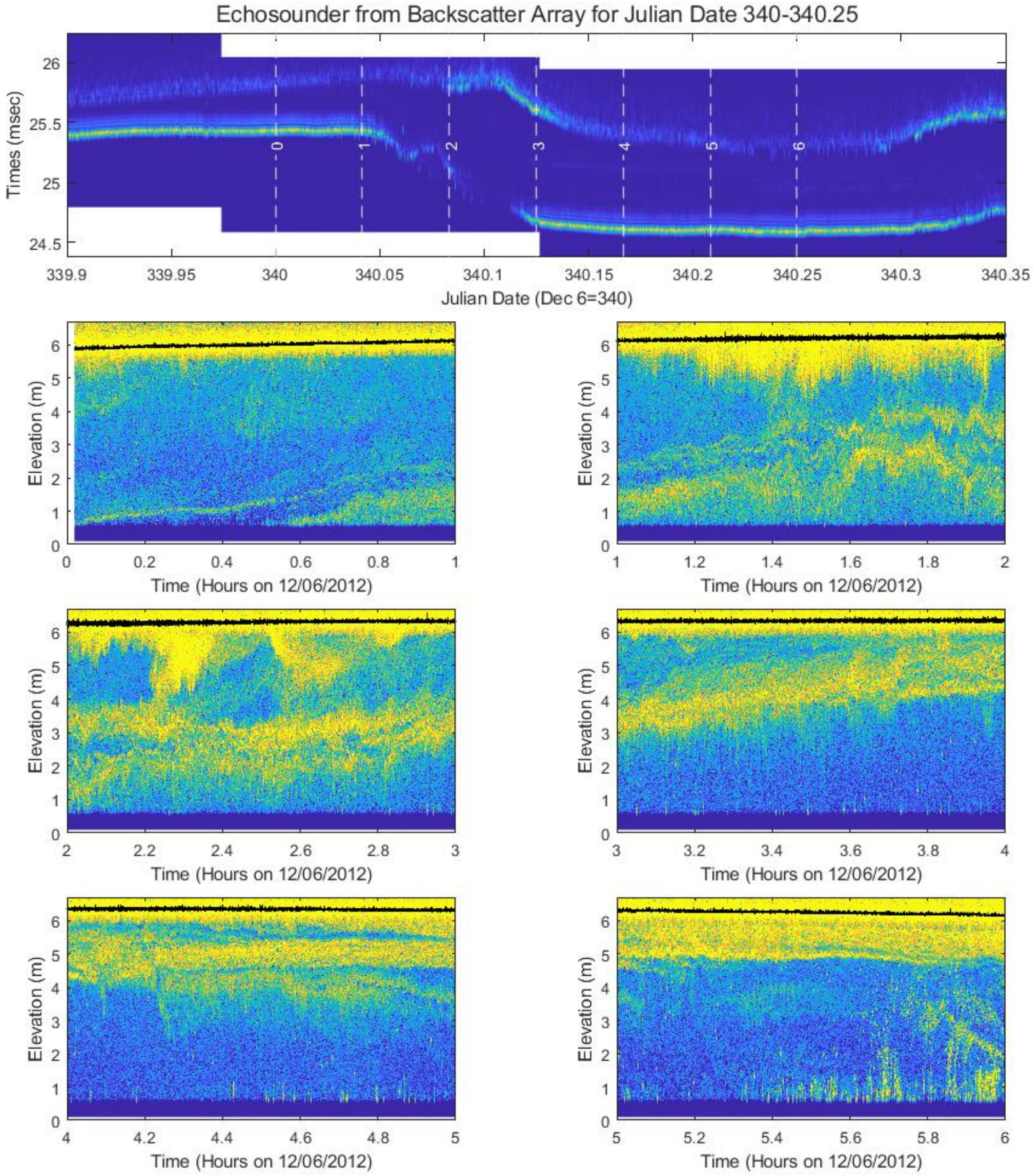

Figure 3.6: Upward looking Echo sounder from backscatter array (75 cm above river bed). Shows variability in the water column over time (Julian Date 340-340.25). Black line shows surface of CT river.

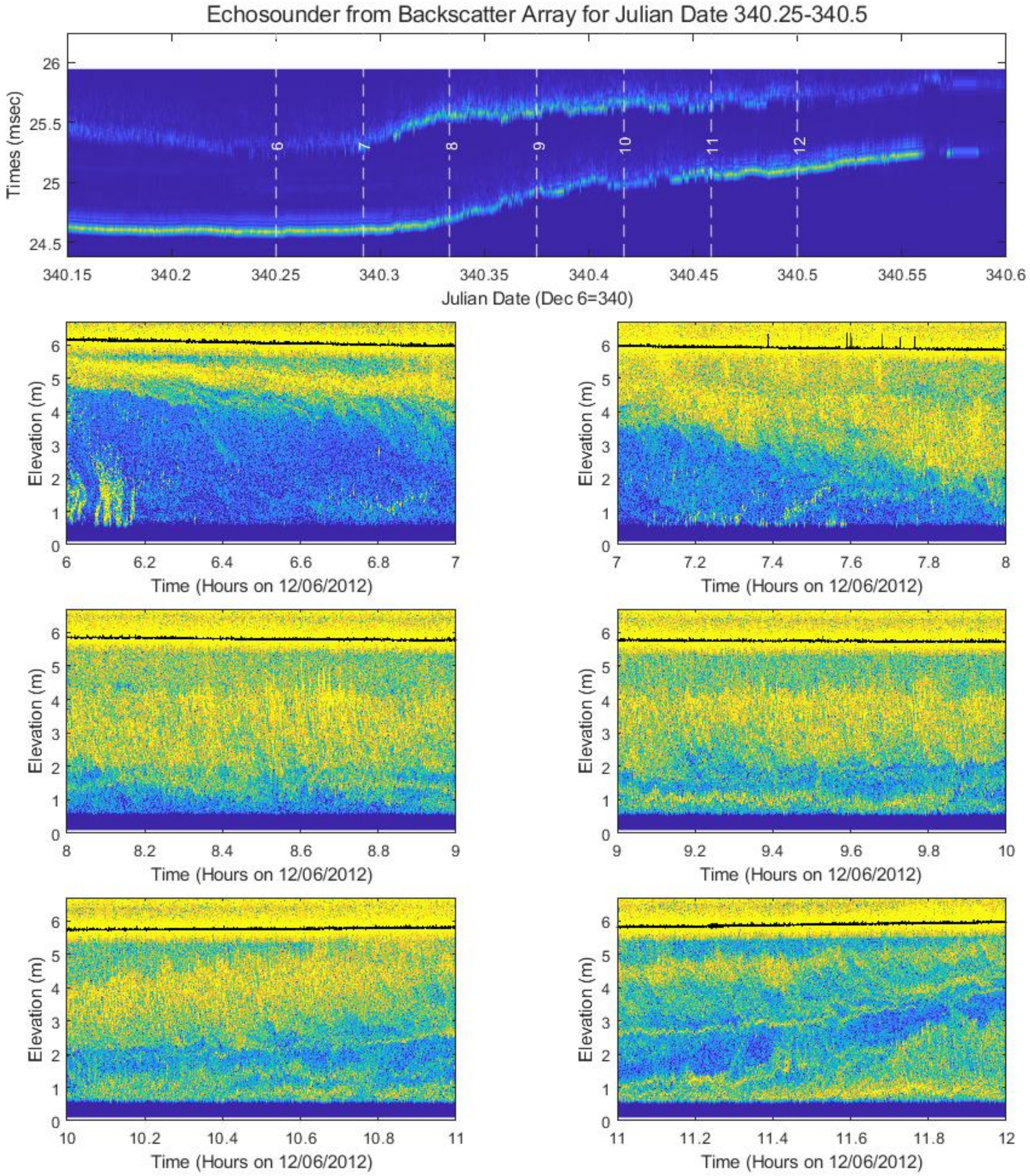

Figure 3.7: Upward looking Echo sounder from backscatter array (75 cm above river bed). Shows variability in the water column over time (Julian Date 340.25-340.5). Black line shows surface of CT river.

mix up from the shear instabilities, causing the highest variability throughout the course of the tidal cycle. Additional echo soundings can be found in the Appendix.

3.2 Initial Modeling and Arrival Times

BELLHOP is now used to try and model arrival times, as seen in Figure 2.11. Most of the modeling is done comparing main transducer A to remote transducer A. As a reminder to this, they both sit 3 meters off the bottom across the river 36.5 meters apart. The biggest questions of the environment that significantly impact the environment are the depth and the SSP, since these measurements were not taken at the exact location of the scintillation system.

3.2.1 Main Beam Width

The modeling run utilizing the depth profile using the tides data matched to the CTD profile and shifted 60 cm up as mentioned in the techniques section is shown in Figure 3.8. It is the same depth profile seen in Figure 3.1. Here we have two different case runs. The first run, shown in magenta, was done with a ±5.5°beam, as that is the half power beam width of the transducer used. There is good matching of the curve of the slower bottom arrival times curve that is from the direct arrivals. The upper more faded arrival times curve is from the surface reflections. This can be seen later in the the TL plots as will are the arrival times plots. Here we see a mismatch of the results coupled with large portions of the data missing. Looking at the ray travel paths we can see that we are just missing the surface reflection coming back down in these areas. Since there is still energy outside the -3dB main beam, the modeled beam was widened to ±8°to the -6dB level. This widening of the beam now does show much better overall coverage across the duration of the collected data. This now leaves just leaves the mismatch of the modeled arrival times from surface reflections which are less than what was actually observed. This shows that the water depth is likely deeper in this area, as deeper water depths would increase the overall distance a surface reflection would have traveled and thus the arrival times would take longer.

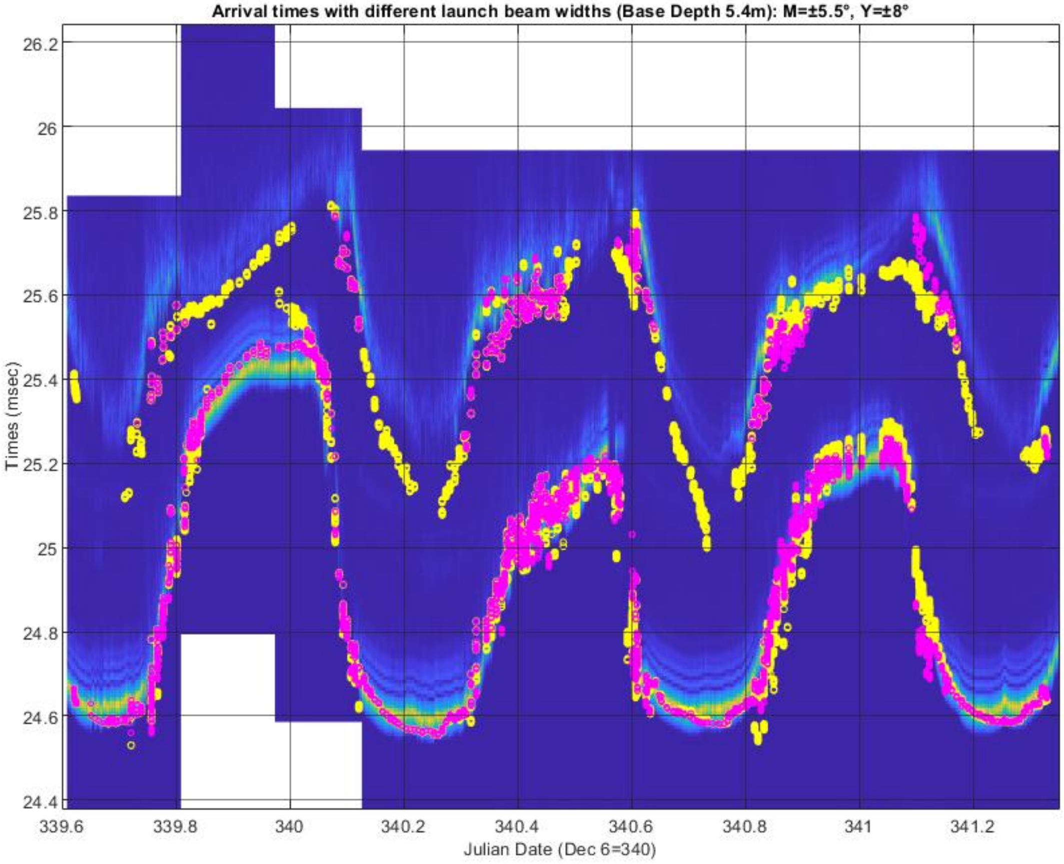

Figure 3.8: Arrival times from BELLHOP modeling plotted over scintillation system measurements from transducer A_M to A_R. Showing both ±5.5°beam (magenta) vs ±8°beam (yellow). Both runs with depth modeling at 5.4 m base using tide data.

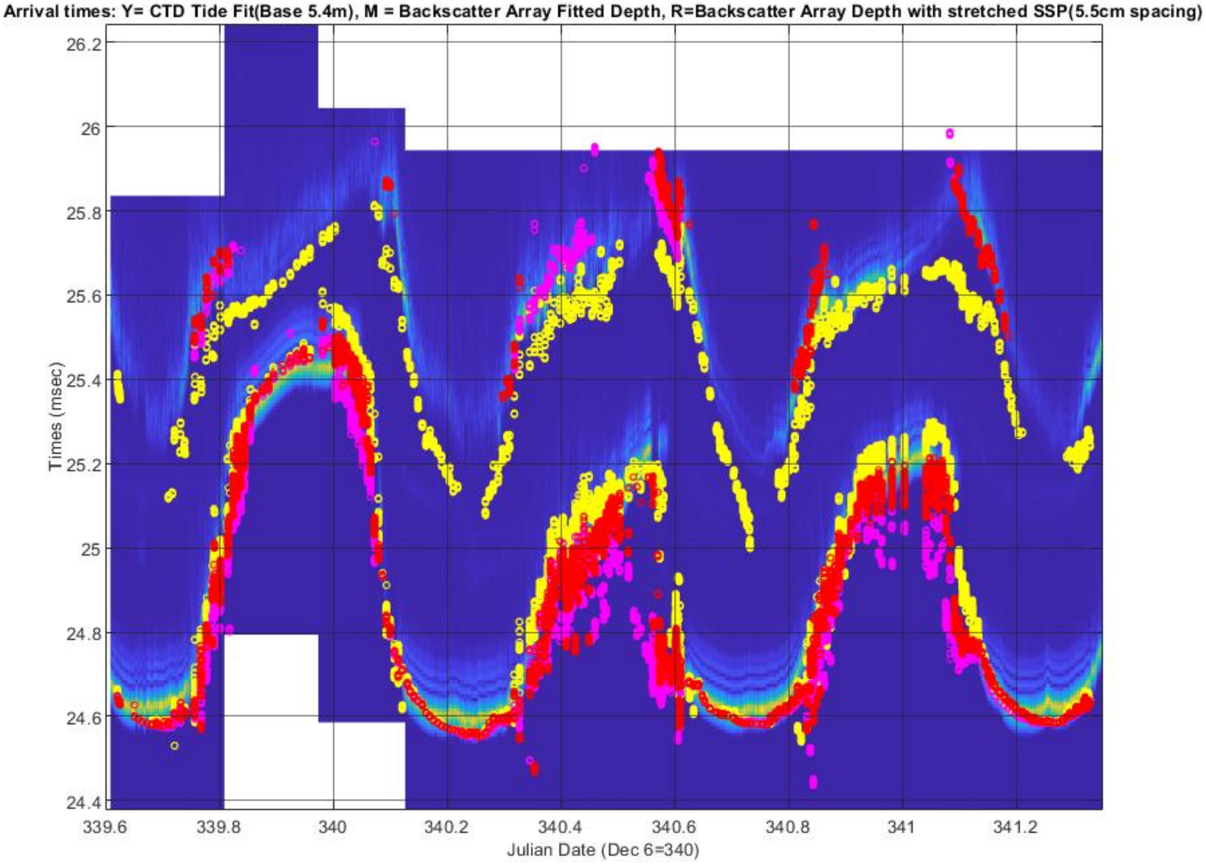

Figure 3.9: Arrival times from BELLHOP modeling plotted over scintillation system measurements from transducer A_M to A_R. Showing shallower depth from 5.4 m base fitted to CTD data and a deeper depth of 6.27 m base from the backscatter system with two different SSPs (Colors labeled at the top). All with the wider ±8°main beam.

3.2.2 Depth and SSP

Figure 3.9 shows three different modeling runs comparing different depth and SSP profiles. All three have the ±8°launch beam as discussed above, which is plotted in green in the previous run with the shallower depth profile. The red and magenta show two new runs. The magenta is simply the deeper depth profile seen in Figure 2.10 using a depth profile fitted to the recorded depth data from the nearby backscatter system. Since the two systems are so near together, this depth is likely to be more accurate. It demonstrates both areas of enhanced matching with real data and areas that are plainly correct. The timing of the first third of the run up until roughly Julian data 340.4 is quite close. We also find an overall improvement in surface reflection timing where there are surface reflection returns. This is because the deeper depth lengthens the distance between the more direct arrival and the surface reflection from the shallower modeling. However, we have a significantly larger amount of missing surface reflection collected. Additionally, in the direct arrival areas between Julian dates 340.4-340.6 and again 340.9-341.1 we observed a significant mismatch with the recorded data. This is most likely because the SSP profile employed is inaccurate when the water depth is deeper, and the SSP was simply stretched and believed to be isovelocity from the CTD data in the shallower area. In an attempt to determine a possible more correct SSP to go along with the deeper backscatter depth profile, the CTD data is stretched by 10% using 5.5cm spacing of its data points vice the actual 5cm spacing. This is plotted in red. This leads to improvement in the direct path arrivals in the two previous noted time periods. It does also manage to maintain similar arrival times in surface reflection area. However we still have decent amounts of missed surface reflections at high tides with increased water depths. There is also the region of near Julian date 340.4 that does have missing surface reflections even though the other deep non-stretched SSP modeling shows arrivals that match well with the collected data there.

3.3 Rays and Multi-path Arrivals

Figures 3.10 through 3.15 use the BELLHOP *plotshd* function along with the edited *plotarr* function. These graphs can help visualize what is going on over the first tidal cycle. These figures are in chronological order, and the time of each event is indicated as the title and denoted as a vertical dotted white line on the recorded scintillation data. The appendix contains supplementary figures for the remaining two tidal cycles.

All figures, 3.10 through 3.15 are using the SSP profile fitted to the backscatter data with the 5.5 cm SSP spacing and a main beam of 0±8°. Note: the direction of the depth on the y-axis between the shade TL and the arrival times plots are reverse.

3.3.1 Critical Angle

When we look at some ray figures, such as Figure 3.13,we can see that the rays never reach the bottom and are reflected up off the salt water layer. This total reflection is known as the hypocritical grazing angle, $thetac$ from Snell's equation, and is provided by the *critical grazing angle*, θ_c from Snell's law, and is given by the equation:[2]

$$\theta_c = arccos(c_1/c_2) \tag{3.1}$$

This only happens when c_2 is greater than c_1. This can happen when the source transducer is above the salt wedge and the rays are transmitting down. It does not have to happen to all of the sound, just the portion that is below the θ_c. An excellent example of this is in Figure 3.14, where we see the multiple shallow incident angles being reflected up, but at the steeper angles this does not occur. Plotted in Figure 3.16 are the maximum critical angles of the SSP, along with the depth of these critical angles and the source depth. In this study we observed that the critical angle is only valid if our source is above the critical angle depth as we are looking at cases where c_2 is higher than c_1.

3.3.2 Surface and Multi-path Arrivals

In Figure 3.9 where the was missing points in the surface reflection portion of the model but clearly some faint data in the recorded data. To verify is some of the missing data could result from looking at a wider beam width more runs were down and rays looked at. Figure 3.17 shows a few of the TL plots that also show the ray structure. We can see that in these cases, there are a few instances where these different launch angles could help generate the seen signals. As we saw above, once the water depth was increased, even a main beam of ±8°did not always result in a surface reflection. There just was not enough water in these deeper cases. Due to the fact that by the time the signal reached the surface it did not have enough distance to get back down to the receiver, over their separation at 36.5 meters. To get surface reflections in these cases, larger

---

[2] Jensen *et al.*, *Computational Ocean Acoustics*.

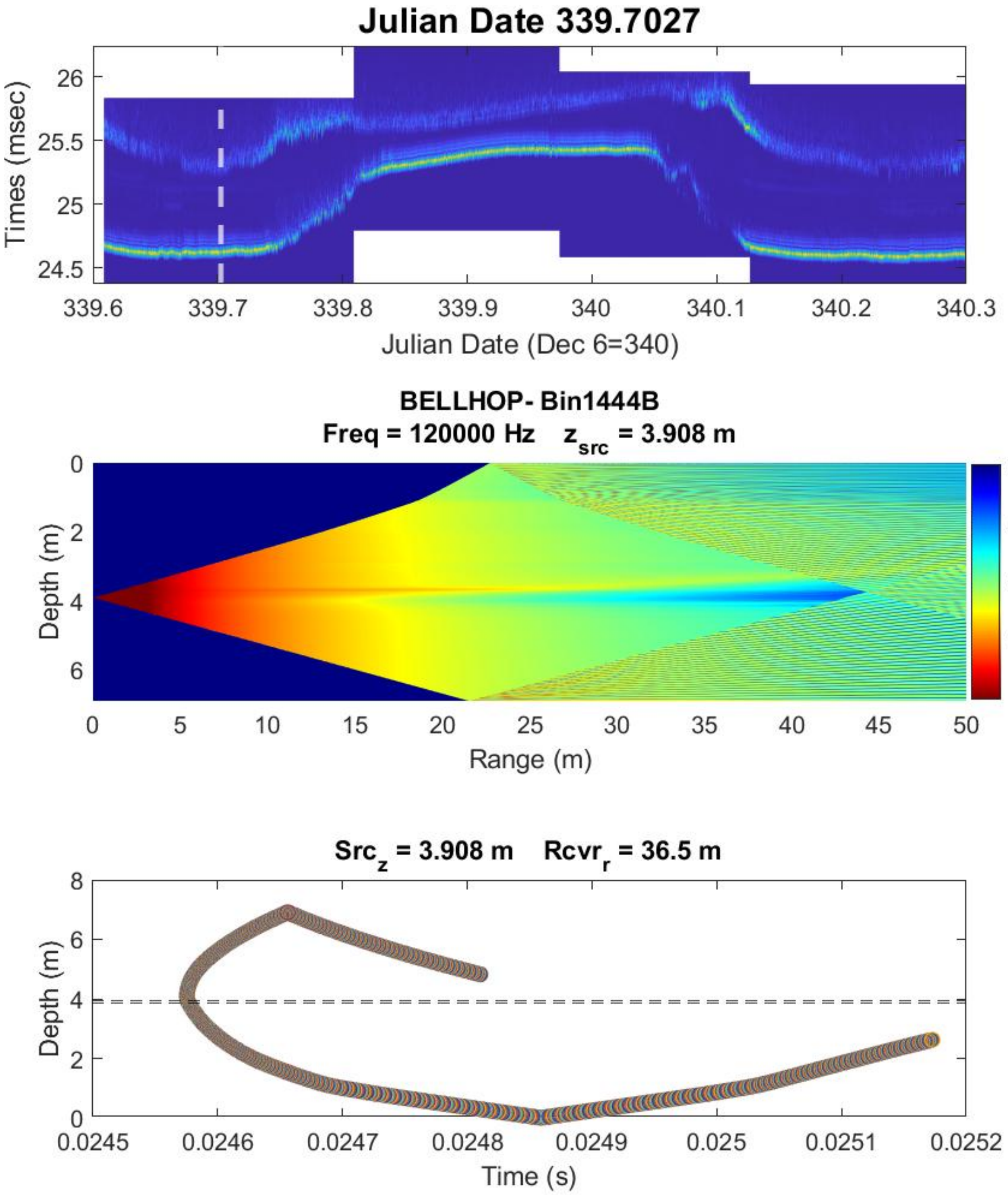

Figure 3.10: Plots for Julian date 339.7027. Top: recorded arrival time data from scintillation system. Middle: Transmission loss for main beam with of ±8°. Bottom: Modeled arrival times from BELLHOP.

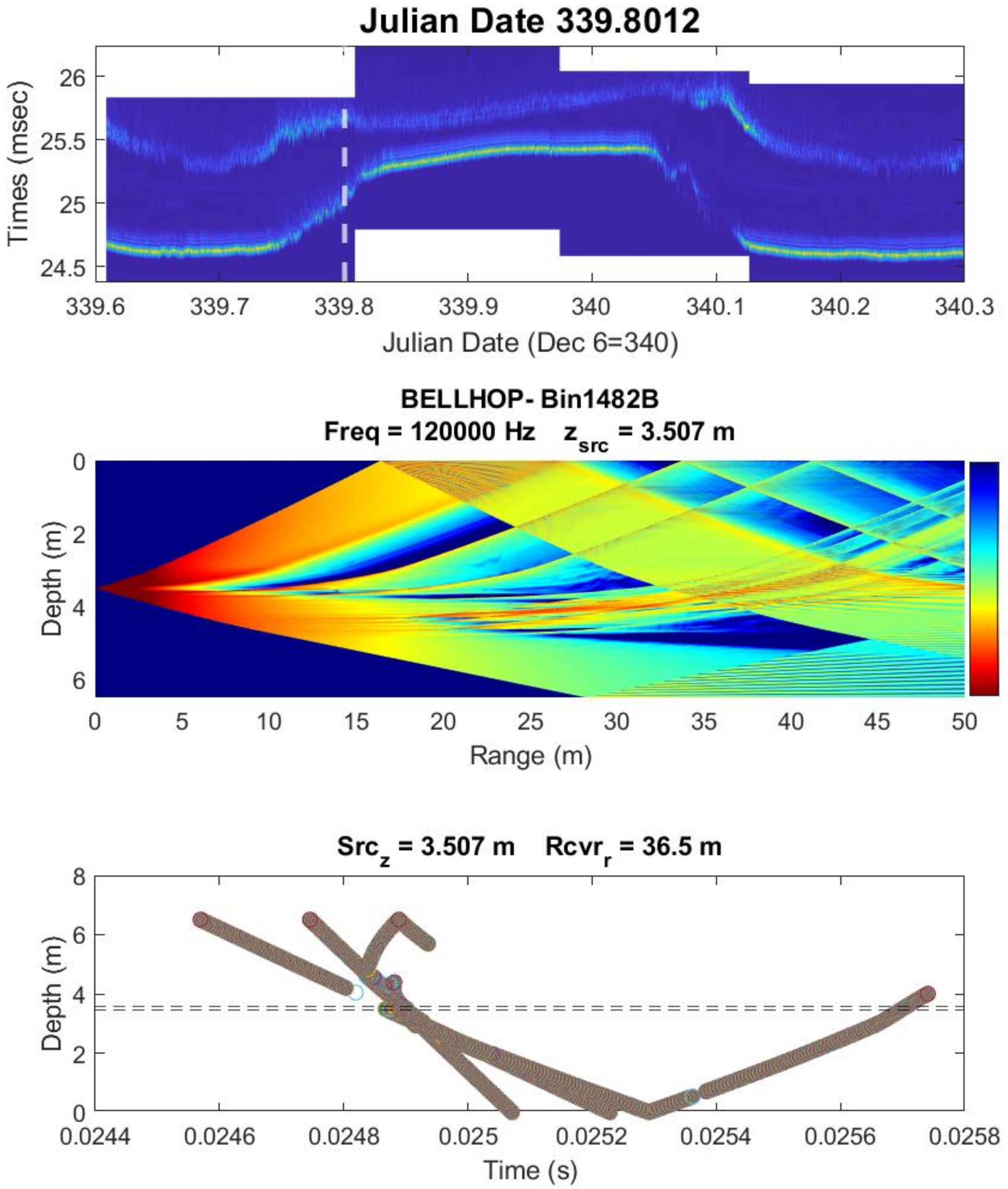

Figure 3.11: Plots for Julian date 339.8012. Top: recorded arrival time data from scintillation system. Middle: Transmission loss for main beam with of ±8°. Bottom: Modeled arrival times from BELLHOP.

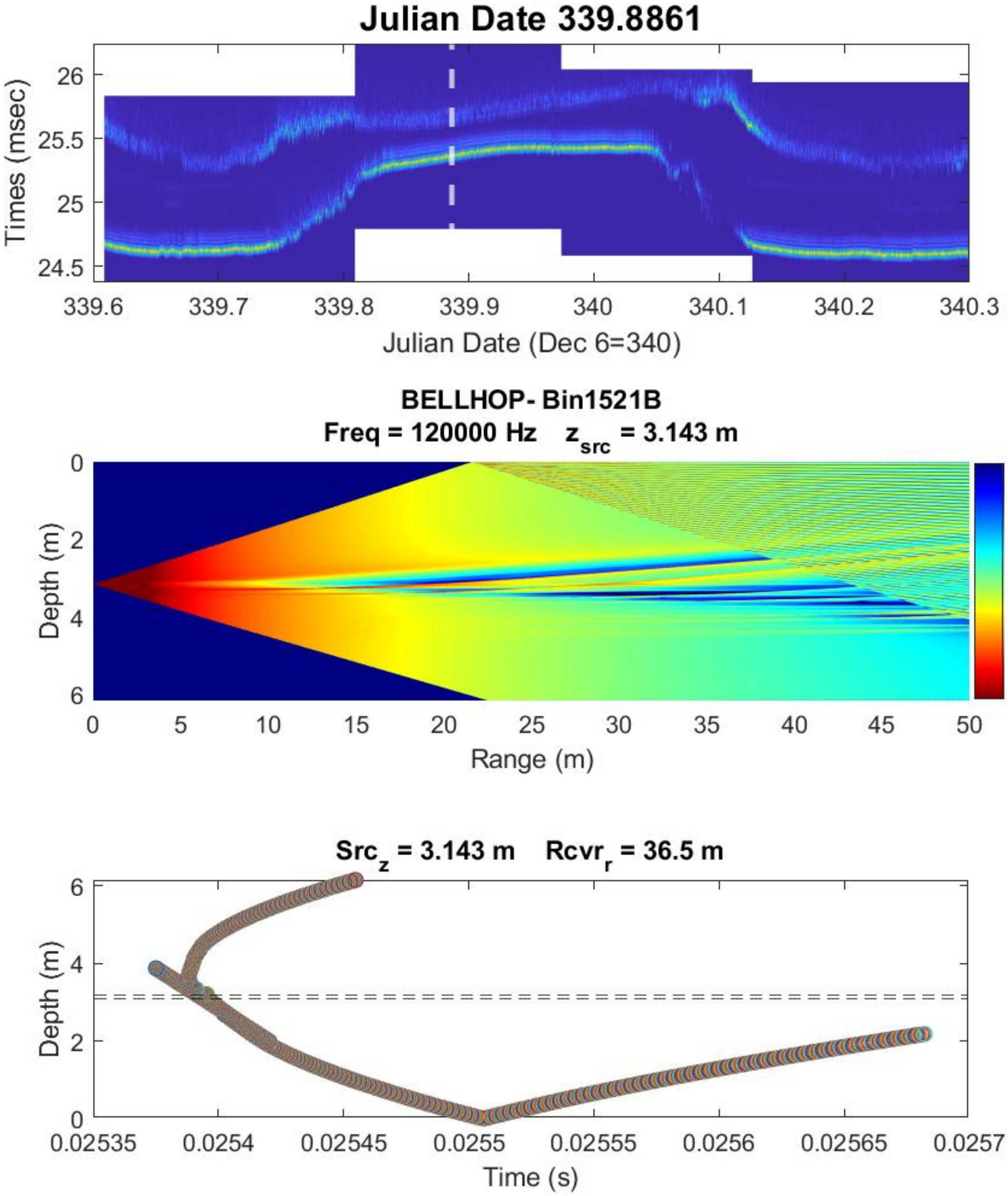

Figure 3.12: Plots for Julian date 339.8861. Top: recorded arrival time data from scintillation system. Middle: Transmission loss for main beam with of ±8°. Bottom: Modeled arrival times from BELLHOP.

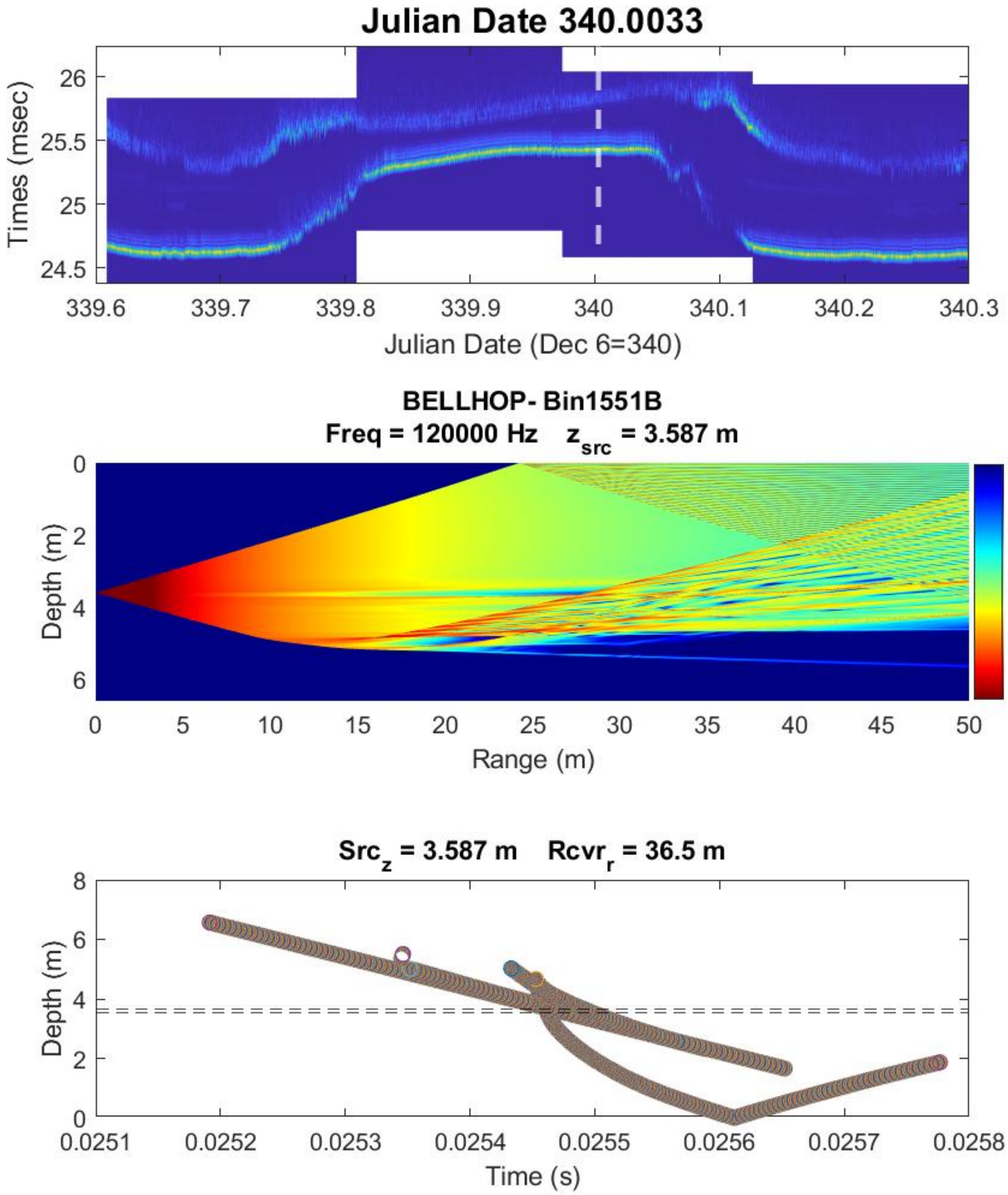

Figure 3.13: Plots for Julian date 340.0033. Top: recorded arrival time data from scintillation system. Middle: Transmission loss for main beam with of ±8°. Bottom: Modeled arrival times from BELLHOP.

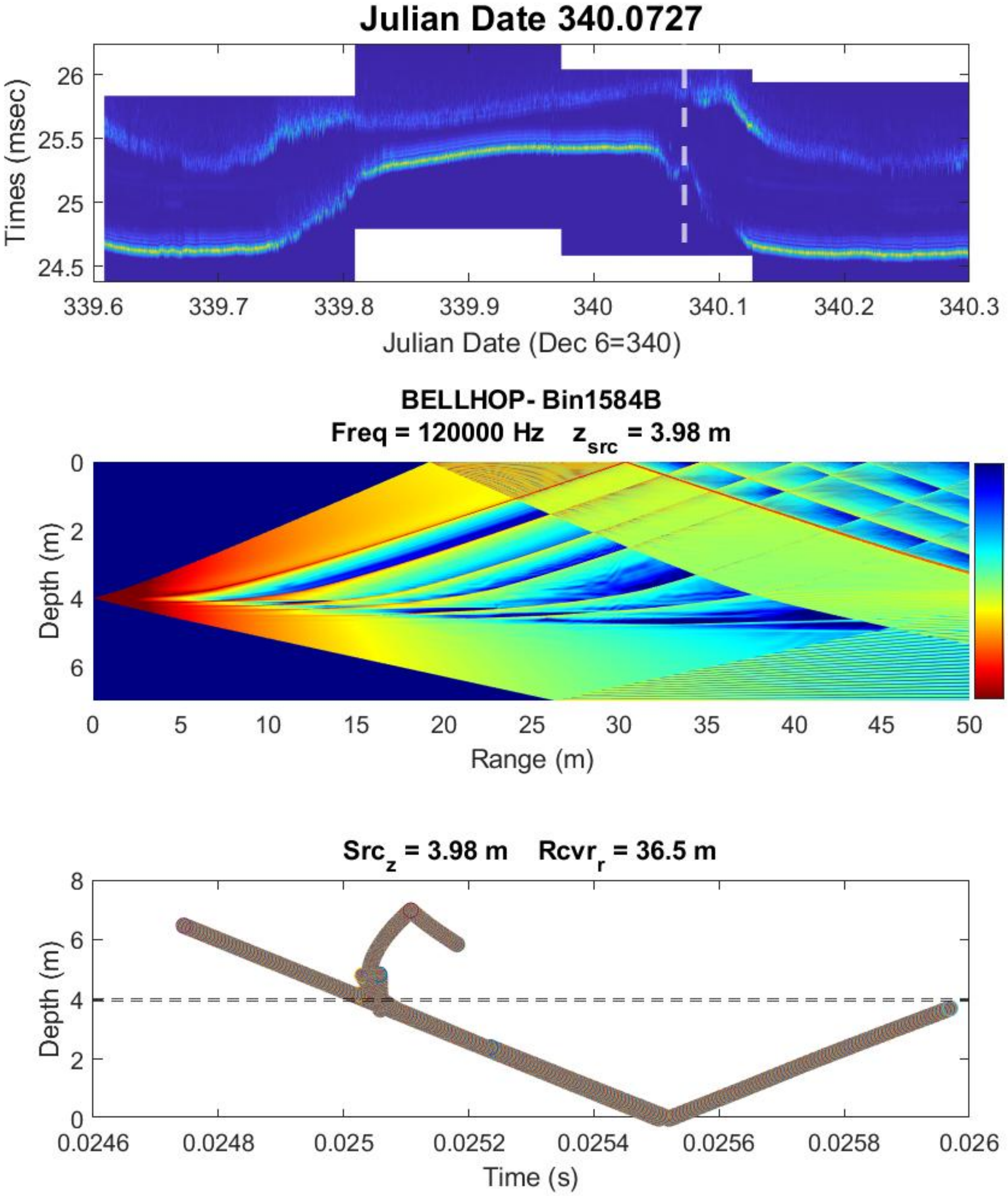

Figure 3.14: Plots for Julian date 340.0727. Top: recorded arrival time data from scintillation system. Middle: Transmission loss for main beam with of ±8°. Bottom: Modeled arrival times from BELLHOP.

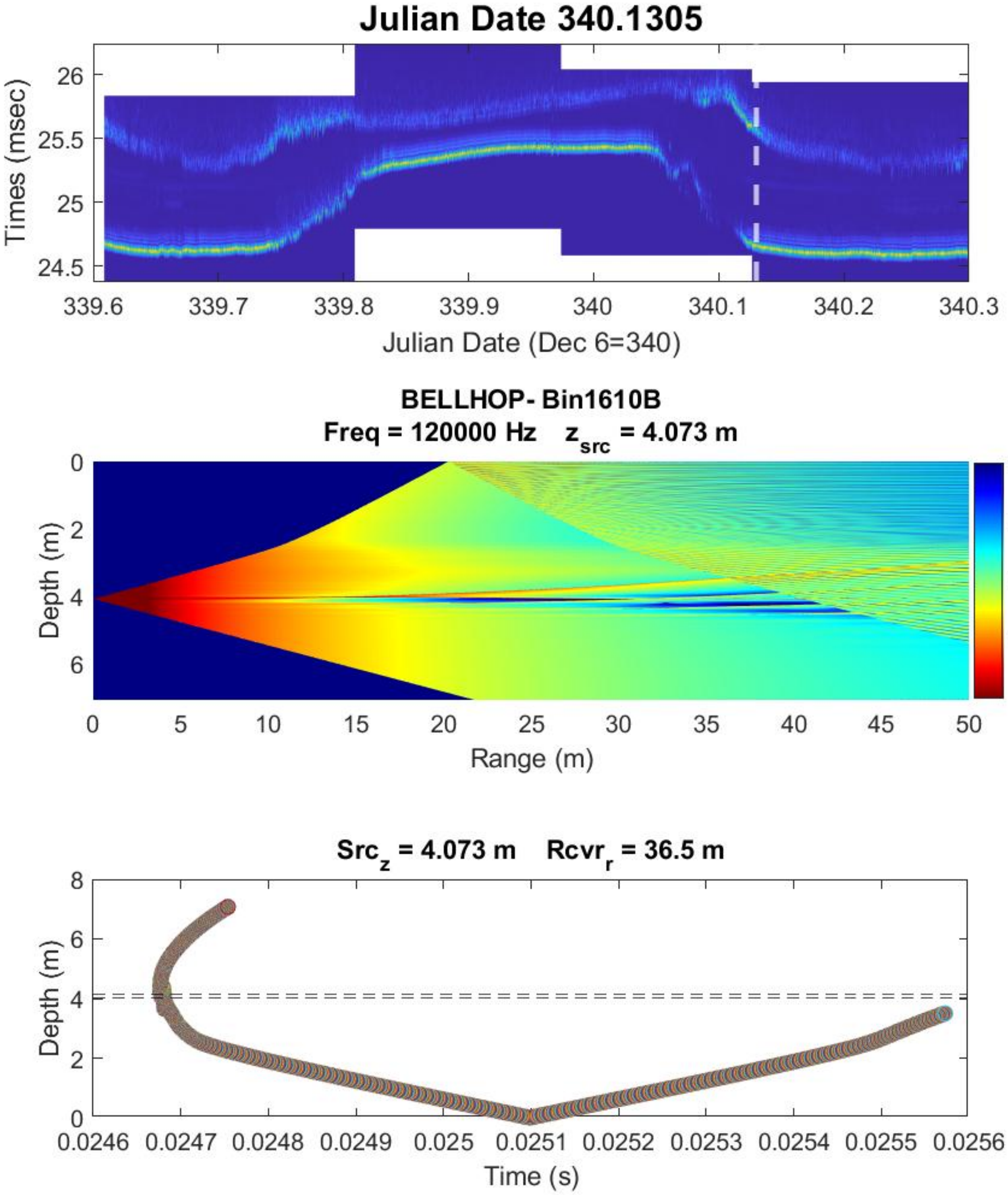

Figure 3.15: Plots for Julian date 340.1305. Top: recorded arrival time data from scintillation system. Middle: Transmission loss for main beam with of ±8°. Bottom: Modeled arrival times from BELLHOP.

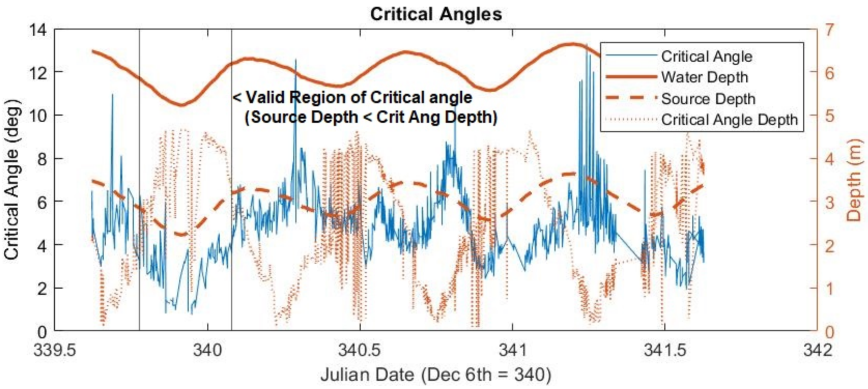

Figure 3.16: Critical angles. Note that the source depth must be above the depth location of the critical angles.

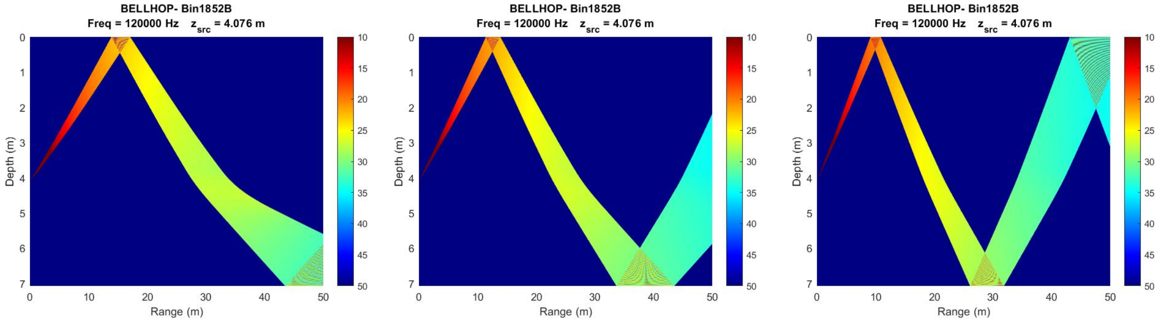

(a) Beam at 11±2°

(b) Beam at 15±2°

(c) Beam at 20±2°

Figure 3.17: BELLHOP TL plot for 3 different launch angles at Julian date 340.57.

launch angles would be needed. There are also potential side lobes right off the main beam seen in the transducer beam pattern Figure 2.5 at around 17°.

To test this, additional modeling runs of beams were done. Three different cases were run: 11±2°, 15±2°, and 20±2°. These runs were done on both the shallower depth model and on the deeper depth model with the stretched SSP. Figure 3.18 shows the results for the deeper depth model with the stretched SSP using the 5.5 cm spacing of the CTD data. Here we can see that a side lobe of 11±2°could account for some coverage of the originally missing portions of the main beam modeled results from the real data. It should be noted that here is a missing 1°band between 8-9°from the red data and the yellow data for the surface reflection between Julian date 340.3 and 340.5 in the plot. The 15±2°tests were run but came up with no results and therefore resulted in no plot. The angle resulted in ray paths between surface reflection and surface reflection to bottom bounce into our receiver. We do once again get arrivals if we increase to a beam of 20±2°. This arrival is a multi-path surface reflection to bottom bounce.

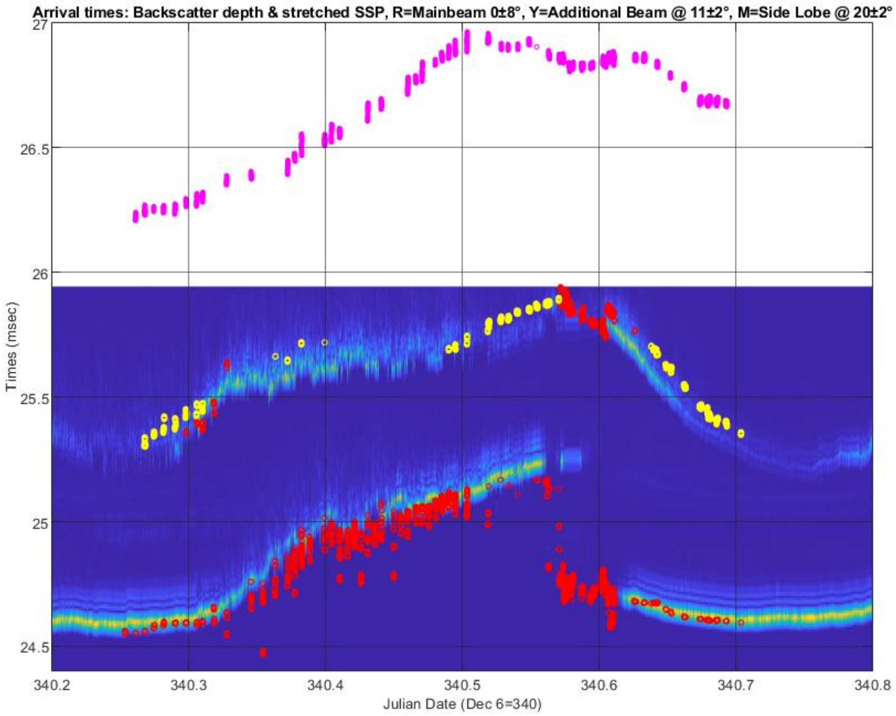

Figure 3.18: Arrival times from BELLHOP modeling plotted over scintillation system measurements from transducer A_M to A_R with deeper depth profile and stretched SSP. Red shows the main beam of 0±8°, yellow an additional beam at 11±2°, magenta a side lobe at 20±2°

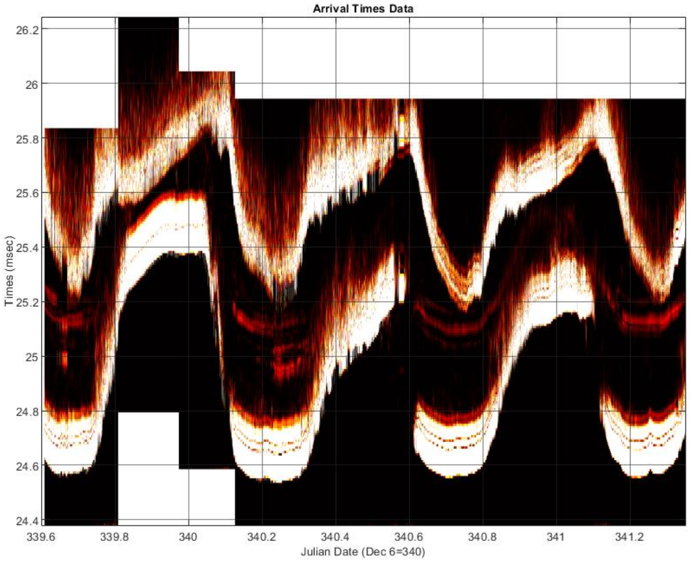

Figure 3.19: Arrival times from scintillation system measurements from transducer A_M to A_R with exaggerated 'white hot' color scale to help show faint bottom bounce arrival.

This could potentially be a side lobe of our transducer, but is definitely out of the main beam area. However, when compared to the data, we can determine that this is not part of our missing modeling. This route results in a much greater overall travel distance and, as a result, significantly longer arrival times. This is seen in magenta in Figure 3.18 as out of scale of the recorded data. The same results would be observed in the shallower depth profile, with surface to bottom bounce having increased arrival times that did not correspond to the data reported. This is also unlikely to be recorded because the TL from several bounces is large, as seen in Figure 2.5 are already at around -18dB. Therefore, these are not really seen in comparison to direct or single reflection arrivals, compared to the stronger main beam.

3.3.3 Bottom Bounce Reflection

Another observation from the recorded data is that there are some very faint returns that fall in the middle of the bottom curve of the direct arrival times and the top curve of the arrival times from the surface reflections. To better highlight this, the color scale was changed with a different color map applied to the recorded data and is shown in Figure 3.19. However, for the most part, all the previous modeling runs of do not show a bottom bounce case. This can be more individually seen in the arrival times curves for Figures 3.10 through 3.15 and the others in the appendix. Here we can sometimes see there are reflections off the bottom but they do not fully make it back up to the receiver depth. Therefore, steeper angles than ±8°are needed to be bottom reflections (in the case of a flat bottom). This indicates that there is still a small amount of energy at a wider beam angles, which matches what is seen with the surface reflection modeling as seen in Figure 3.18.

3.4 Improved Model

Figure 3.20 is a middle ground between the other two modeling runs to try and get a better match. Here, the base water depth is changed to 5.95 m. Scintillation arrays are positioned closer to the backscatter system, resulting in a similar deeper depth. However, employing backscatter depths has the disadvantage of the surface reflection arrival times being longer than the recorded data, resulting in a somewhat lesser depth being required. With a decrease in overall water depth. The SSP stretching was reduced to 5.3 cm spacing rather than the prior 5.5 cm spacing. This nevertheless resulted in a minor reduction in the total need to extend the SSP by 10 cm. Finally, the main beam band was expanded to ±11°as this would allow for full coverage of the main beam from Table 2.1. Ensuring that the modeling has a chance to notice the surface reflection at deeper depths, as well as perhaps allowing for some bottom bounce reflections seen faintly in Figure 3.19 even if signal intensity is lower on the edges. The wider beam would also help show that arrivals were possible even if the geometry of the tripods were not perfectly level on the river bed.

Overall, the modeling of the environment was a very close match, as can be seen in Figure 3.20. Here the surface reflection timings overlay extremely well, indicating a good depth. There are still times when the more direct arrivals approach slightly faster than the recorded data, particularly near the end of the flood. This is most likely owing to the fact that the SSP had to be extrapolated from CTD data for deeper depths because the CTD measurements were taken in a shallower position. With the extended main beam, we can now observe some bottom bounce reflections that appear in the interval between direct arrival and surface reflection arrival timings. In this case, the modeled arrival timings for the bottom bounce are similarly faster than the real data. The pattern, though, is pretty similar. This is most likely due to the same issue as before, in which the SSP is assumed to go isovelocity at the conclusion of the CTD data rather than having direct measurements in the particular location of the scintillation system. This is further

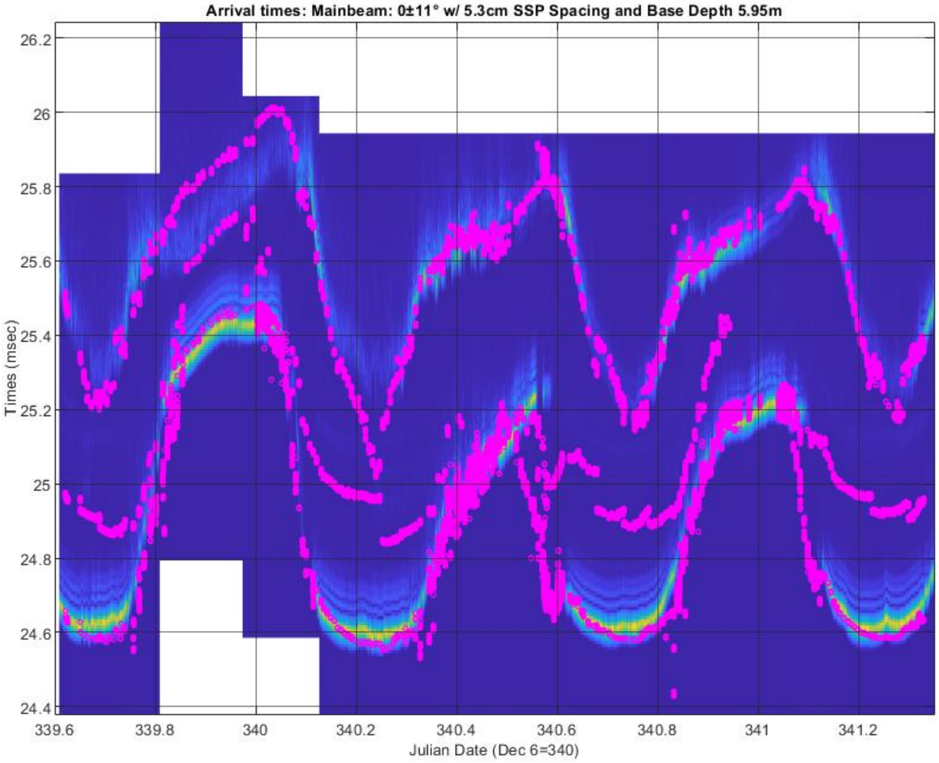

Figure 3.20: Arrival times from BELLHOP modeling plotted over scintillation system measurements from transducer A_M to A_R with an in-between depth profile, plotted in black, (5.95 m Base) and stretched SSP with 5.3 cm spacing. Expanded Main beam of 0±11°.

supported by a review of the results in Figure 3.8 when a shallower depth was used and the SSP had to be extended less for the direct path arrivals overlapping the recorded data very adequately.

Figure 3.21 is an updated BELLHOP Shade TL plot and arrival times for the new wider ±11°full main beam. Here, compared to the previous ±8°beam, we can see that surface reflection is able to reach back down to our receiver depths at 36.5 m range. Additionally, this is true for the bottom bounce as well. The remainder of the transmission loss with single environment arrival times can be found in the Appendix for the remainder of the data set. While the model now indicates the arrival times for the bottom bounce, it is important to remember that the Source strength at the outskirts of the main beam is roughly -10 to -15dB depending on how far away from the center of the beam the indecent rays are originating from. This, along with transmission losses from the bottom reflection, results in possible but weak arrivals.

Another finding made while collecting data was that the lower transducers would begin to receive the signal sooner as the salt wedge was driven in during the flood, until it worked its way up in depth, and they would even out again. A run was performed between Main transducer, A_M, (3 m above the bottom) and Remote transducer, D_R, (2.25 m above the bottom) to see if this is supported by the models. The arrival times are plotted in Figure 3.22 along with the depth profile used for comparison. This agrees with the reported observations that as the salt wedge is forced up the estuary during the flood, there is a period of time when the deeper Transducers C and D are in salt water, causing them to arrive faster than the A_M to A_R. This occurs between roughly Julian date 340 and 340.1, when the flood occurs, and they resume having the same times. The same is true for the ebb, where the deeper transducer D_R is in the salt wedge for a longer period of time, as seen at the time of around 339.8. The bottom bounce is also visible in the illustration, and the surface is slightly delayed. However, this would not have been as noticeable because the bottom bounce was extremely faint in the raw data, and the surface reflection was also quite diffuse. This helps to confirm the model's accuracy.

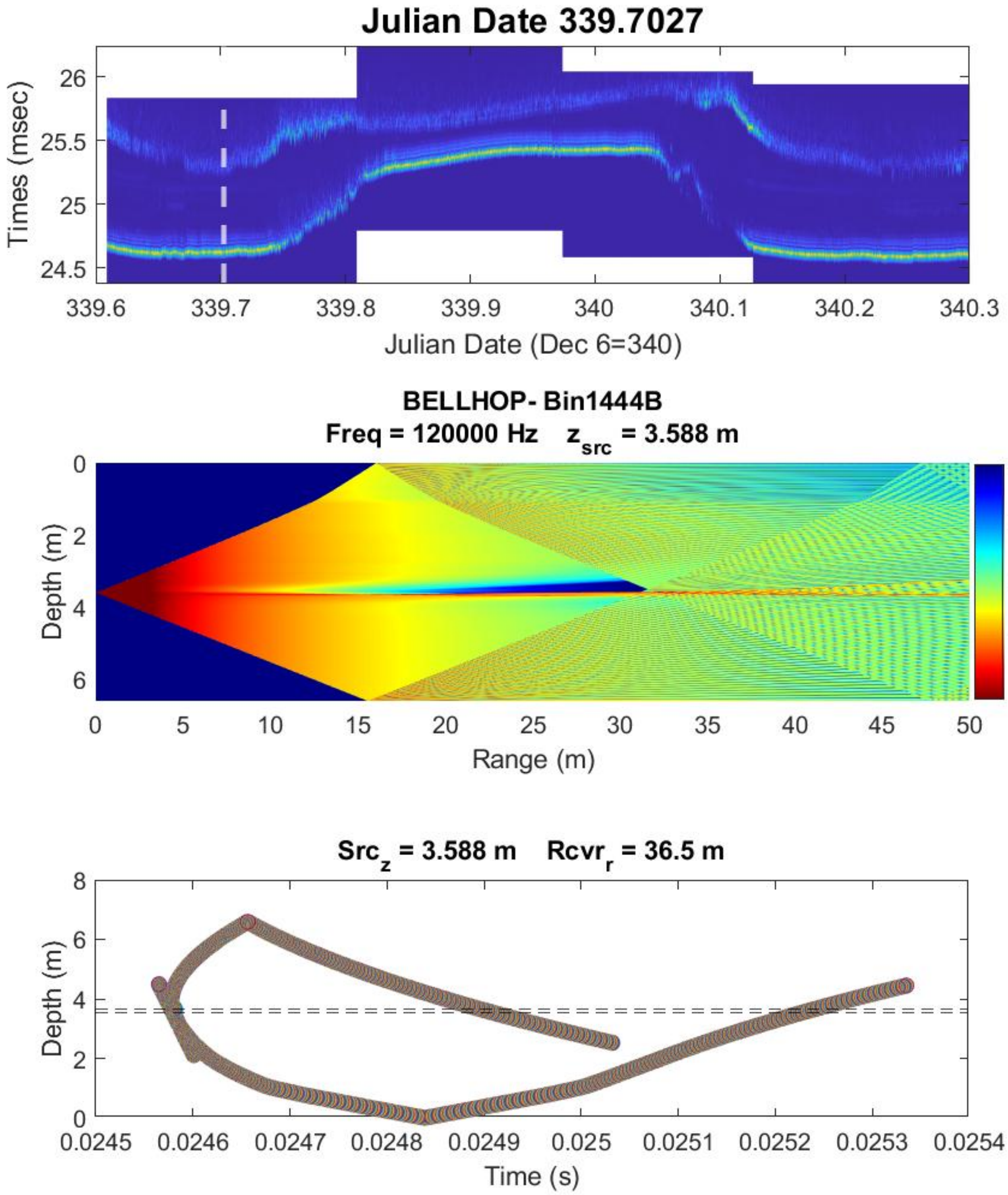

Figure 3.21: Plots for Julian date 339.7027. Top: recorded arrival time data from scintillation system. Middle: Transmission loss for main beam with of ±11°. Bottom: Modeled arrival times from BELLHOP.

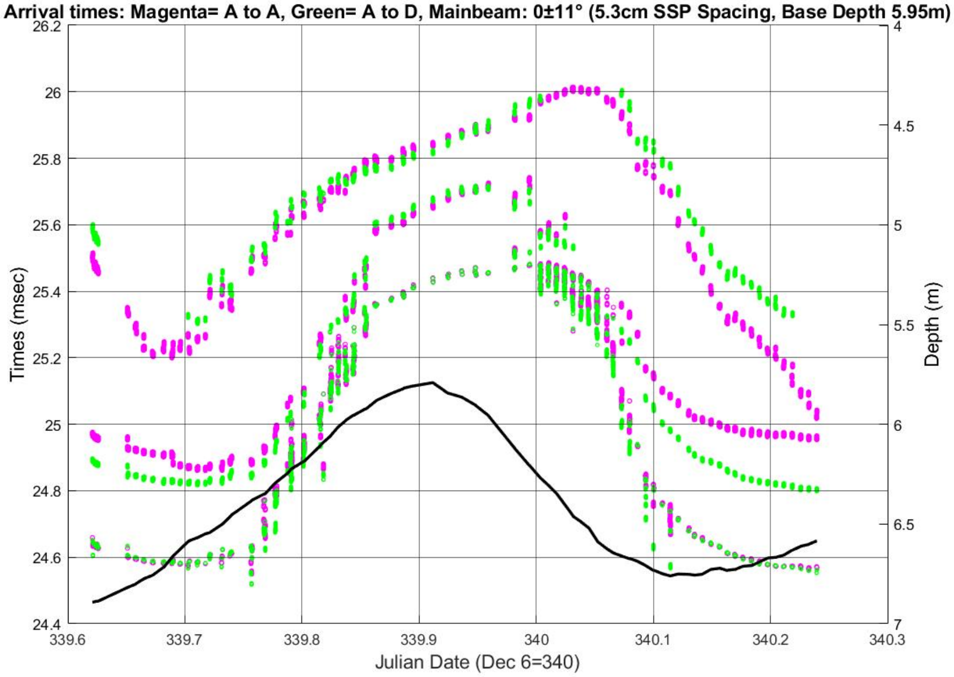

Figure 3.22: BELLHOP modeling comparing transducer A_M to A_R (magenta) vs A_M to D_R (green) arrival times with in-between depth profile (5.95 m Base) and stretched SSP (5.3 cm spacing). Expanded Main beam of 0±11°.

4 Conclusions

This study analyzed a highly stratified and dynamic estuary environment. The tripod scintillation system mounted on the floor of the river bed was very effective at recording time of arrival data with a high resolution. The system was able to observe the temperature and structural changes in the water column by measuring the arrival times between two tripods of transducers over multiple tidal cycles. Overall, the system performed well and demonstrated the advantage of using a fixed-mounted system for time of arrival measurements. A more detailed understanding and depiction of how highly stratified settings occur on a spatial and temporal timescale was seen. Some transducers ceased operating throughout the course of the week due to the volume of wiring. This should be modified in future designs to better manage the cabling under projected high current.

BELLHOP was used to model the environment from available data. Multiple modeling runs were conducted with adjustments to parameters. The modeling runs were then combined into a time series to be able to show the temporal changes to the dynamic estuary environment. The modeling was then compared to the arrival timings of the collected data, which fit pretty well despite some of the model's assumptions and simplifications. This validated that BELLHOP and ray tracing can be used quite accurately to model even a dynamic problem with a challenging environment such as a highly stratified water column that quickly changes between salt and fresh water.

Further experiments would need to be done to better constrain the problem. Unfortunately, no co-located CTD data were available, and even a high fidelity depth measurement, such as a surface-looking ADCP put on the tripods, would have been extremely beneficial. This would allow for better model comparison to known parameters and thus a deeper, more specific analysis can be performed. Specifically, do shear instabilities described by Fincke[1] have a significant impact on the arrival time and structure, such as broadening the transmitted beam via scattering. It would be useful to have

---

[1] Fincke, "Quantification of the spatial and temporal evolution of stratifed shear instabilities at high Reynolds number using quantitative acoustic scattering techniques".

laboratory measurements of the width of the main beam to help determine this. Furthermore, it is plausible that the shear instabilities caused further scattering, broadening the beam. Additionally, BELLHOP does allow for bottom topography, as well as range dependent environmental parameters. Collecting this data as part of a future validation would be beneficial. It would be fascinating to see how accurate such a thorough model to be recorded data is without the need to modify input settings.

The ability to have accurate models that forgo the need for expensive and costly field experiments is extremely advantageous. It is foreseeable that this type of modeling could be used to either install or use already existing remote monitoring stations to track acoustical changes in varying timescales from simple CTD data. This, together with other remote data from moored stations, could aid in other acoustic monitoring problems and be used in research ranging from climate monitoring and patterns such as those observed in the Arctic by Zeh and others.[2] Additionally, it would be very useful and cost-effective in designing or implementing acoustic communication by being able to model and predict dynamic environments. Covert communications, as explored by Walree and others, may be required for military operations if specific environmental factors might be used or avoided.[3]

---

[2] Zeh *et al.*, "Model-data comparison of sound propagation in a glacierized fjord with a simulated brash ice surface".

[3] Walree *et al.*, "UUV Covert Acoustic Communications".

Bibliography

1. *Acoustic Toolbox* Ocean Acoustics Library. http://oalib.hlsresearch.com/AcousticsToolbox/.
2. Fincke, J. R. *Quantification of the spatial and temporal evolution of stratifed shear instabilities at high Reynolds number using quantitative acoustic scattering techniques* MA thesis (Massachusetts Institute of Technology and Woods Hole Oceanographic Institution, 2015).
3. Freeman, S. E., Emokpae, L. E., and Edelmann, G. F. *High-frequency, highly directional short-range underwater acoustic communications* in *OCEANS 2015 - MTS/IEEE Washington* IEEE, Washington, DC, 2015. doi: 10.23919/OCEANS.2015.7401898.
4. Jensen, F. B., Kuperman, W. A., Porter, M. B., and Schmidt, H. *Computational Ocean Acoustics* 2nd ed. Springer, New York, NY, 2011.
5. Lavery, A. *High-Frequency Acoustic Propagation in a Shallow, Energetic, Salt-Wedge Estuary* Woods Hole Oceanographic Institution. 2015.
6. Menn, M. L. *Instrumentation and Metrology in Oceanography* John Wiley & Sons, Hoboken, NJ, 2012.
7. *NOAA Tides and Currents* https://tidesandcurrents.noaa.gov. Accessed: 2022-06-12.
8. Porter, M. B. *The BELLHOP Manual and User's Guide* Heat, Light, and Sound Research, Inc. La Jolla, CA, 2011.
9. Porter, M. B. and Liu, Y.-C. *Finite-Element Ray Tracing* technical report. Theoretical and Computational Acoustics - Vol 2 (New Jersey Institute of Technology, Newark, NJ, 1994).
10. Walree, P., Ludwig, T., Solberg, C., Sangfelt, E., Laine, A., Bertolotto, G., Ishøy, A., Tno, A., Fincantieri, F., Cantieri, and Italiani, N. UUV Covert Acoustic Communications, 2022.

11. Zeh, M. C., Ballard, M. S., Glowacki, O., Deane, G. B., and Wilson, P. S. Model-data comparison of sound propagation in a glacierized fjord with a simulated brash ice surface. *The Journal of the Acoustical Society of America* **151.** doi: 10.1121/10.0010046, 2022.

A Additional Figures

This section contains additional figures.

A.1 Echo Sounder from Backscatter Array

Figures A.1 to A.4 are additional plots of the echo sounder from the backscatter array. Time markers, vertical dotted white lines, are seen in the arrival times plot at the top of each for reference.

A.2 BELLHOP Shade TL and Arrival Times

Here are several graphs of the environment during the first three tidal cycles. These are shown in chronological sequence, with the time of each incident listed as the title and denoted as a vertical dotted white line on the recorded scintillation data.

A.2.1 Beam: ±8°, 6.27m Base Depth & 5.5cm SSP Spacing

All figures A.5 through A.20 are plotted using the SSP profile fitted to the backscatter data with the 5.5cm SSP spacing and a main beam of 0±8°. Note: The direction of the depth on the y-axis between the shade TL and the arrival times plots are reverse.

A.2.2 Beam: ±11°, 5.95m Base Depth & 5.3cm SSP Spacing

All figures A.21 through A.41 are plotted using the SSP profile fitted to the backscatter data with the 5.3cm SSP spacing and a main beam of 0±11°. Note: the direction of the depth on the y-axis between the shade TL and the arrival times plots are reverse.

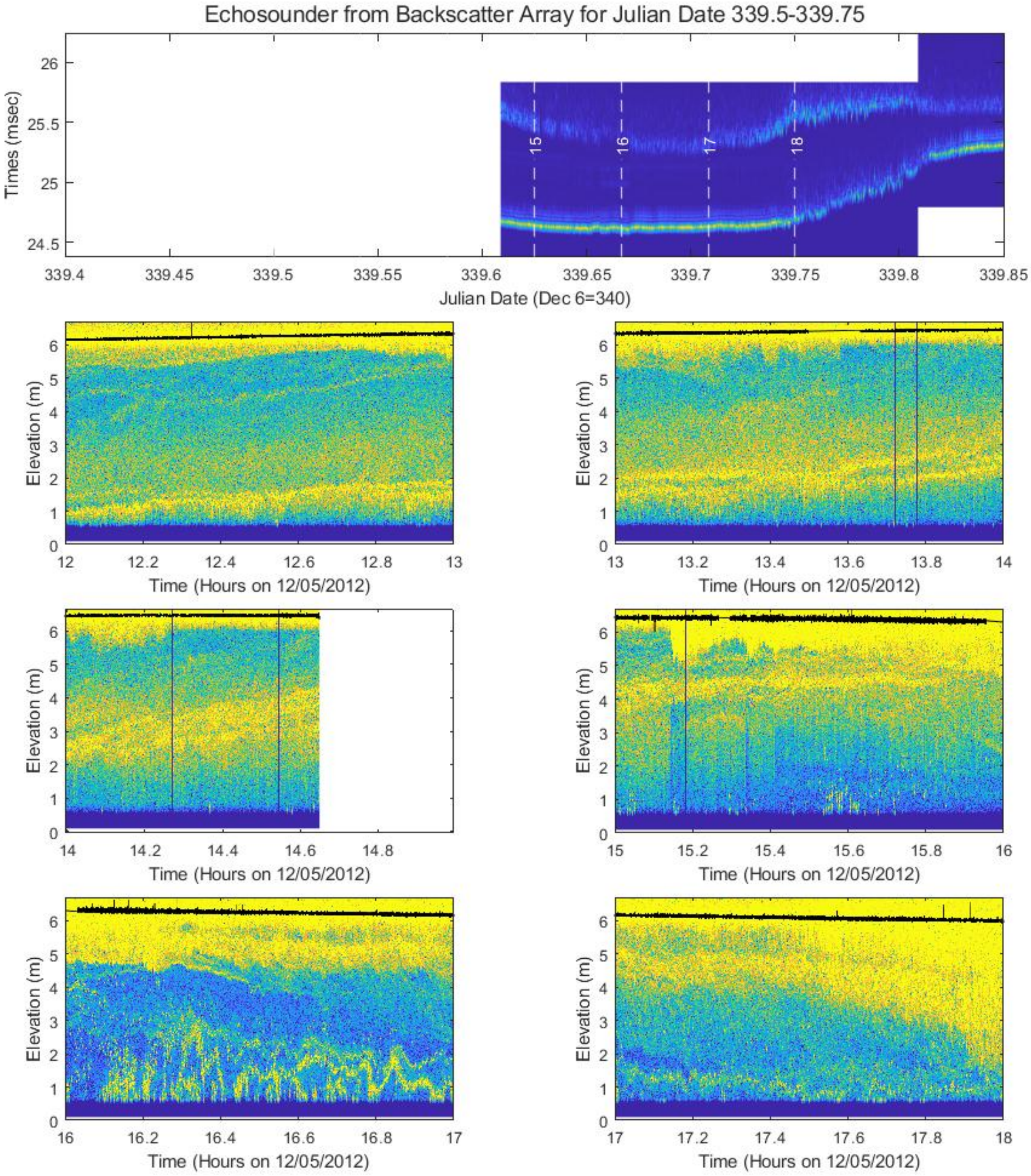

Figure A.1: Upward looking Echo sounder from backscatter array (75cm above river bed) shows variability in the water column over time (Julian Date 339.5-339.75). Black line shows surface of CT river.

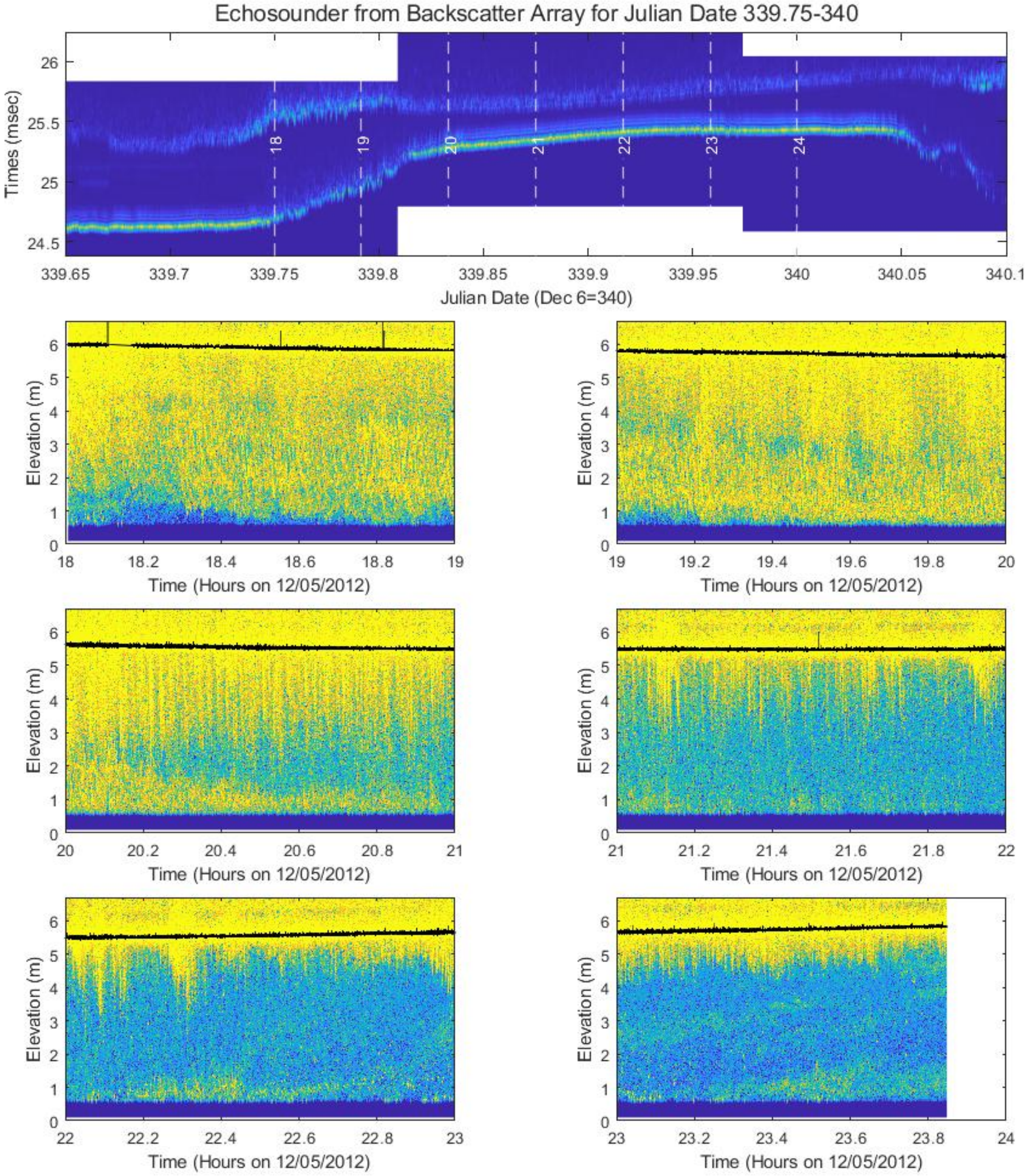

Figure A.2: Upward looking Echo sounder from backscatter array (75cm above river bed) shows variability in the water column over time (Julian Date 339.75-340). Black line shows surface of CT river.

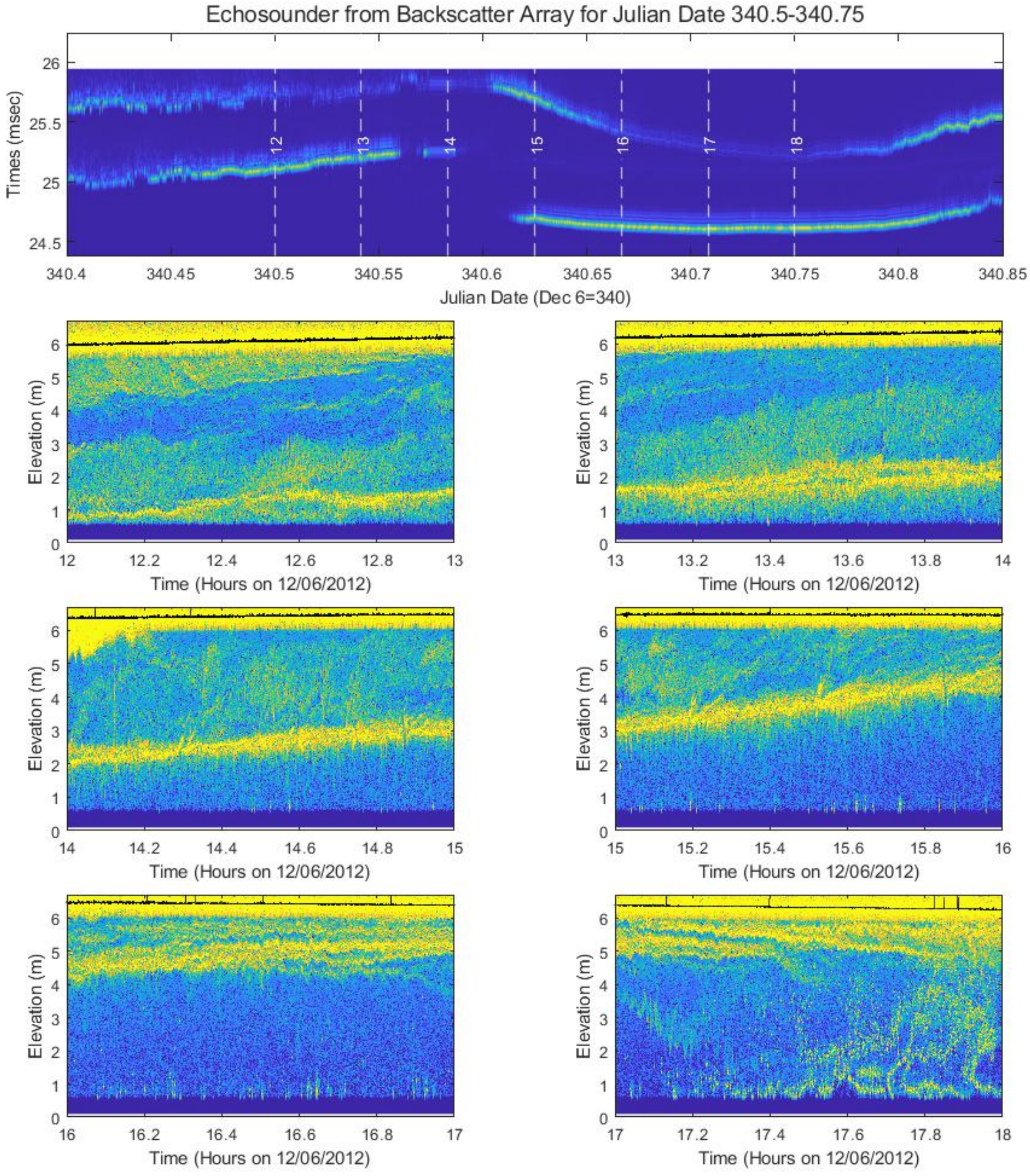

Figure A.3: Upward looking Echo sounder from backscatter array (75cm above river bed) shows variability in the water column over time (Julian Date 340.5-340.75). Black line shows surface of CT river.

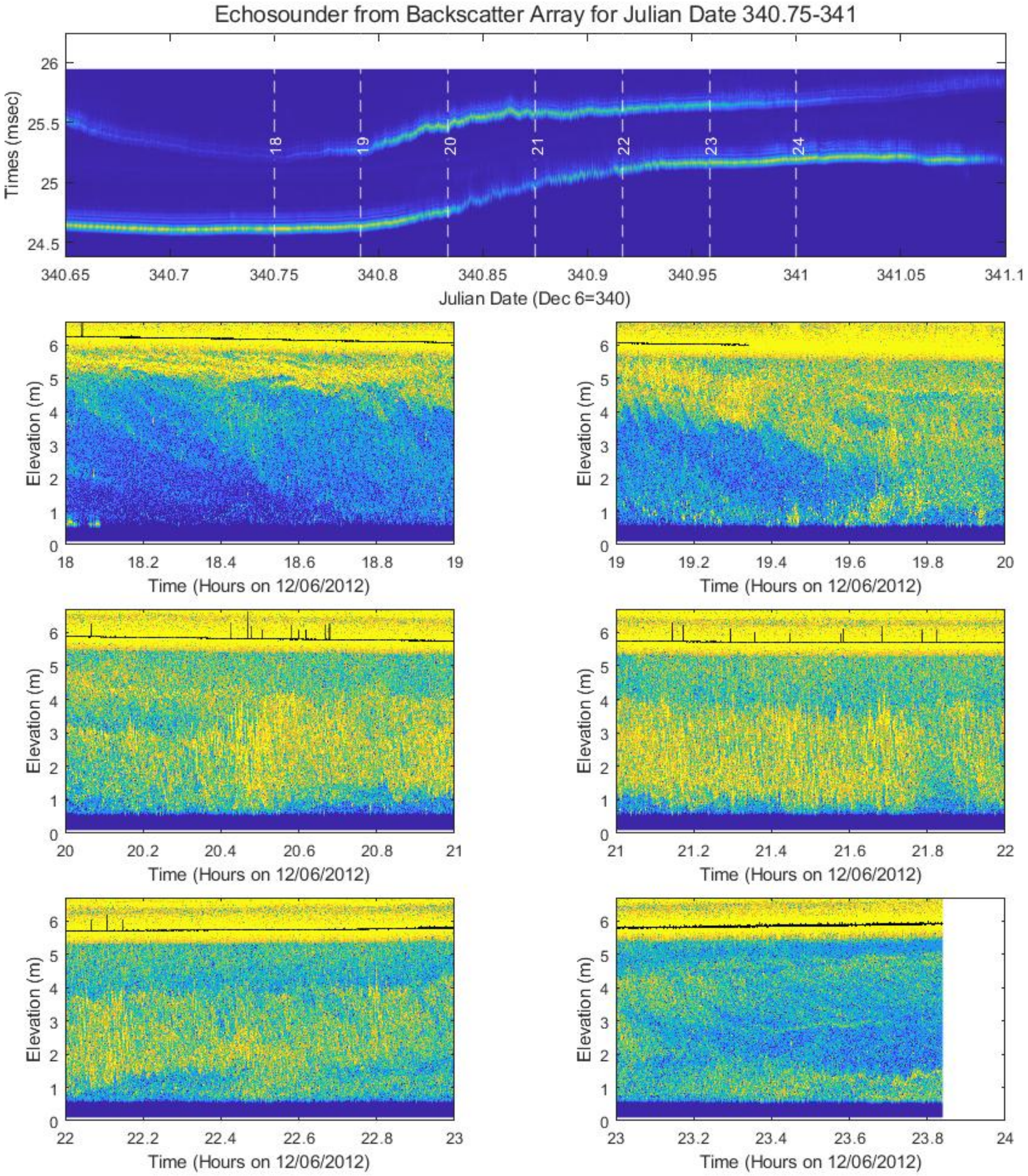

Figure A.4: Upward looking Echo sounder from backscatter array (75cm above river bed) shows variability in the water column over time (Julian Date 340.75-341). Black line shows surface of CT river.

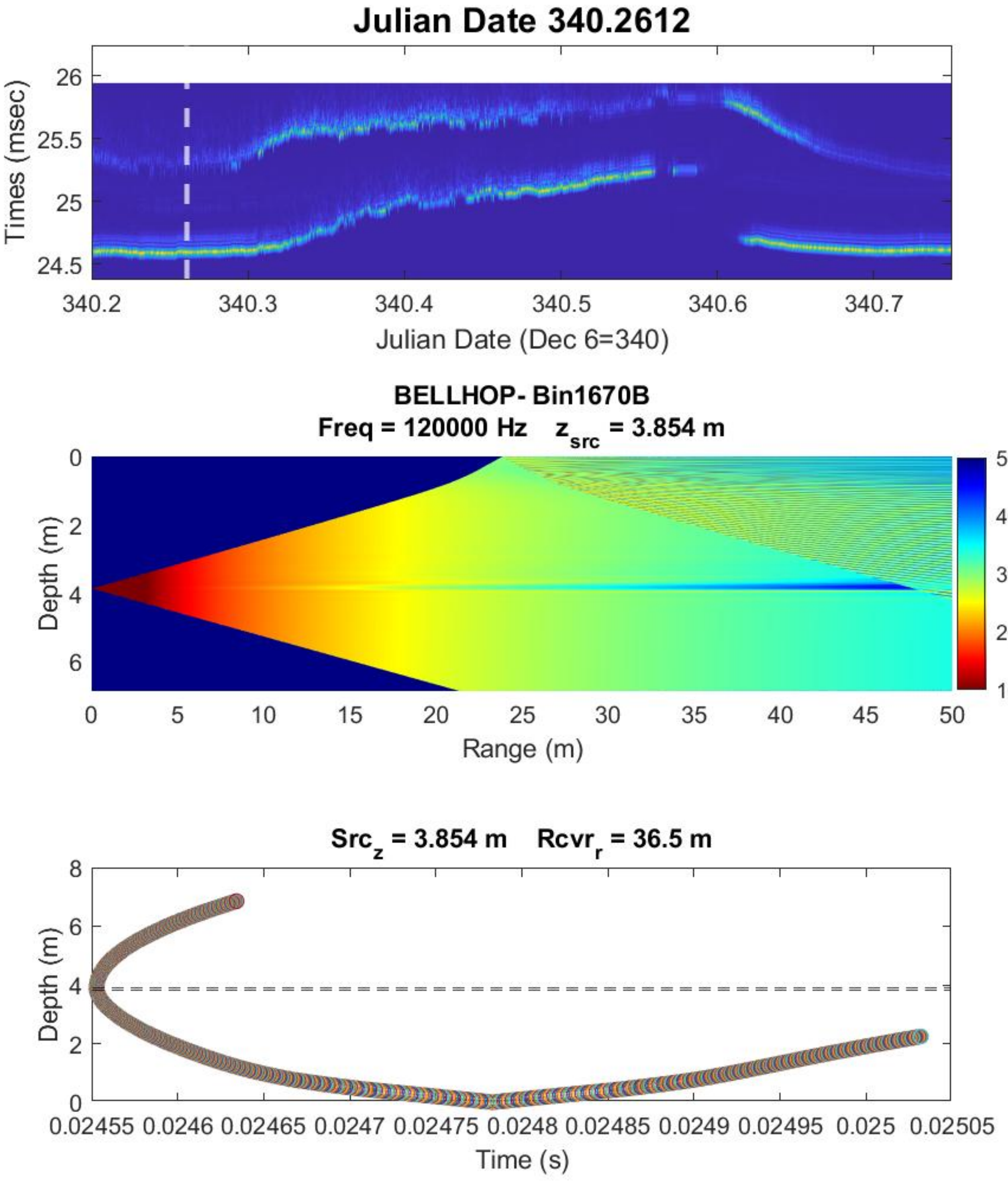

Figure A.5: Plots for Julian date 340.2612. Top: recorded arrival time data from scintillation system. Middle: Transmission loss for main beam with of ±8°. Bottom: Modeled arrival times from BELLHOP.

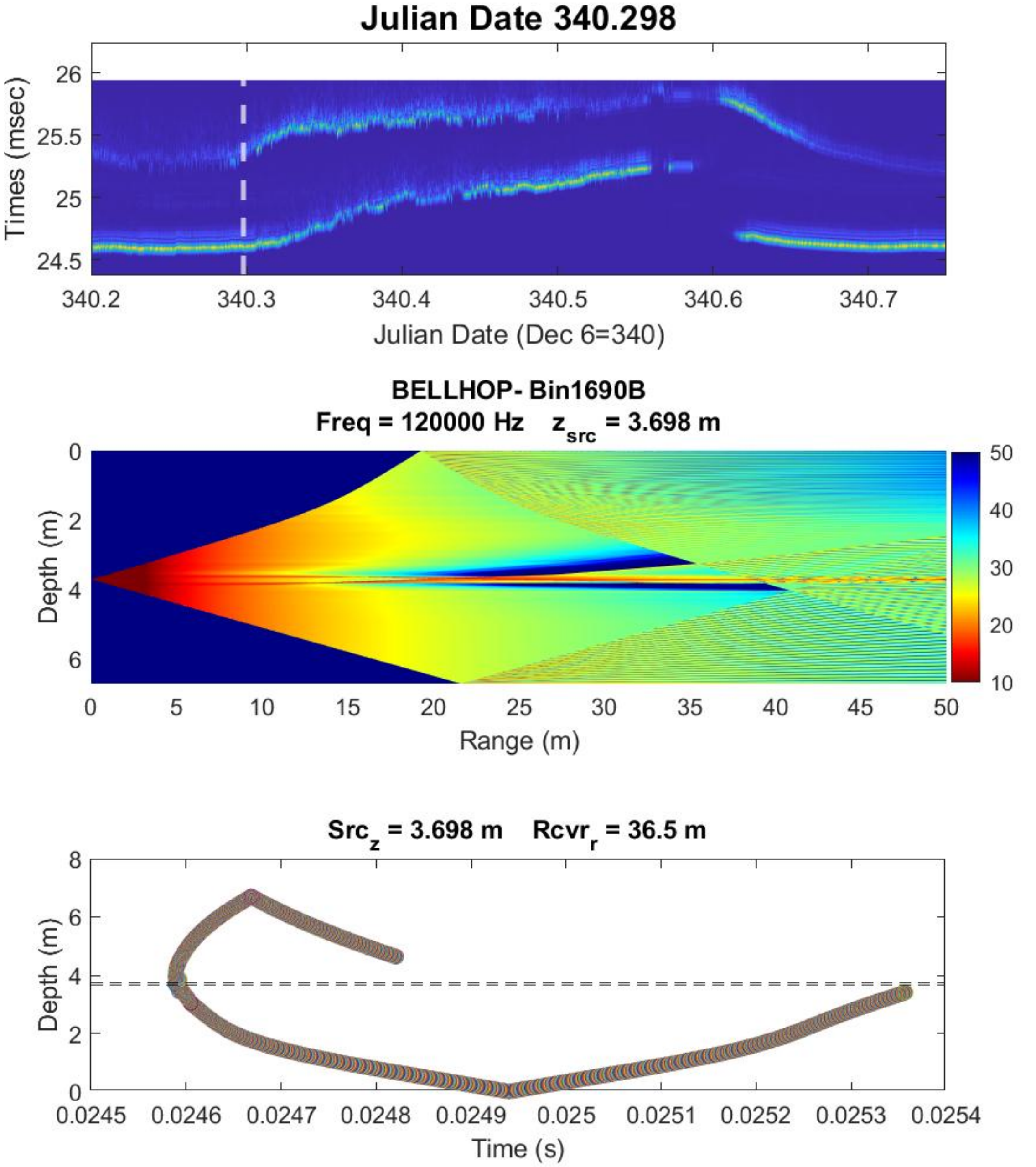

Figure A.6: Plots for Julian date 340.298. Top: Recorded arrival time data from scintillation system. Middle: Transmission loss for main beam with of ±8°. Bottom: Modeled arrival times from BELLHOP.

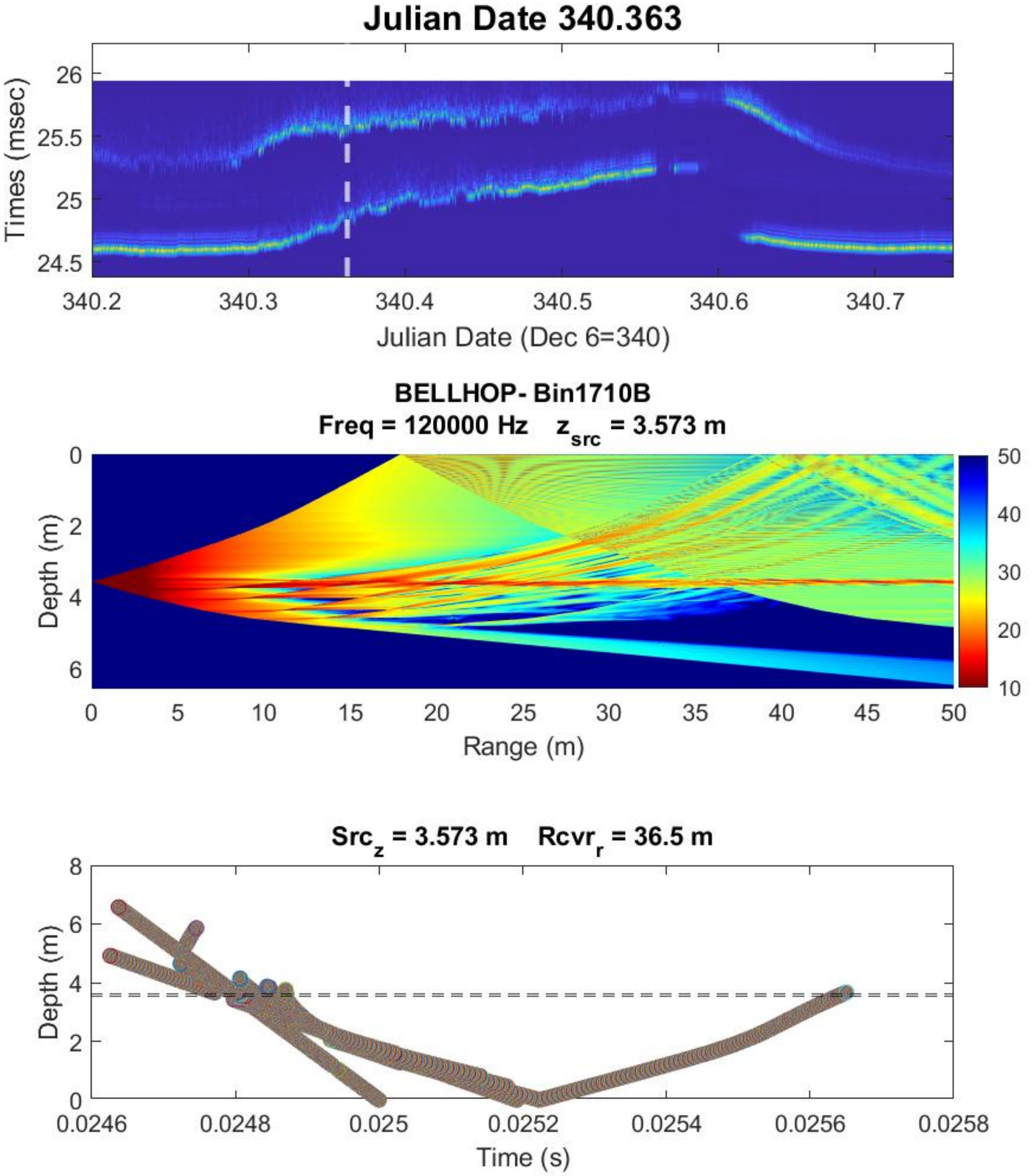

Figure A.7: Plots for Julian date 340.363. Top: Recorded arrival time data from scintillation system. Middle: Transmission loss for main beam with of ±8°. Bottom: Modeled arrival times from BELLHOP.

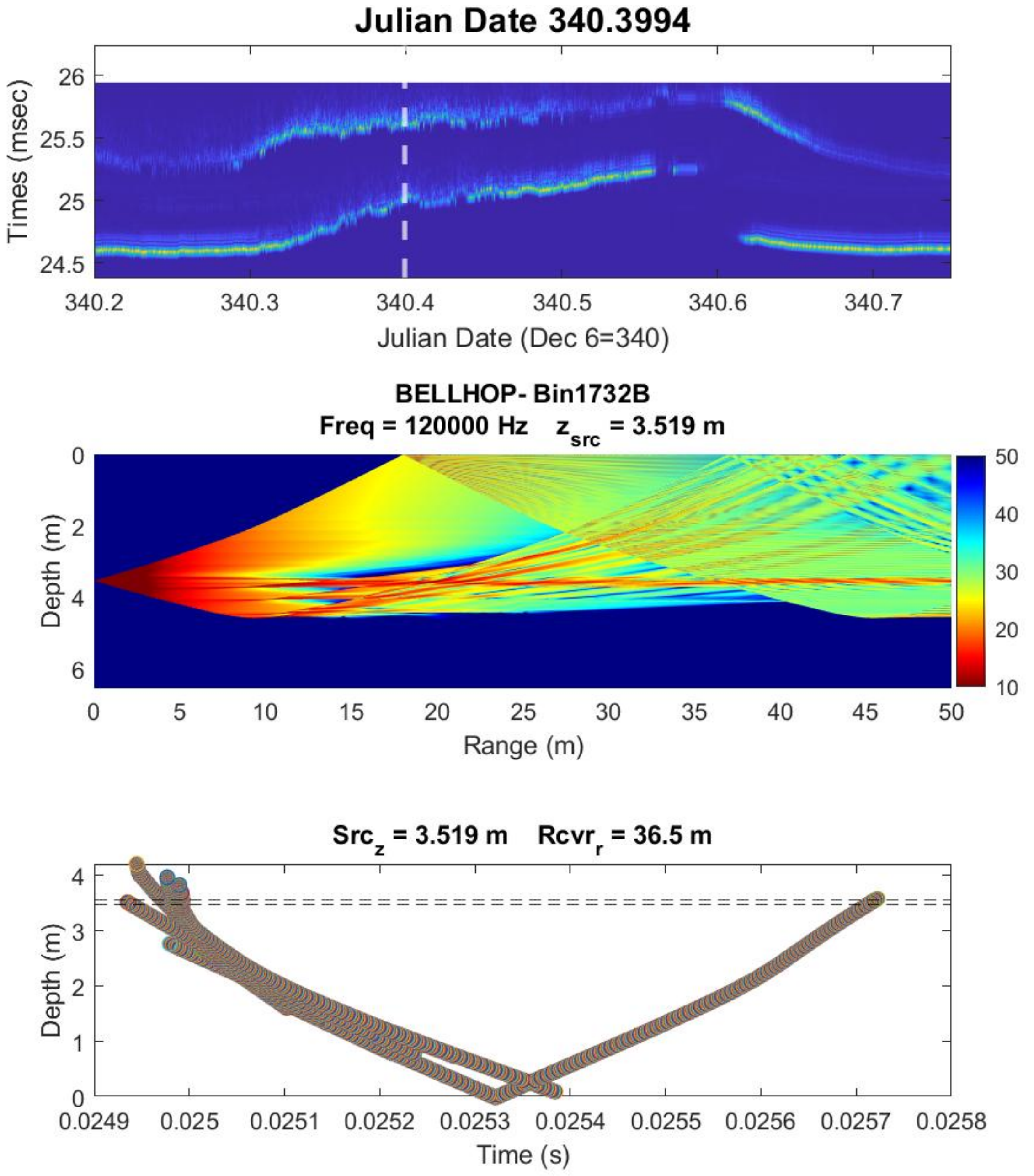

Figure A.8: Plots for Julian date 340.3994. Top: Recorded arrival time data from scintillation system. Middle: Transmission loss for main beam with of ±8°. Bottom: Modeled arrival times from BELLHOP.

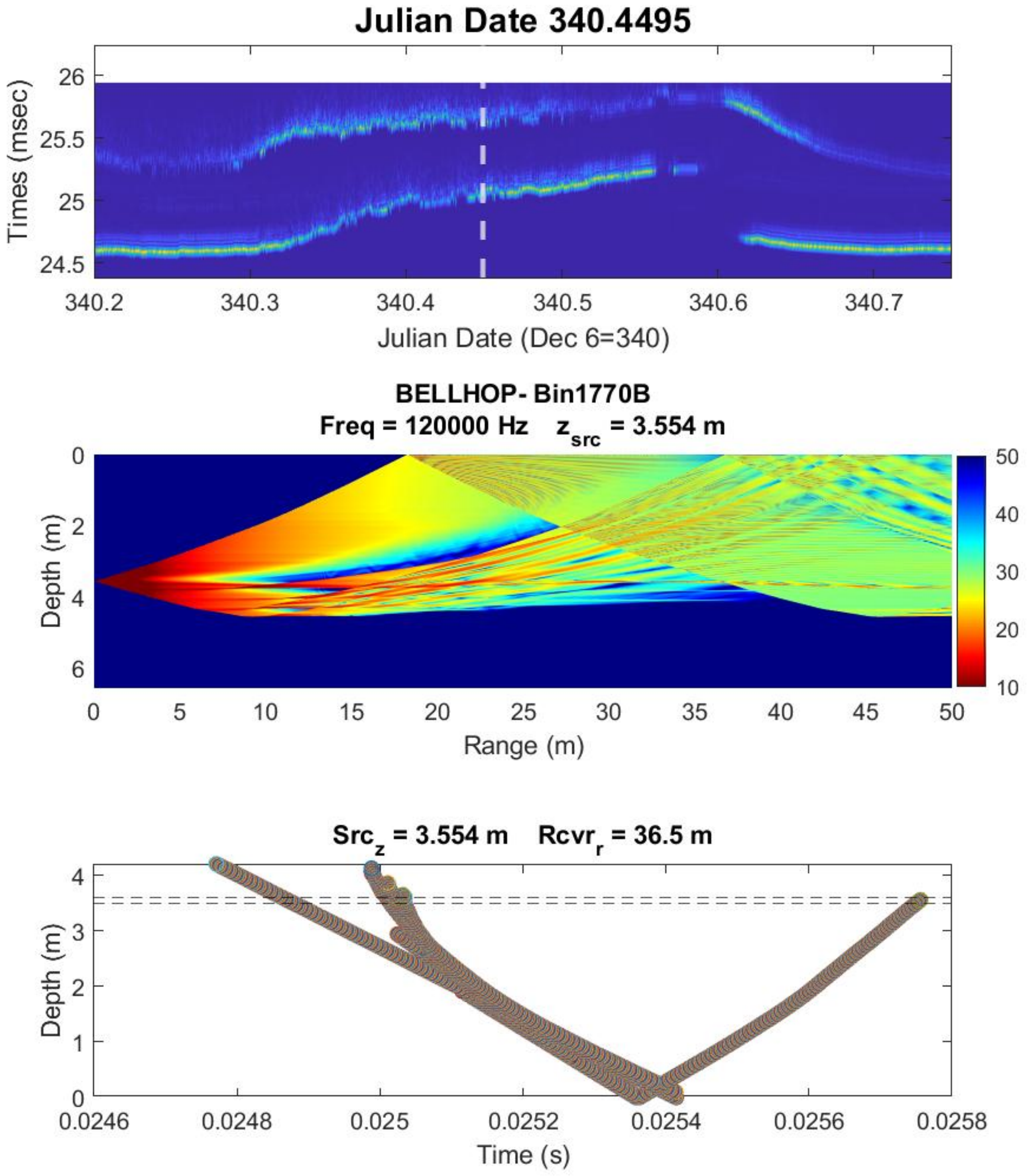

Figure A.9: Plots for Julian date 340.4495. Top: Recorded arrival time data from scintillation system. Middle: Transmission loss for main beam with of ±8°. Bottom: Modeled arrival times from BELLHOP.

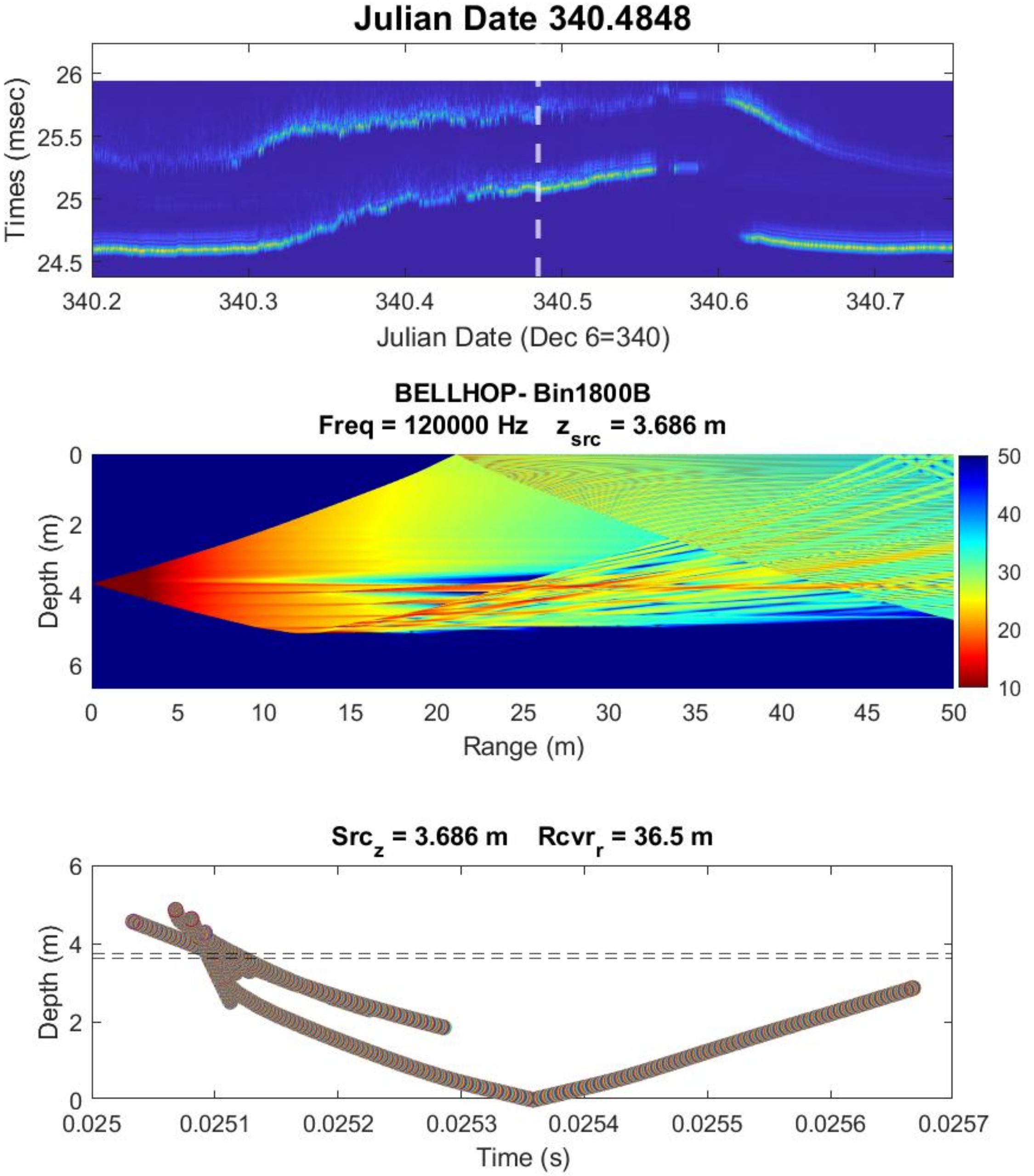

Figure A.10: Plots for Julian date 340.4848. Top: Recorded arrival time data from scintillation system. Middle: Transmission loss for main beam with of ±8°. Bottom: Modeled arrival times from BELLHOP.

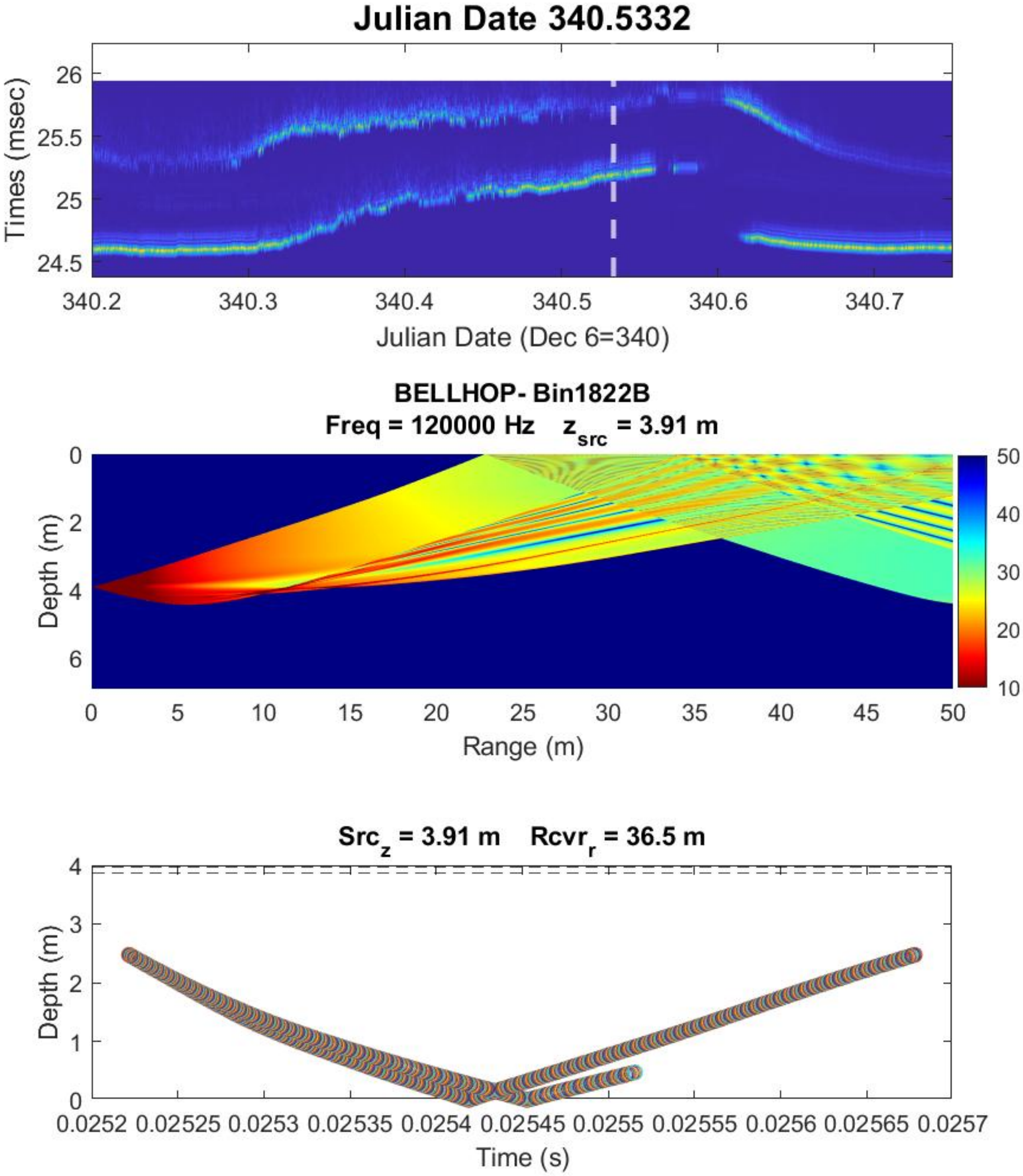

Figure A.11: Plots for Julian date 340.5332. Top: Recorded arrival time data from scintillation system. Middle: Transmission loss for main beam with of ±8°. Bottom: Modeled arrival times from BELLHOP.

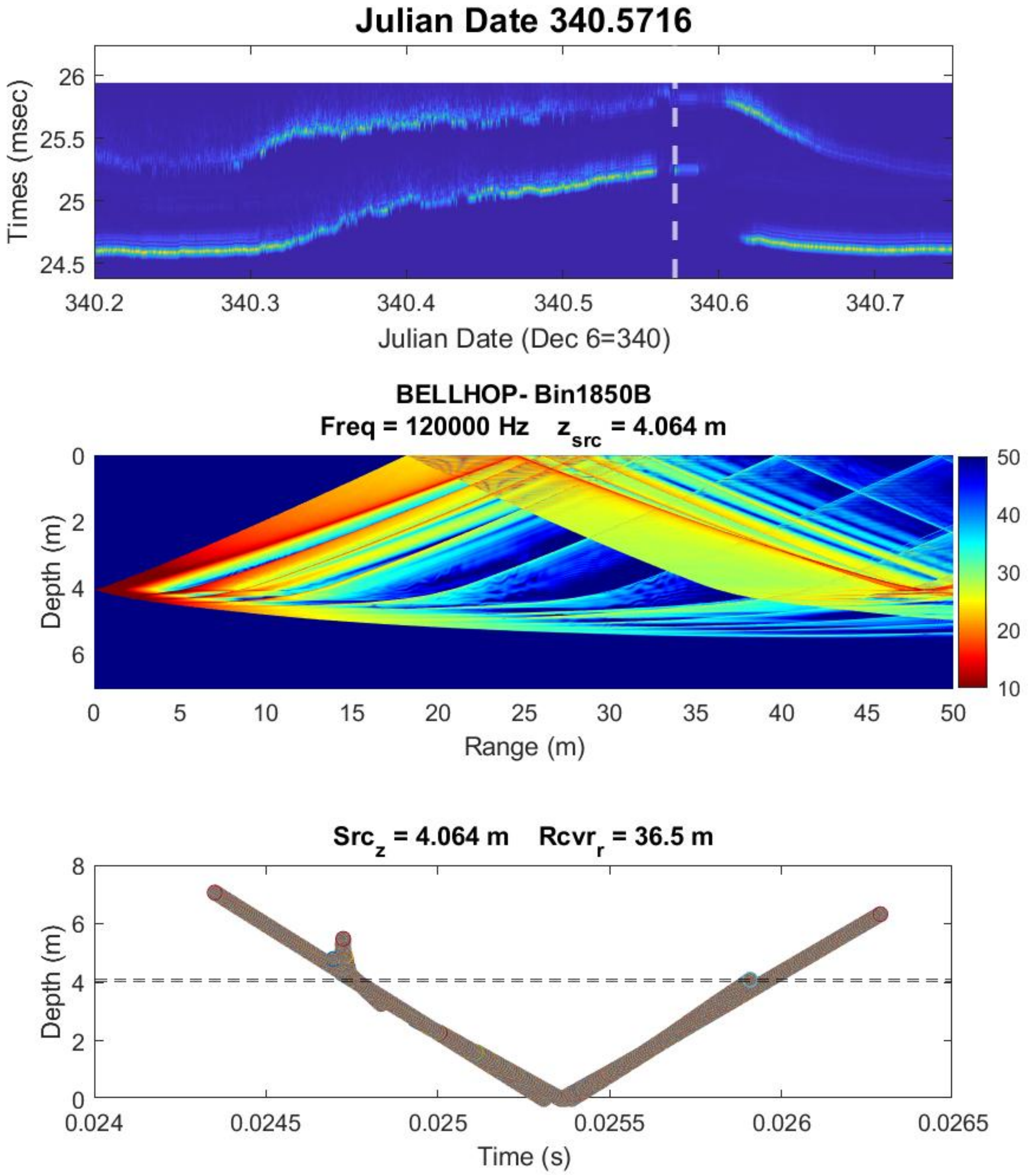

Figure A.12: Plots for Julian date 340.5716. Top: Recorded arrival time data from scintillation system. Middle: Transmission loss for main beam with of ±8°. Bottom: Modeled arrival times from BELLHOP.

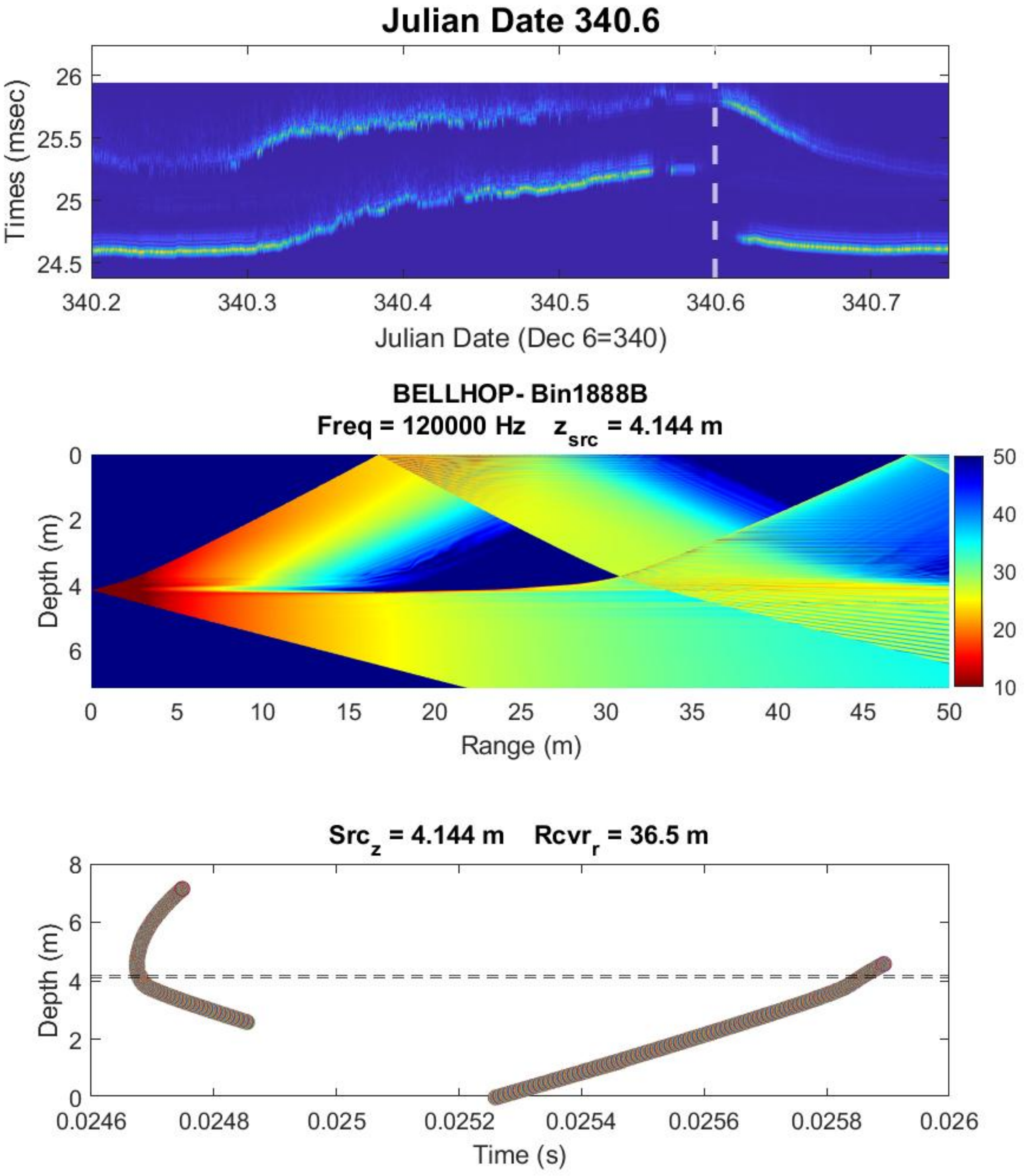

Figure A.13: Plots for Julian date 340.6. Top: Recorded arrival time data from scintillation system. Middle: Transmission loss for main beam with of ±8°. Bottom: Modeled arrival times from BELLHOP.

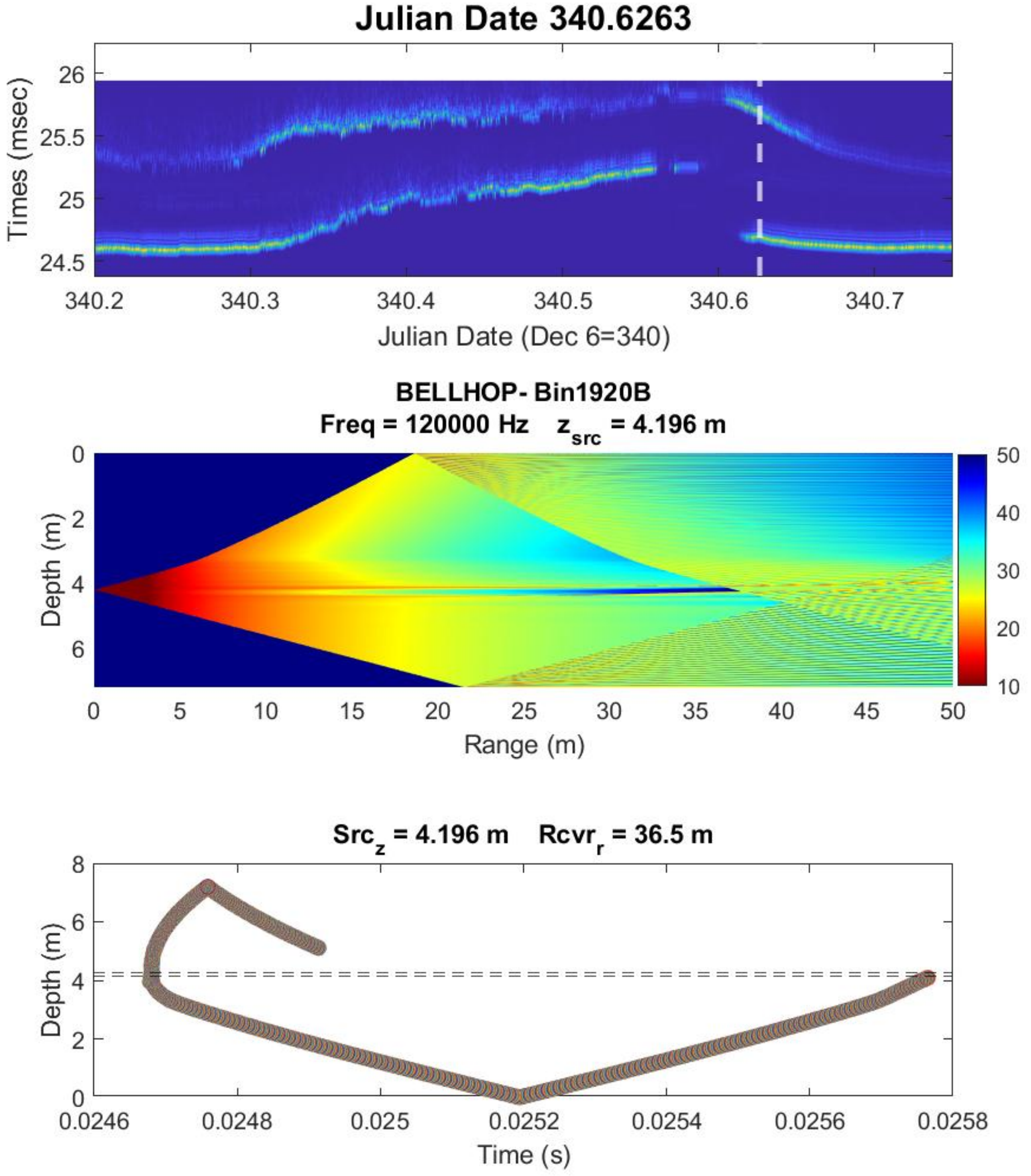

Figure A.14: Plots for Julian date 340.6263. Top: Recorded arrival time data from scintillation system. Middle: Transmission loss for main beam with of ±8°. Bottom: Modeled arrival times from BELLHOP.

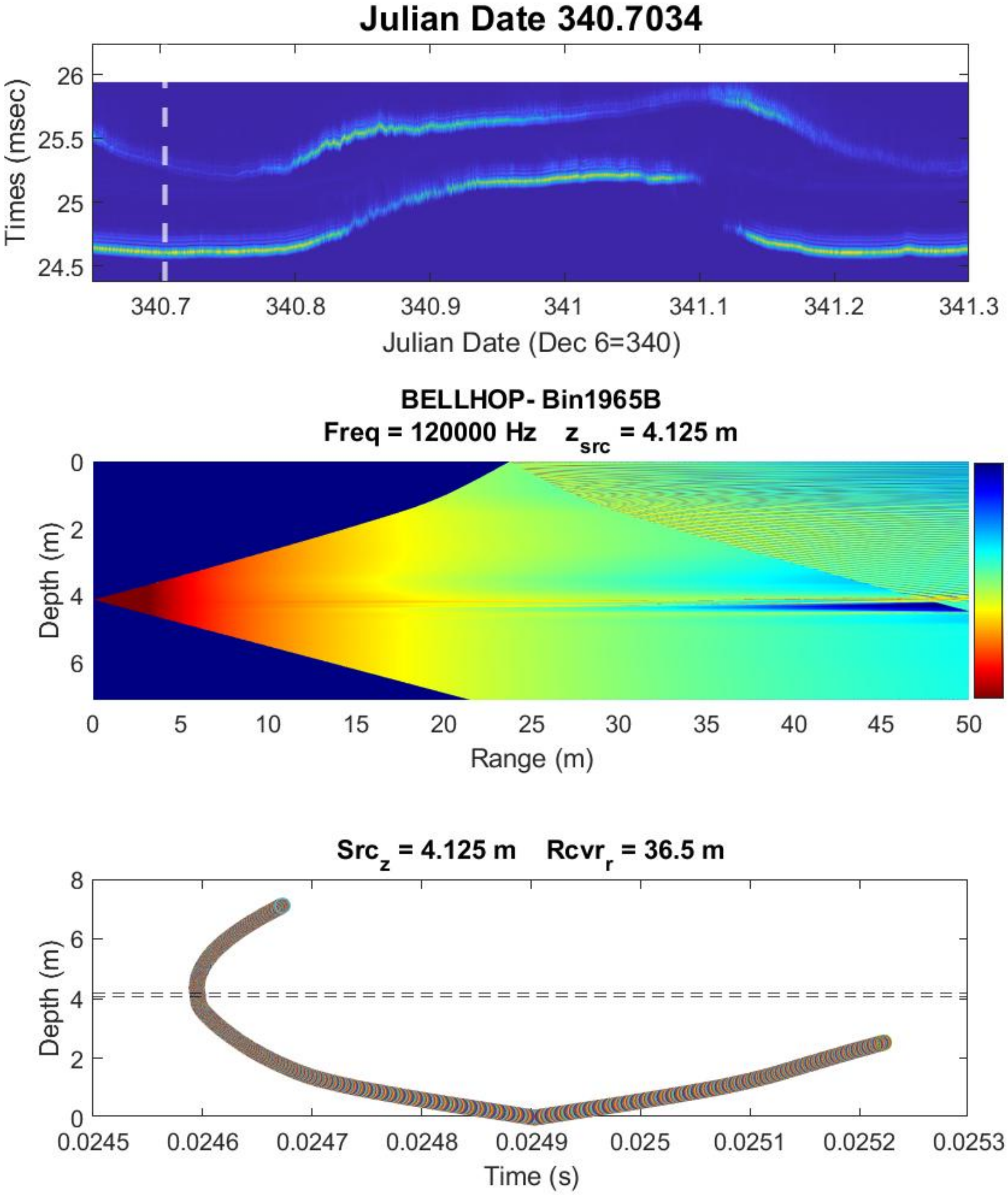

Figure A.15: Plots for Julian date 340.7037. Top: Recorded arrival time data from scintillation system. Middle: Transmission loss for main beam with of ±8°. Bottom: Modeled arrival times from BELLHOP.

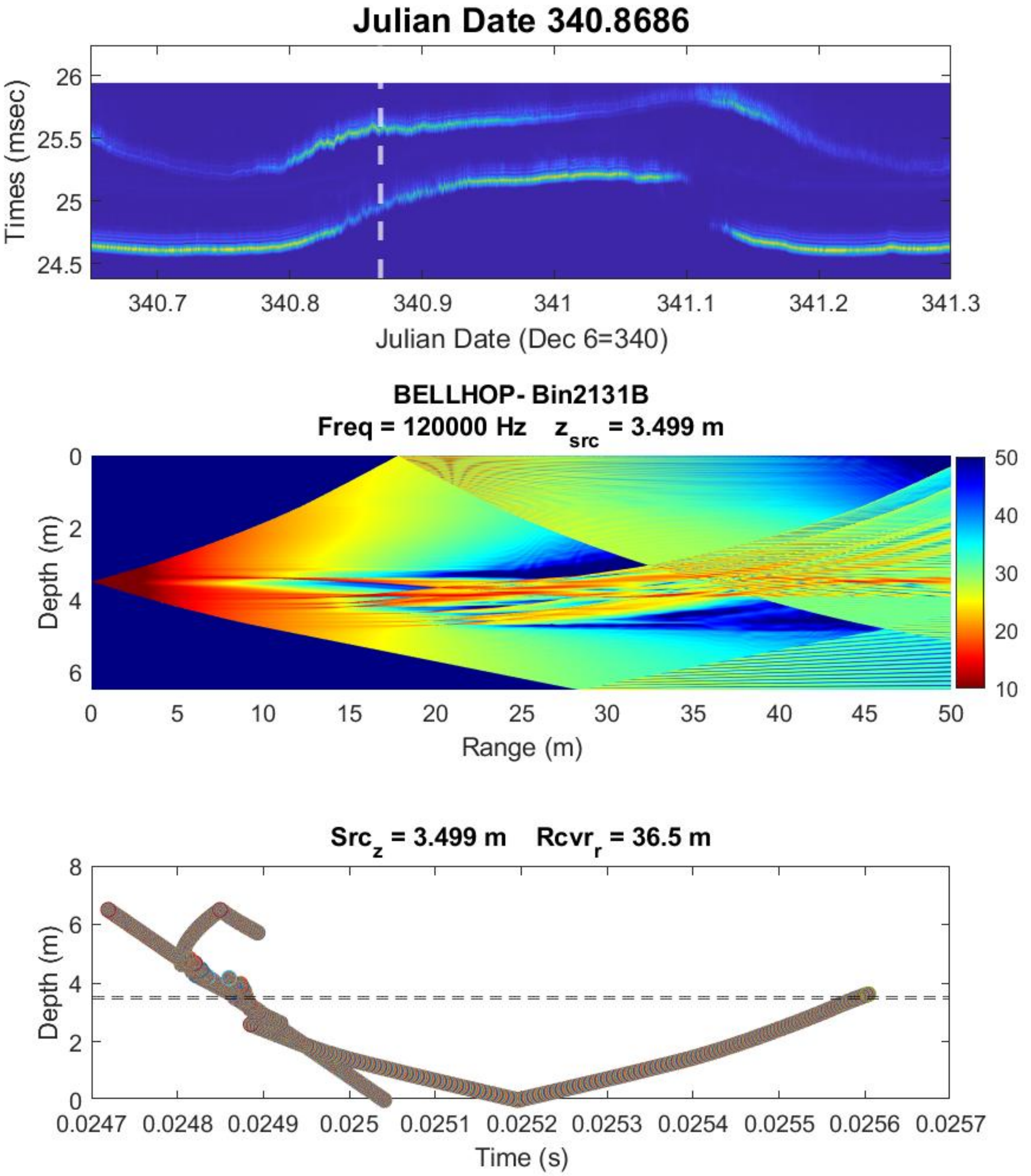

Figure A.16: Plots for Julian date 340.8686. Top: Recorded arrival time data from scintillation system. Middle: Transmission loss for main beam with of ±8°. Bottom: Modeled arrival times from BELLHOP.

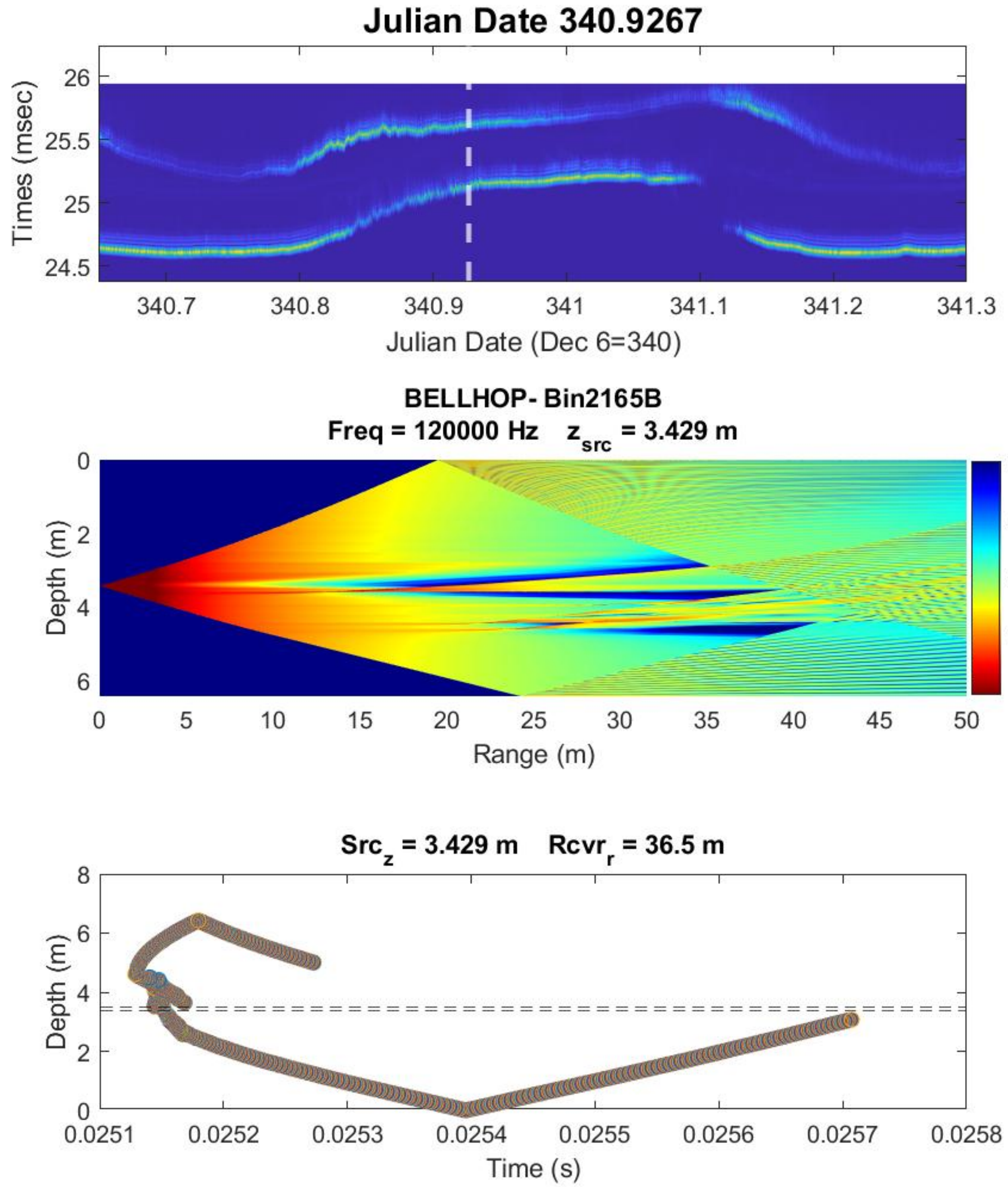

Figure A.17: Plots for Julian date 340.9267. Top: Recorded arrival time data from scintillation system. Middle: Transmission loss for main beam with of ±8°. Bottom: Modeled arrival times from BELLHOP.

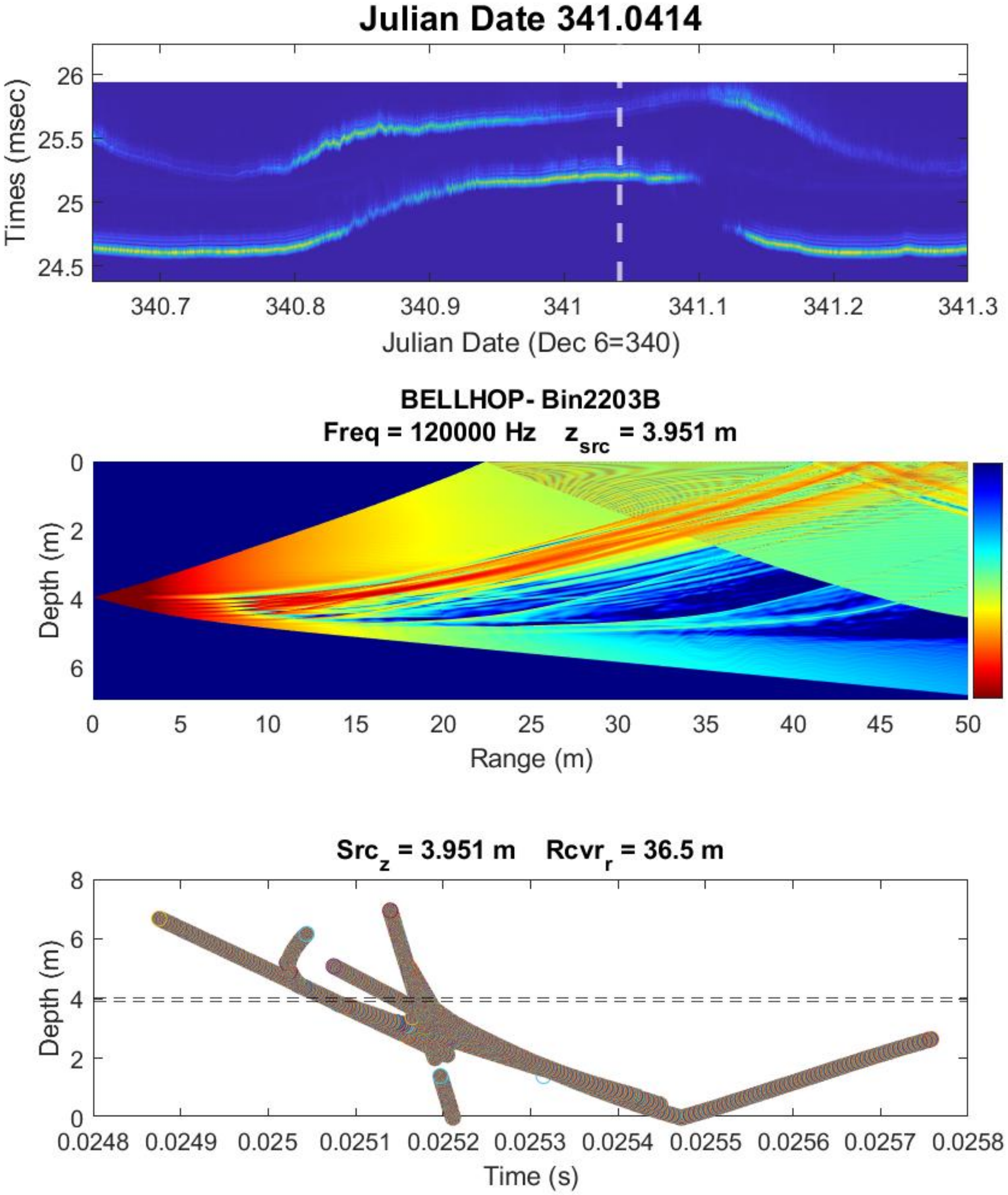

Figure A.18: Plots for Julian date 341.0414. Top: Recorded arrival time data from scintillation system. Middle: Transmission loss for main beam with of ±8°. Bottom: Modeled arrival times from BELLHOP.

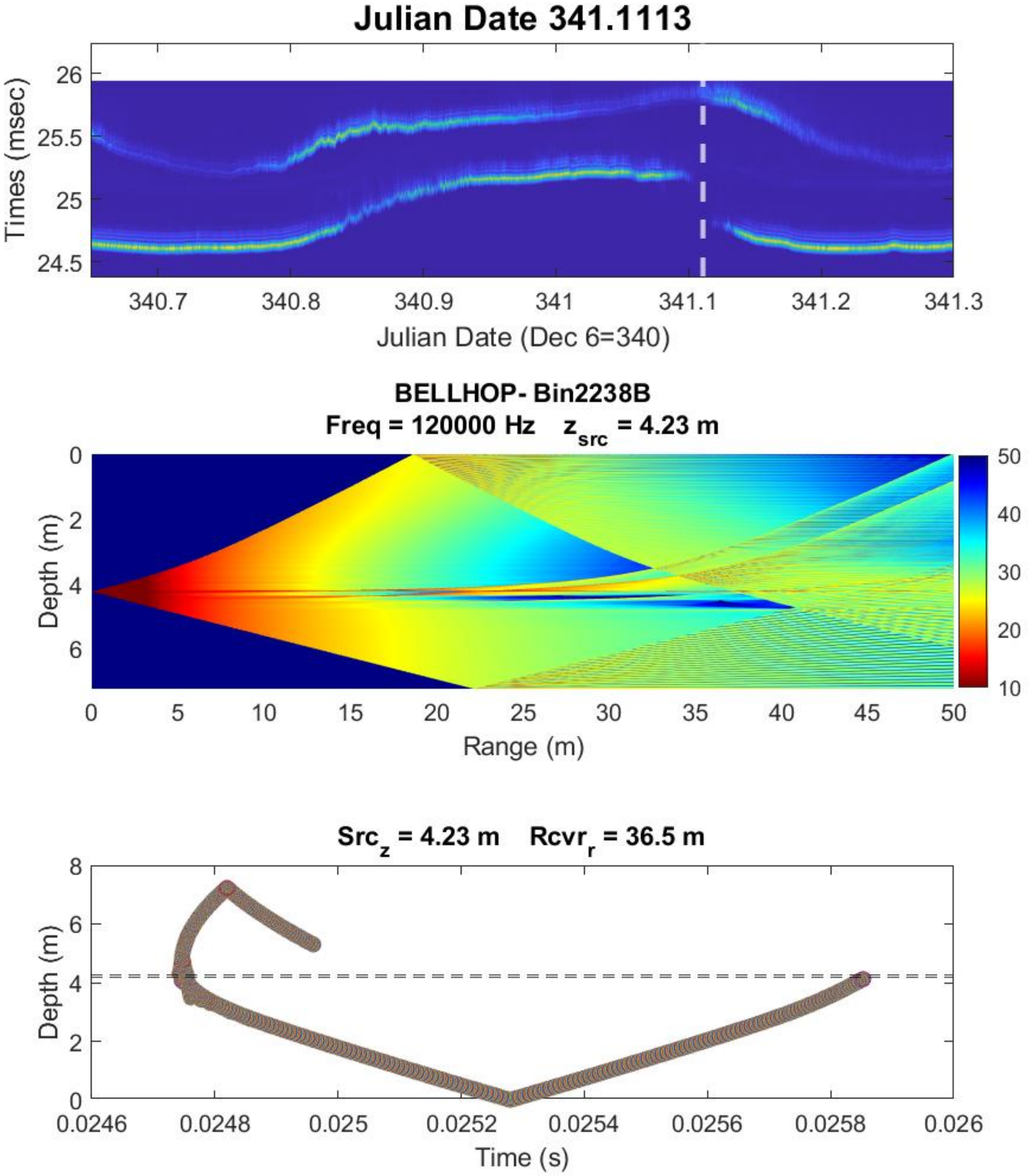

Figure A.19: Plots for Julian date 341.1113. Top: Recorded arrival time data from scintillation system. Middle: Transmission loss for main beam with of ±8°. Bottom: Modeled arrival times from BELLHOP.

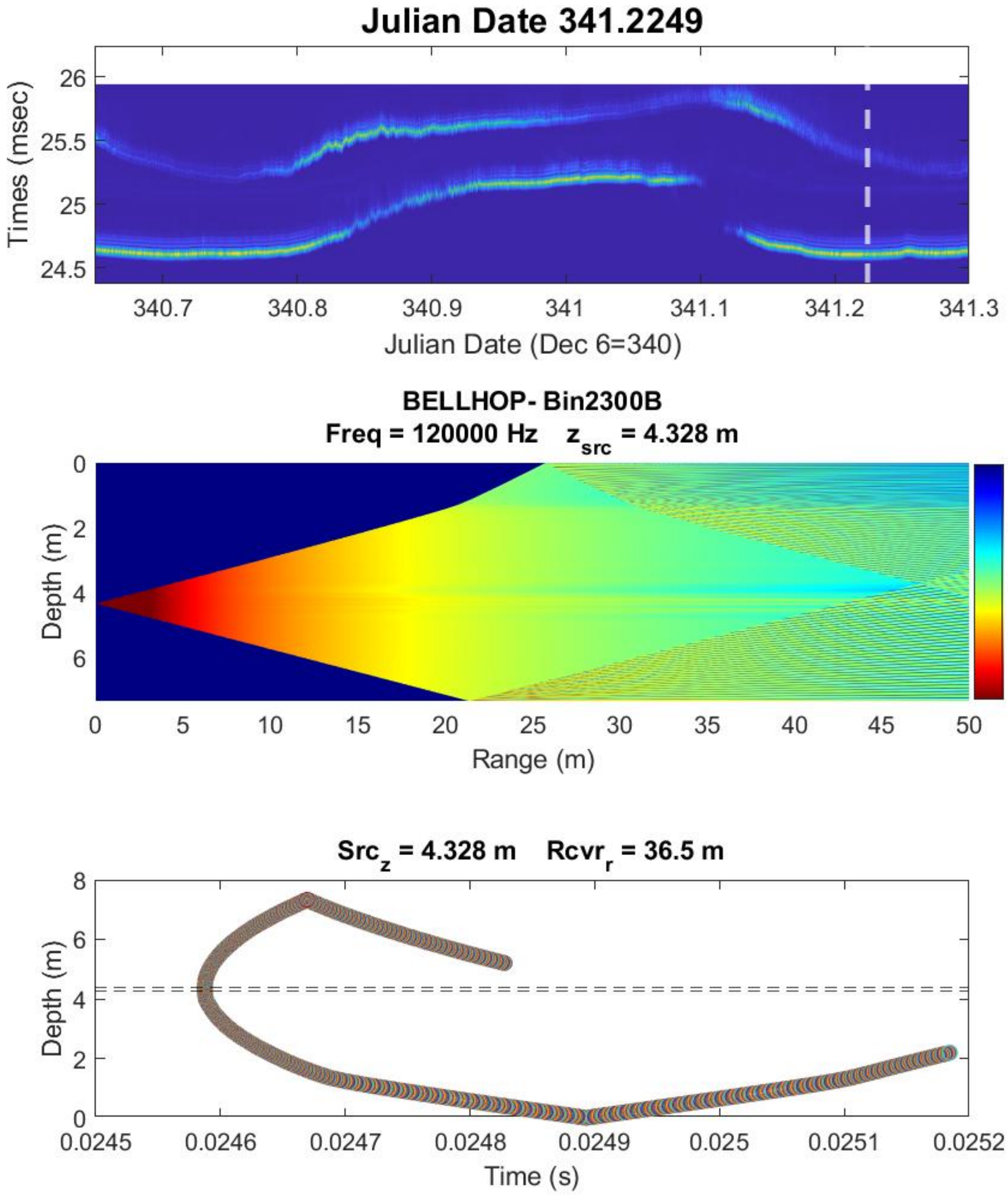

Figure A.20: Plots for Julian date 341.2249. Top: Recorded arrival time data from scintillation system. Middle: Transmission loss for main beam with of ±8°. Bottom: Modeled arrival times from BELLHOP.

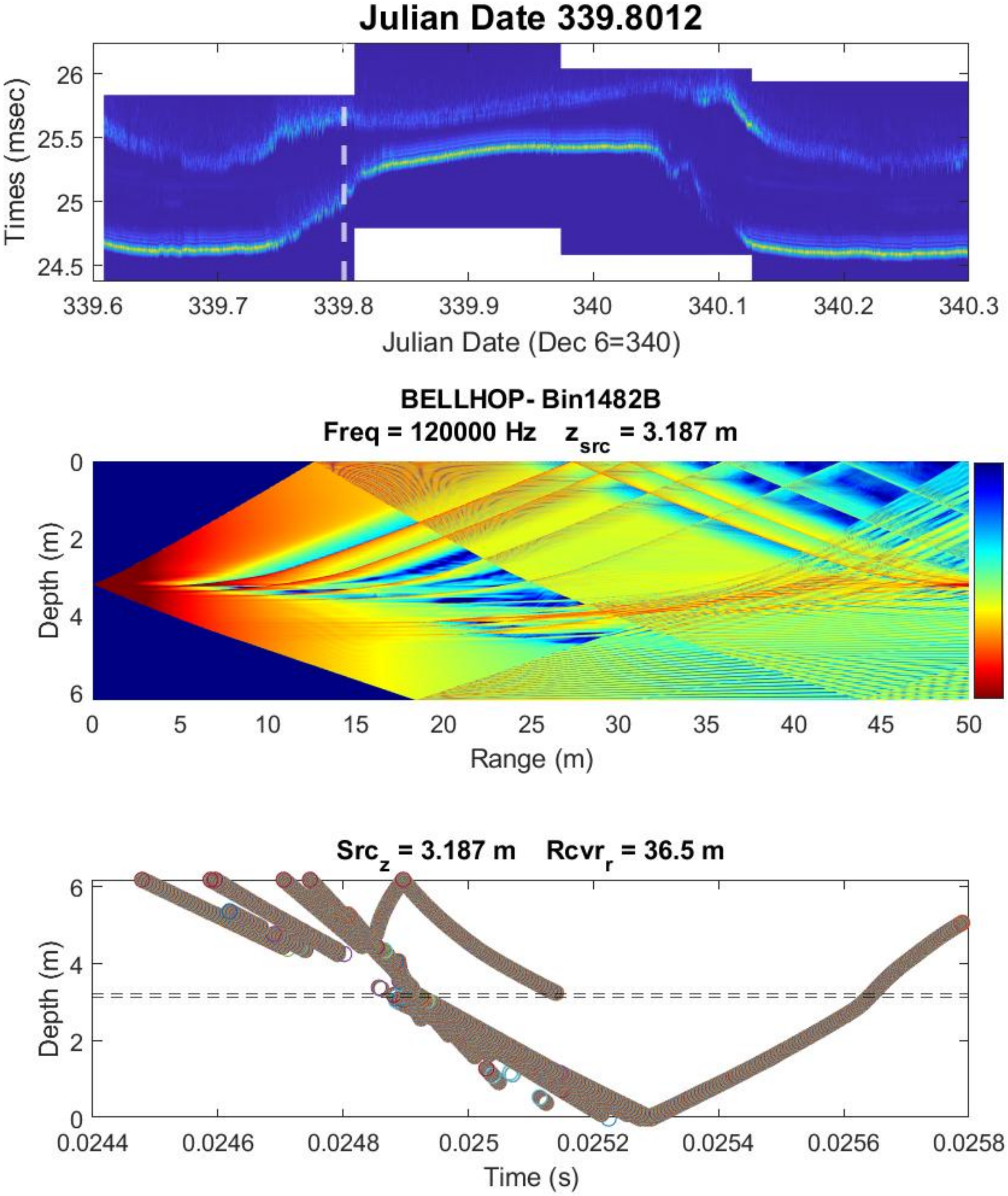

Figure A.21: Plots for Julian date 339.8012. Top: recorded arrival time data from scintillation system. Middle: Transmission loss for main beam with of ±11°. Bottom: Modeled arrival times from BELLHOP.

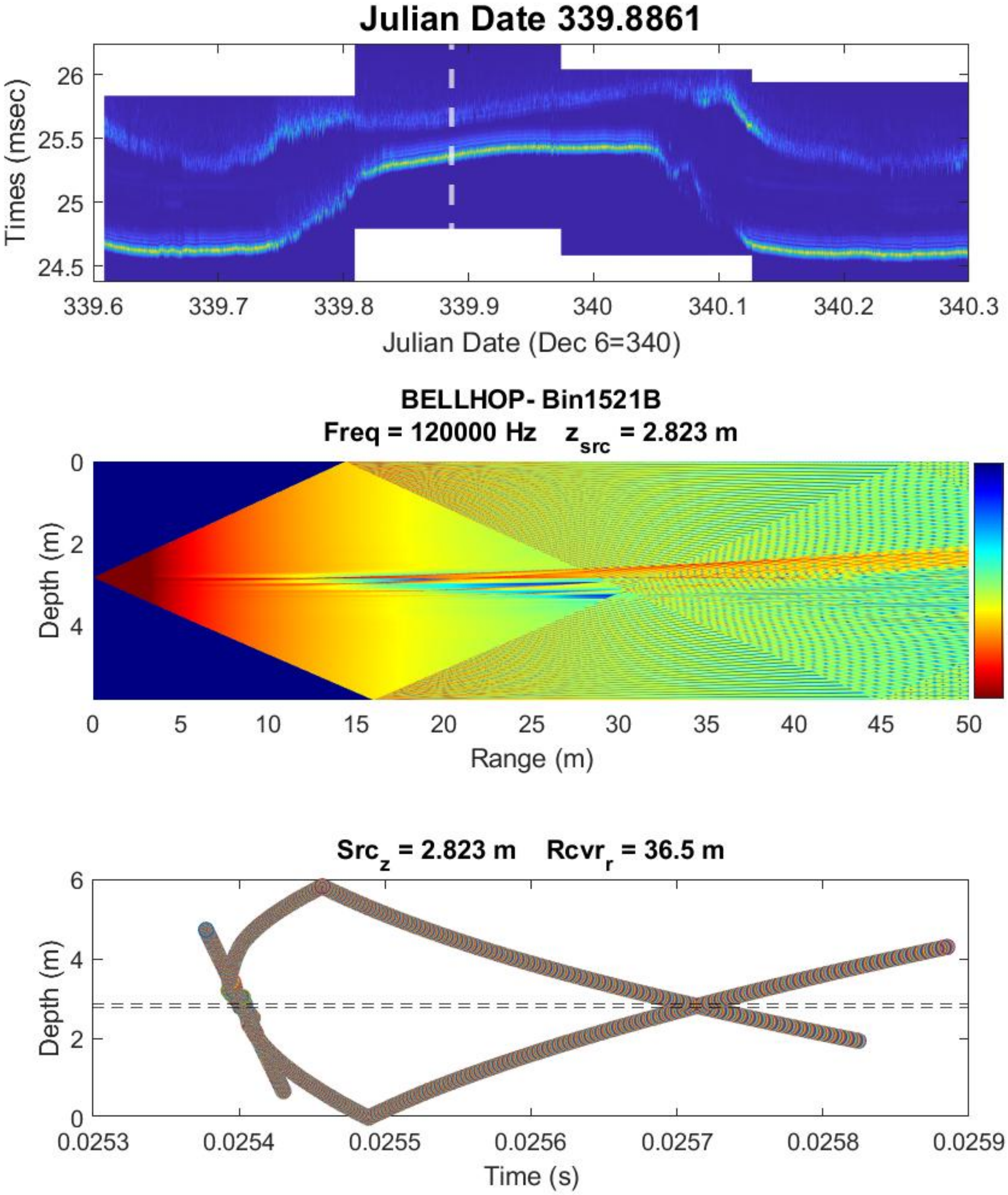

Figure A.22: Plots for Julian date 339.8861. Top: recorded arrival time data from scintillation system. Middle: Transmission loss for main beam with of ±11°. Bottom: Modeled arrival times from BELLHOP.

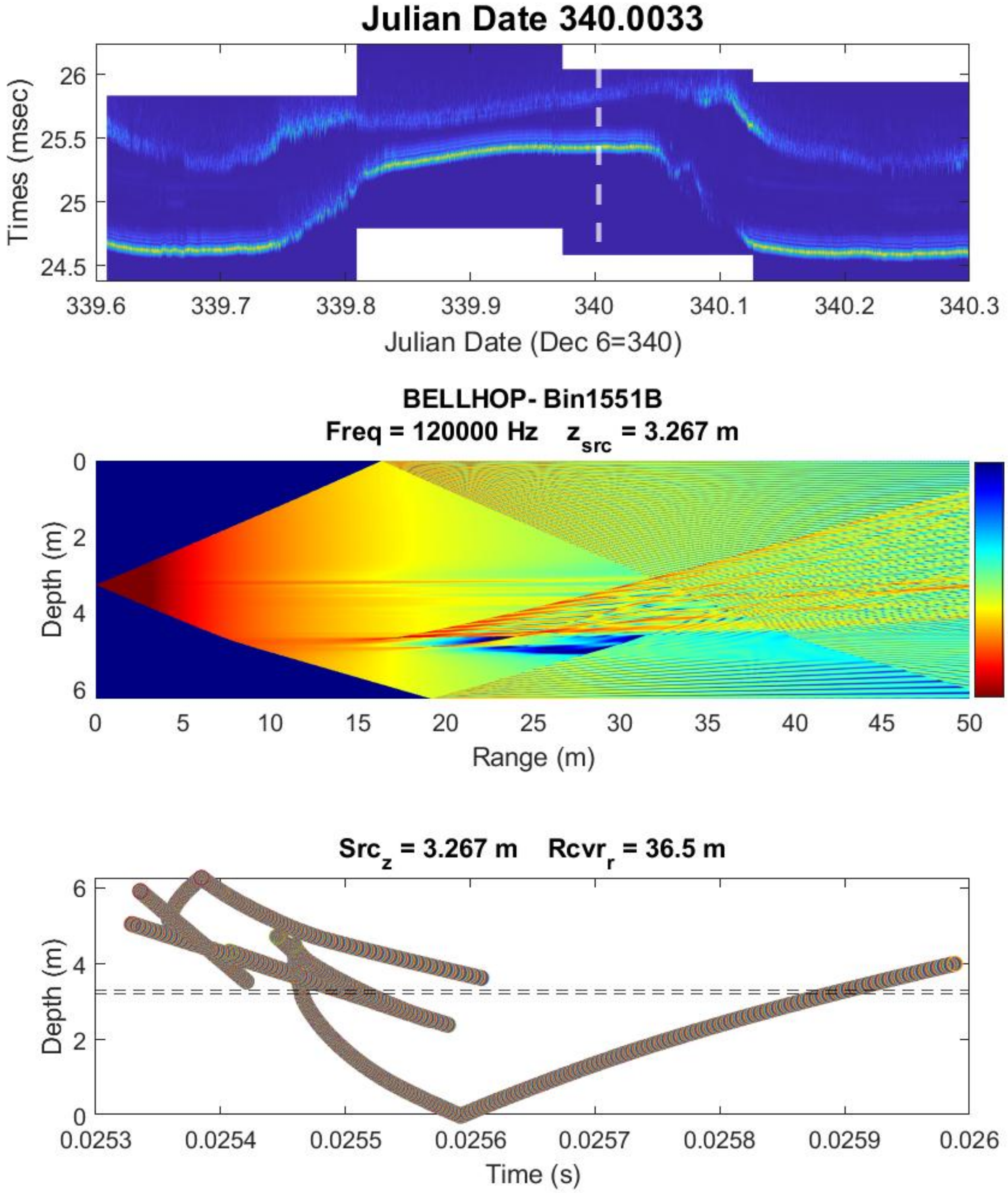

Figure A.23: Plots for Julian date 340.0033. Top: recorded arrival time data from scintillation system. Middle: Transmission loss for main beam with of ±11°. Bottom: Modeled arrival times from BELLHOP.

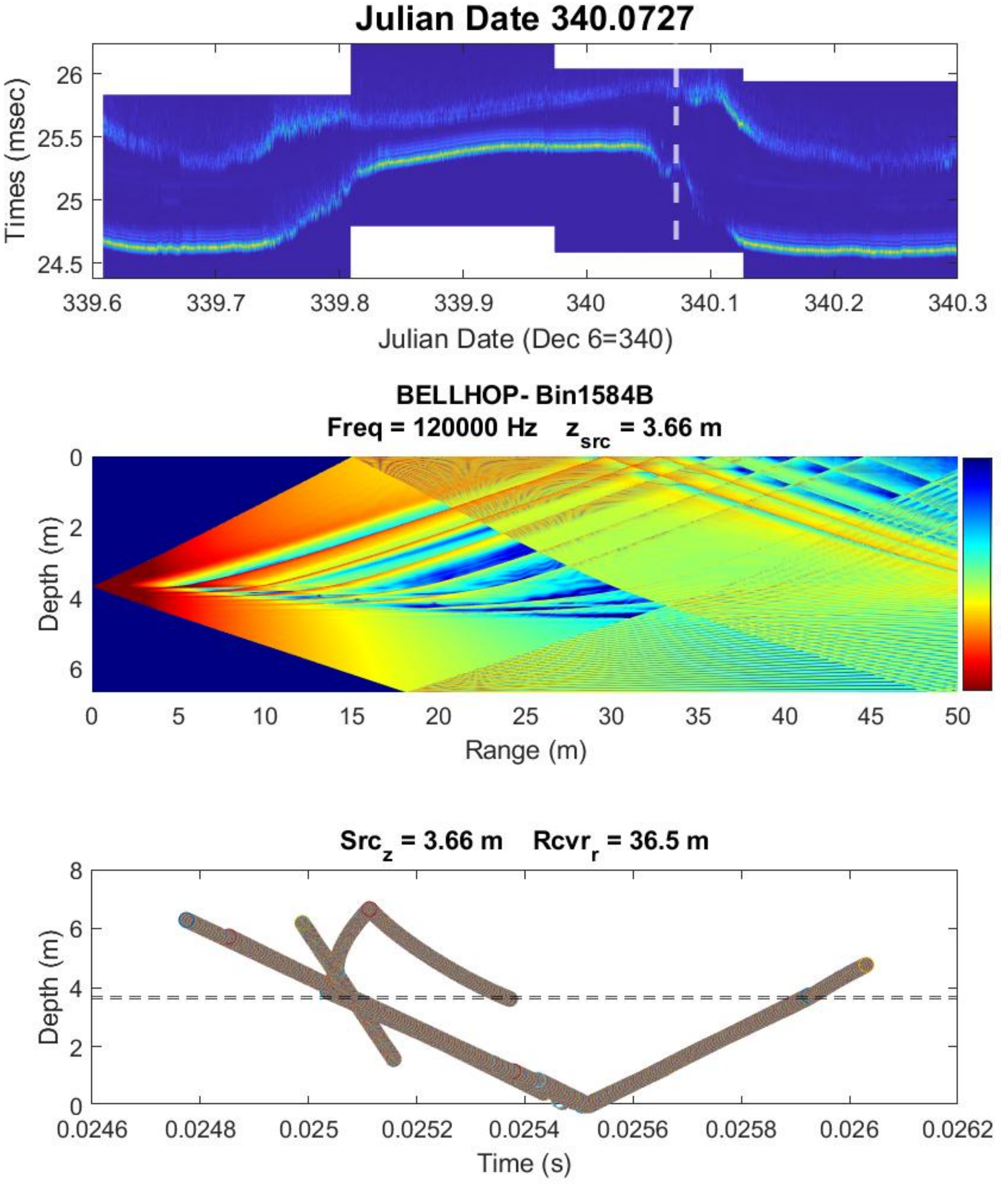

Figure A.24: Plots for Julian date 340.0727. Top: recorded arrival time data from scintillation system. Middle: Transmission loss for main beam with of ±8°. Bottom: Modeled arrival times from BELLHOP.

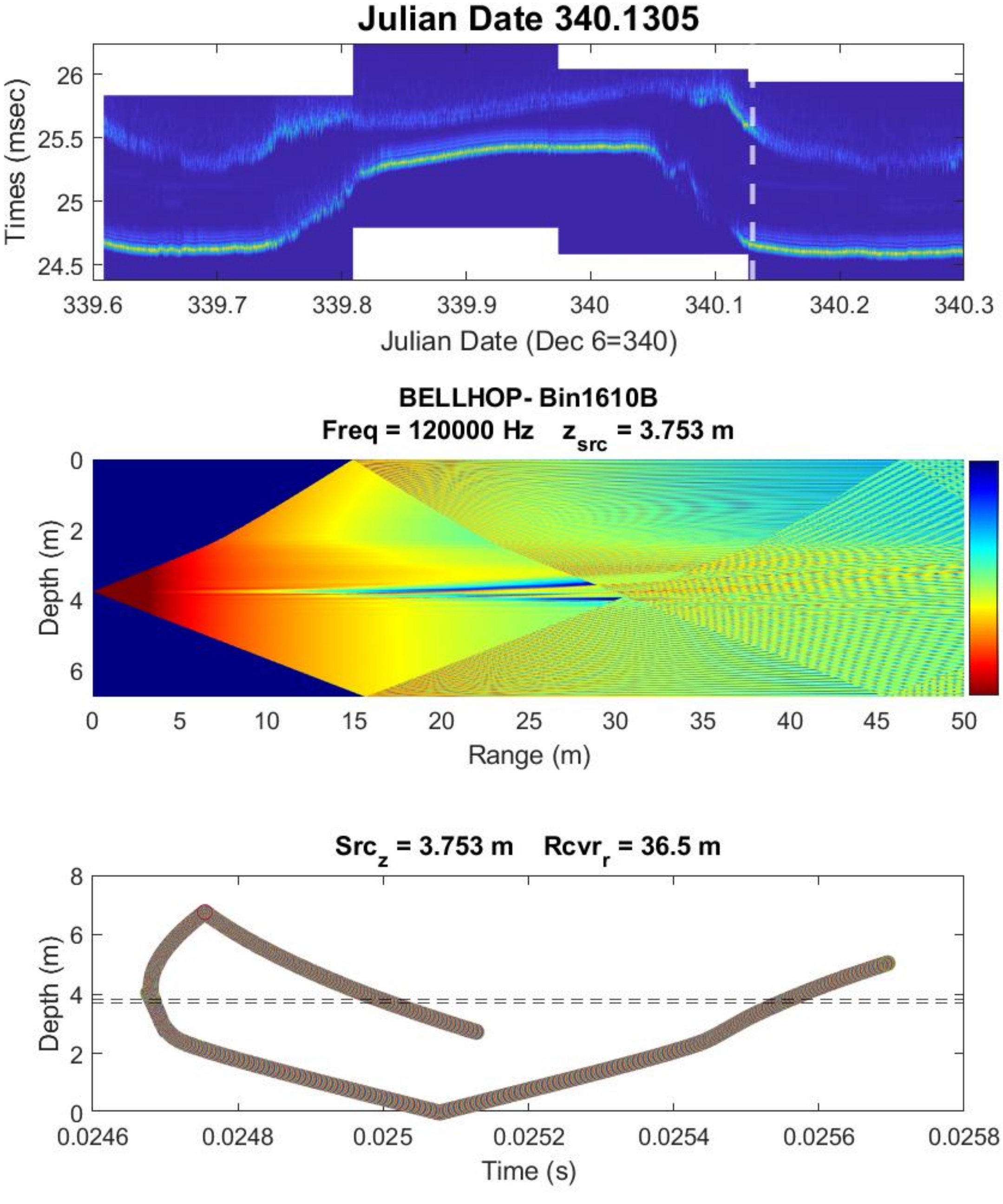

Figure A.25: Plots for Julian date 340.1305. Top: recorded arrival time data from scintillation system. Middle: Transmission loss for main beam with of ±11°. Bottom: Modeled arrival times from BELLHOP.

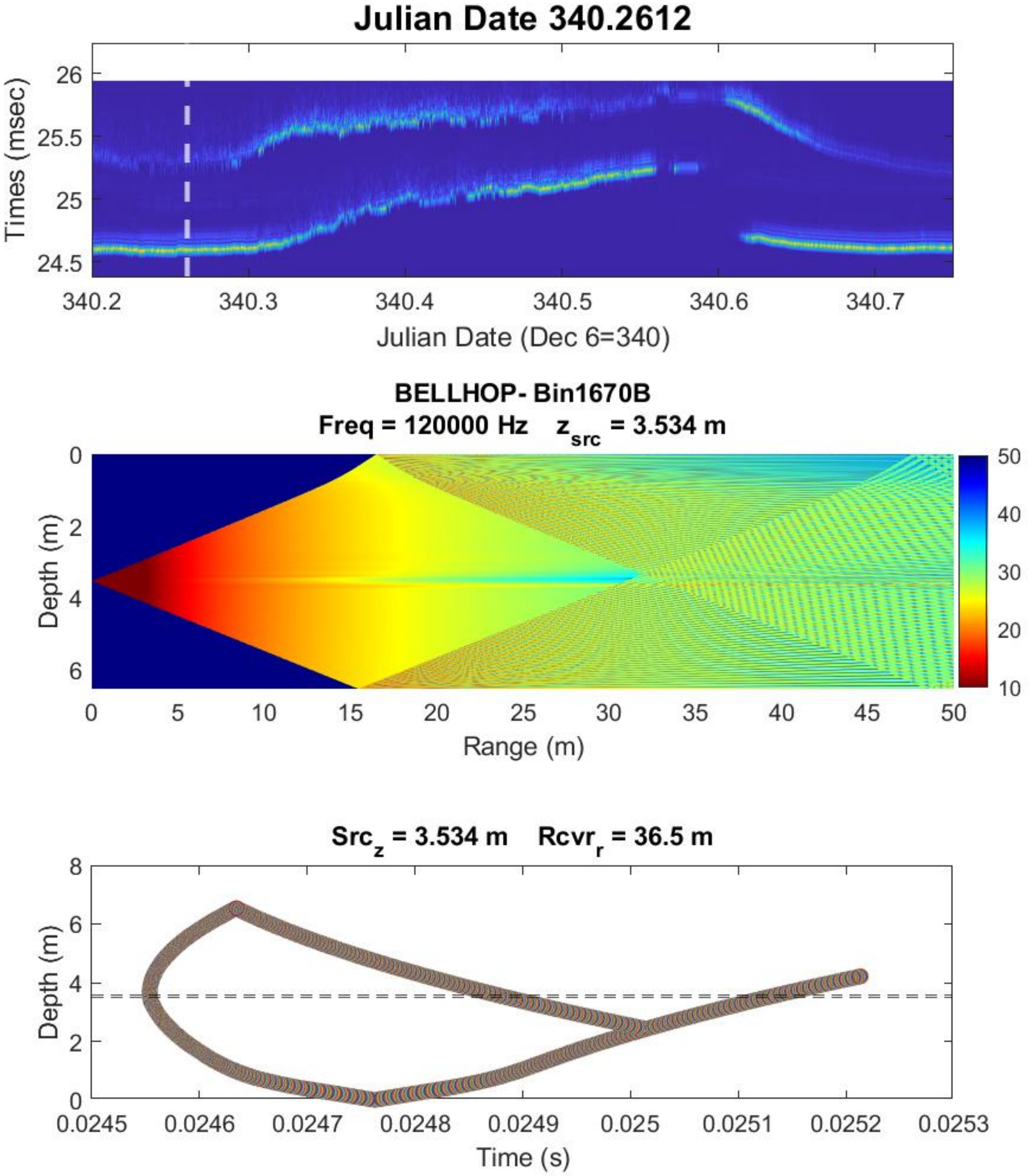

Figure A.26: Plots for Julian date 340.2612. Top: recorded arrival time data from scintillation system. Middle: Transmission loss for main beam with of ±8°. Bottom: Modeled arrival times from BELLHOP.

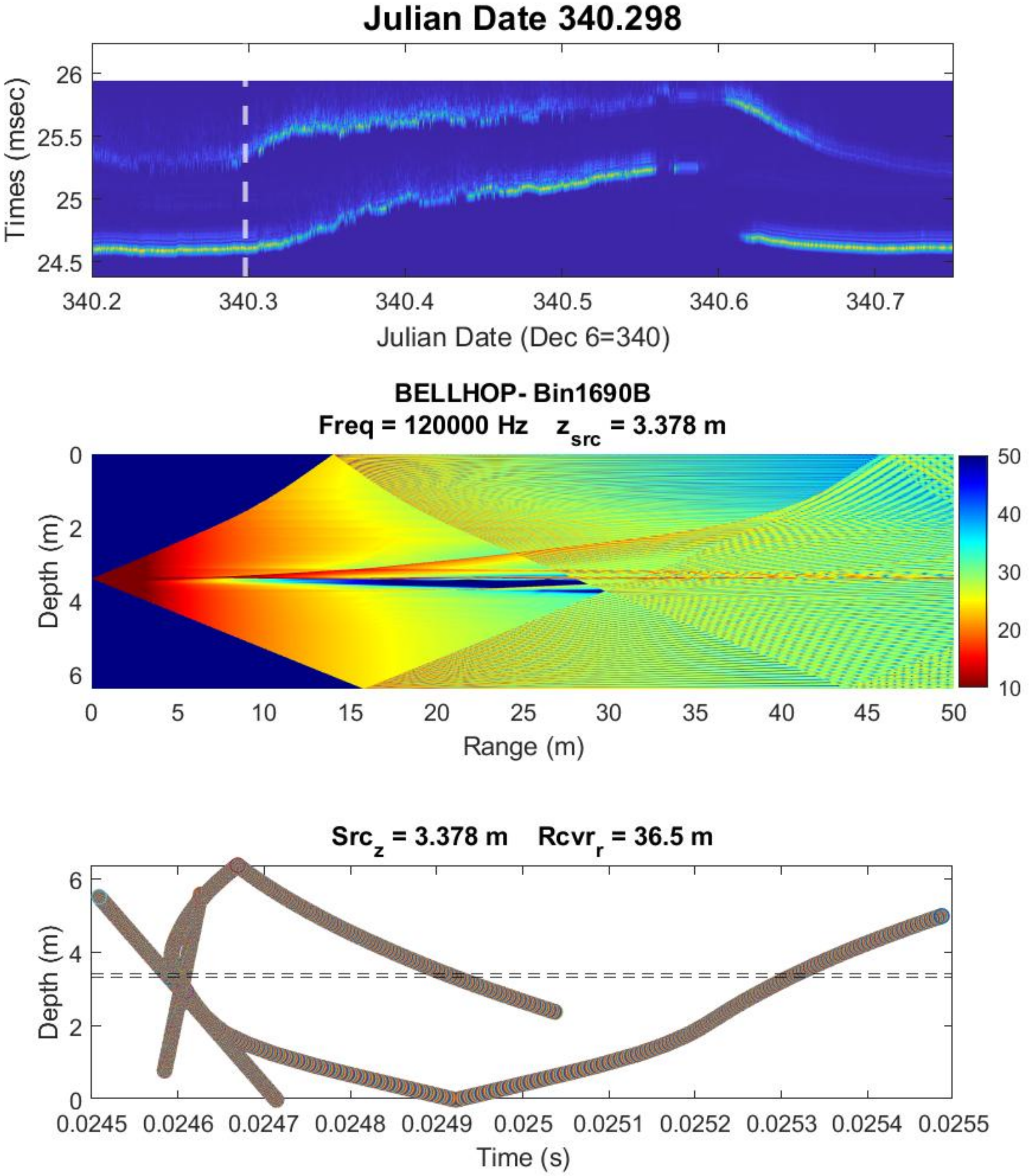

Figure A.27: Plots for Julian date 340.298. Top: Recorded arrival time data from scintillation system. Middle: Transmission loss for main beam with of ±11°. Bottom: Modeled arrival times from BELLHOP.

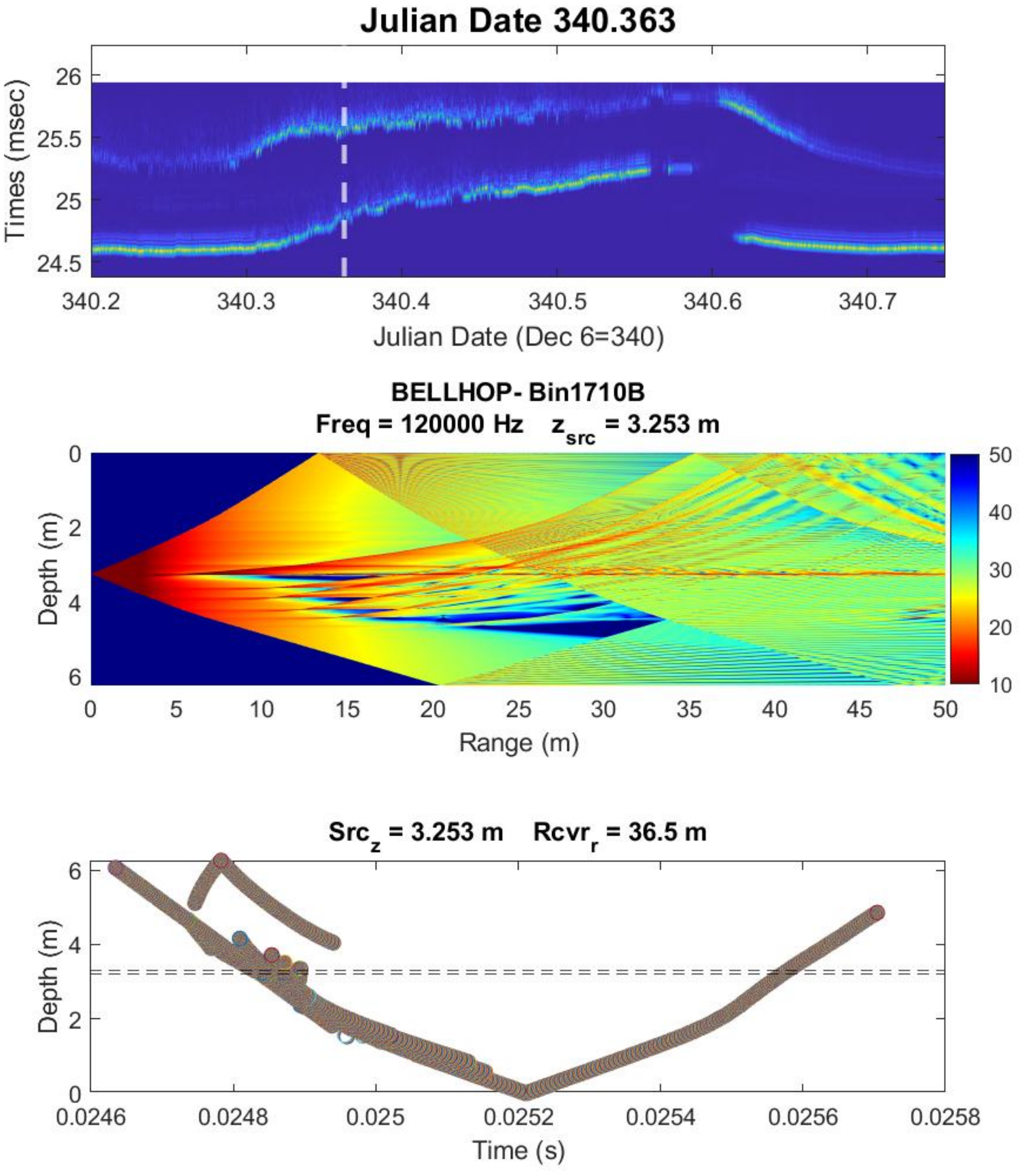

Figure A.28: Plots for Julian date 340.363. Top: Recorded arrival time data from scintillation system. Middle: Transmission loss for main beam with of ±11°. Bottom: Modeled arrival times from BELLHOP.

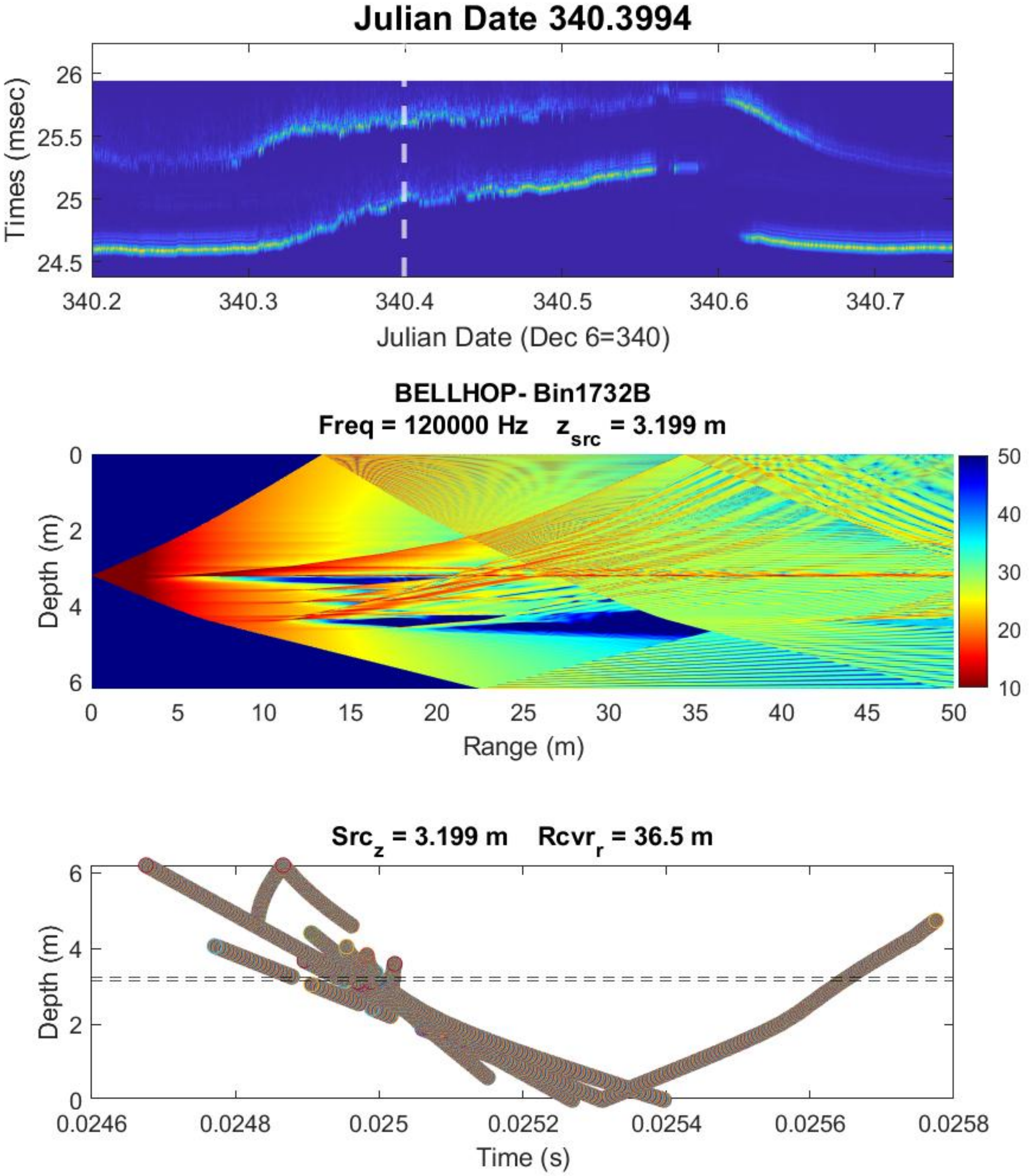

Figure A.29: Plots for Julian date 340.3994. Top: Recorded arrival time data from scintillation system. Middle: Transmission loss for main beam with of ±11°. Bottom: Modeled arrival times from BELLHOP.

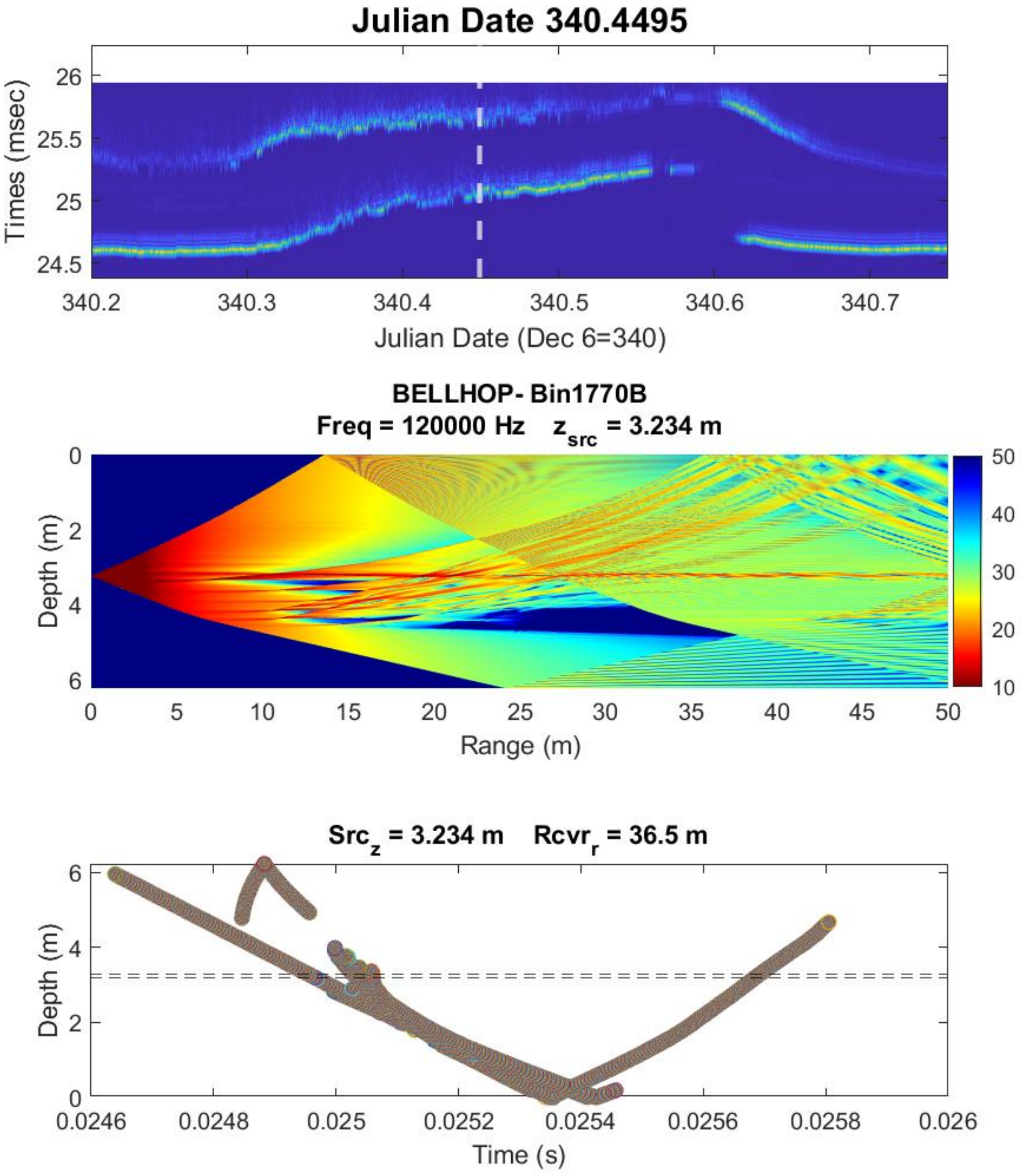

Figure A.30: Plots for Julian date 340.4495. Top: Recorded arrival time data from scintillation system. Middle: Transmission loss for main beam with of ±11°. Bottom: Modeled arrival times from BELLHOP.

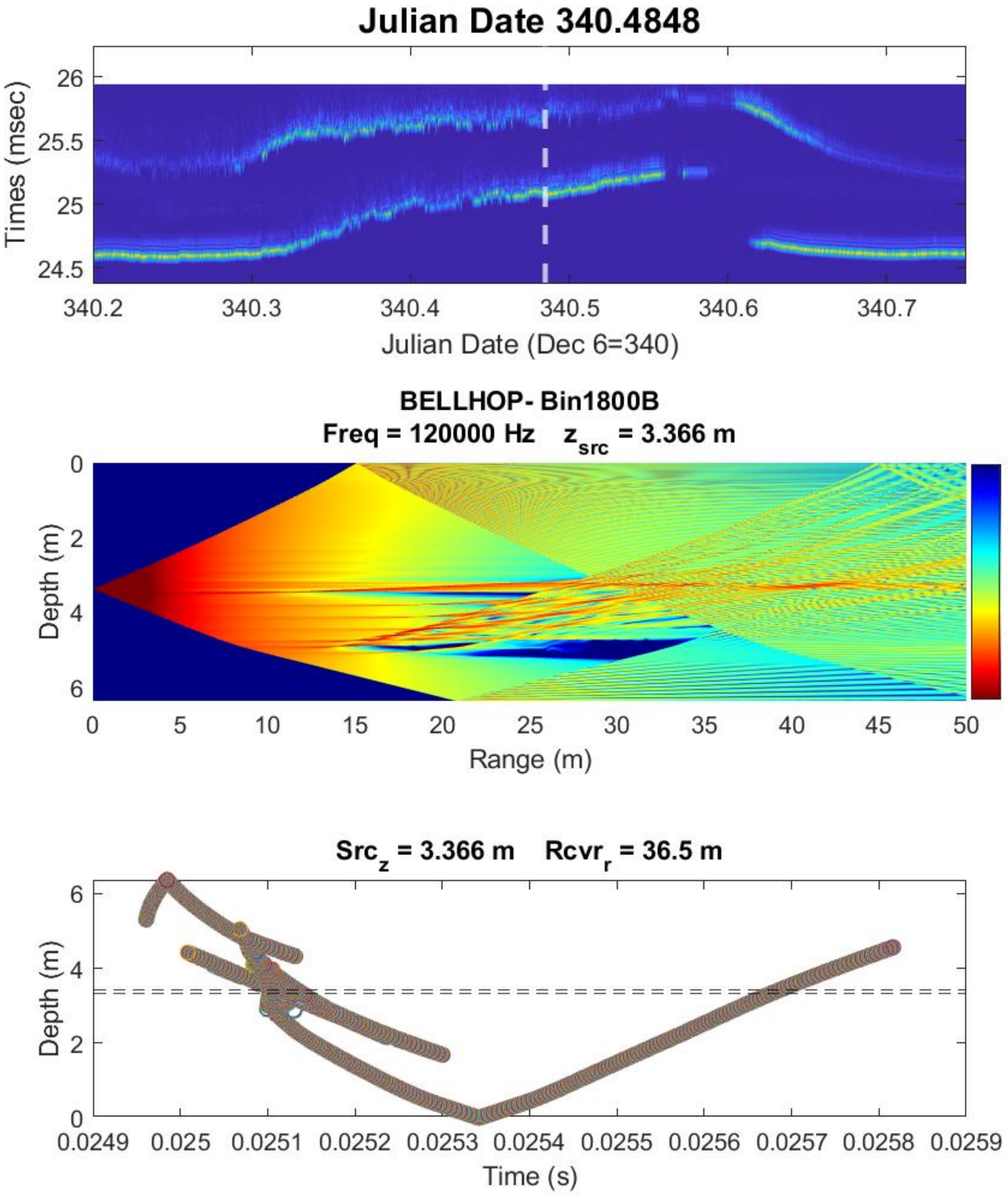

Figure A.31: Plots for Julian date 340.4848. Top: Recorded arrival time data from scintillation system. Middle: Transmission loss for main beam with of ±11°. Bottom: Modeled arrival times from BELLHOP.

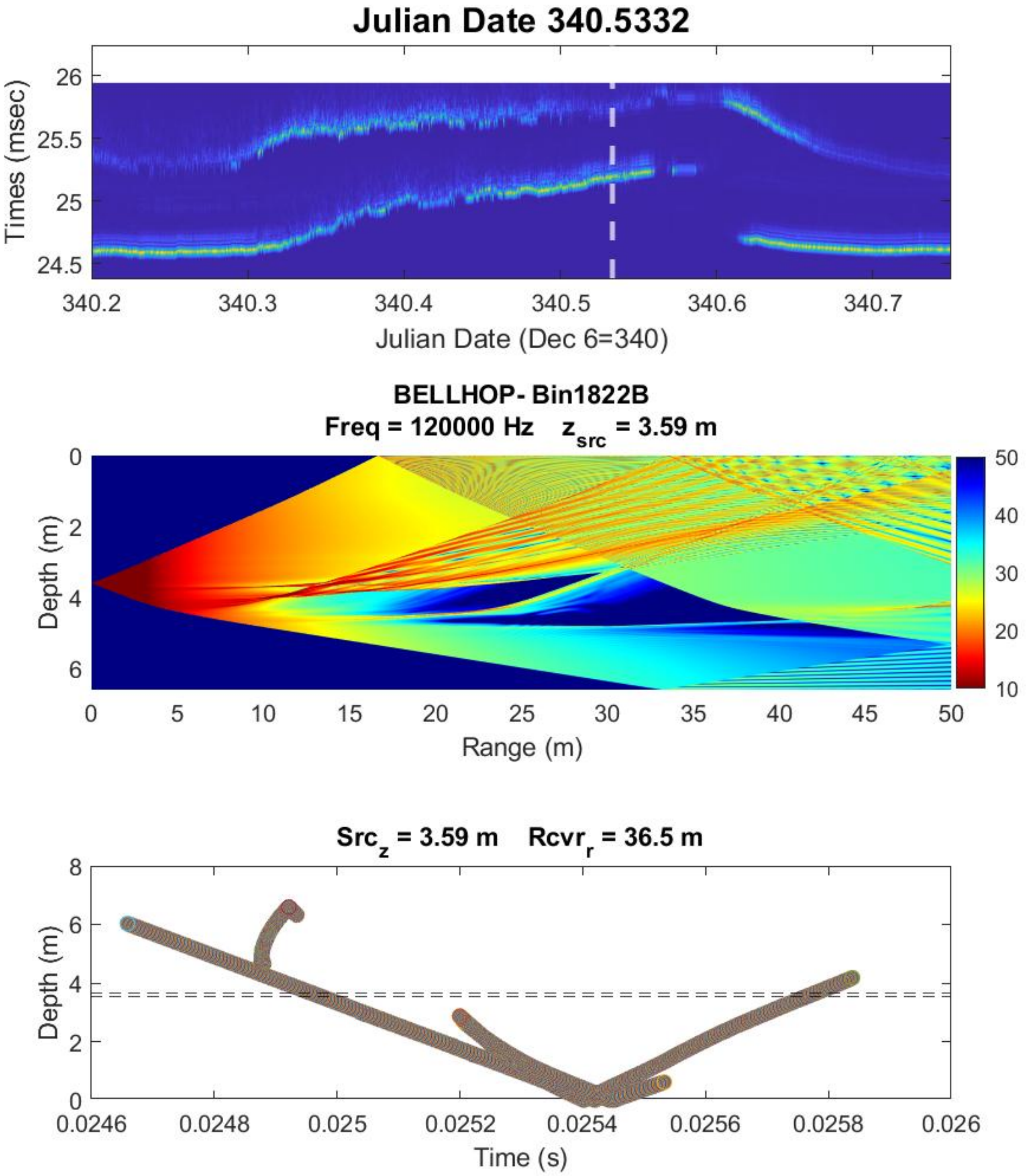

Figure A.32: Plots for Julian date 340.5332. Top: Recorded arrival time data from scintillation system. Middle: Transmission loss for main beam with of ±11°. Bottom: Modeled arrival times from BELLHOP.

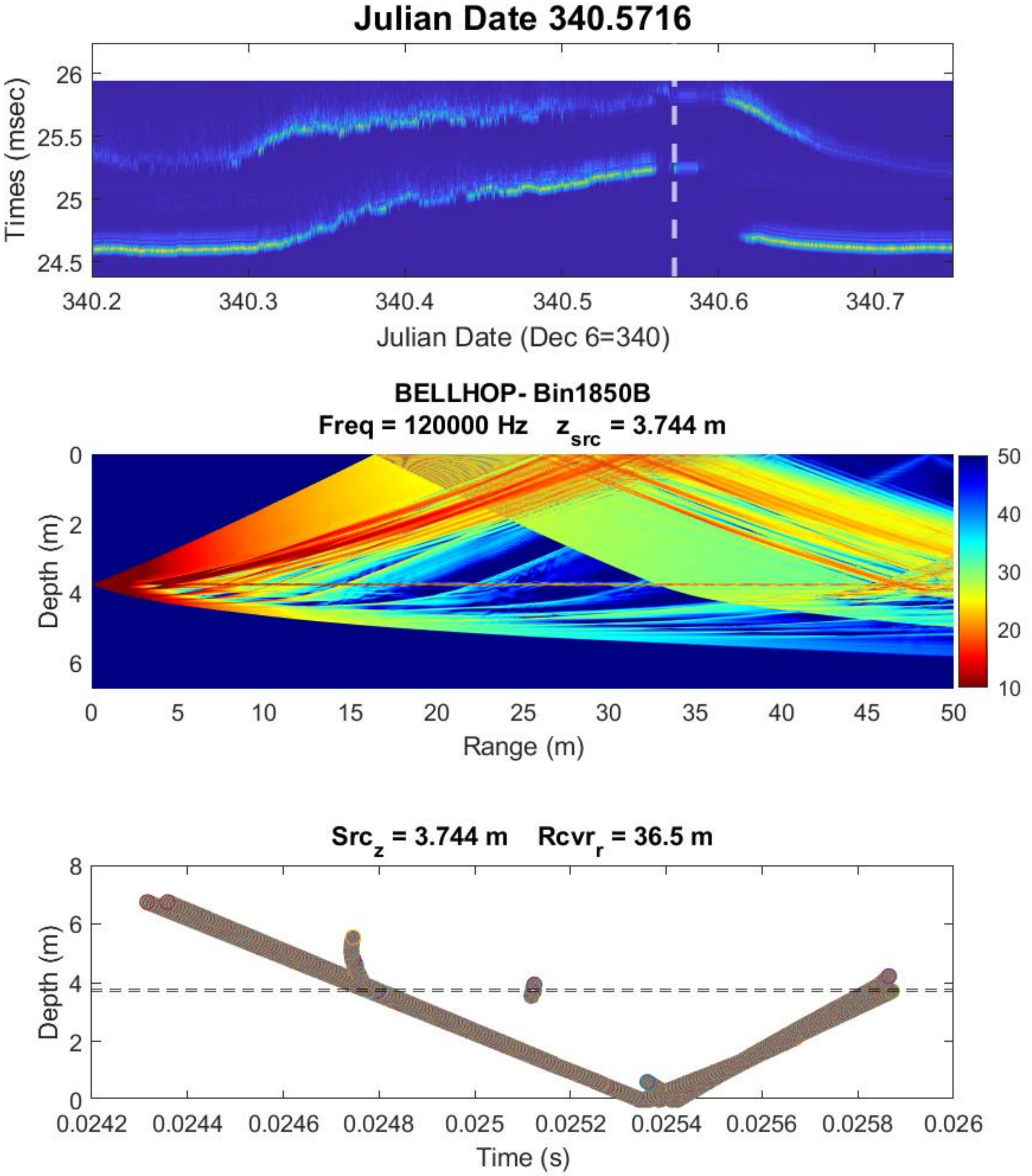
Julian Date 340.5716

BELLHOP- Bin1850B
Freq = 120000 Hz z_{src} = 3.744 m

Src_z = 3.744 m $Rcvr_r$ = 36.5 m

Figure A.33: Plots for Julian date 340.5716. Top: Recorded arrival time data from scintillation system. Middle: Transmission loss for main beam with of ±11°. Bottom: Modeled arrival times from BELLHOP.

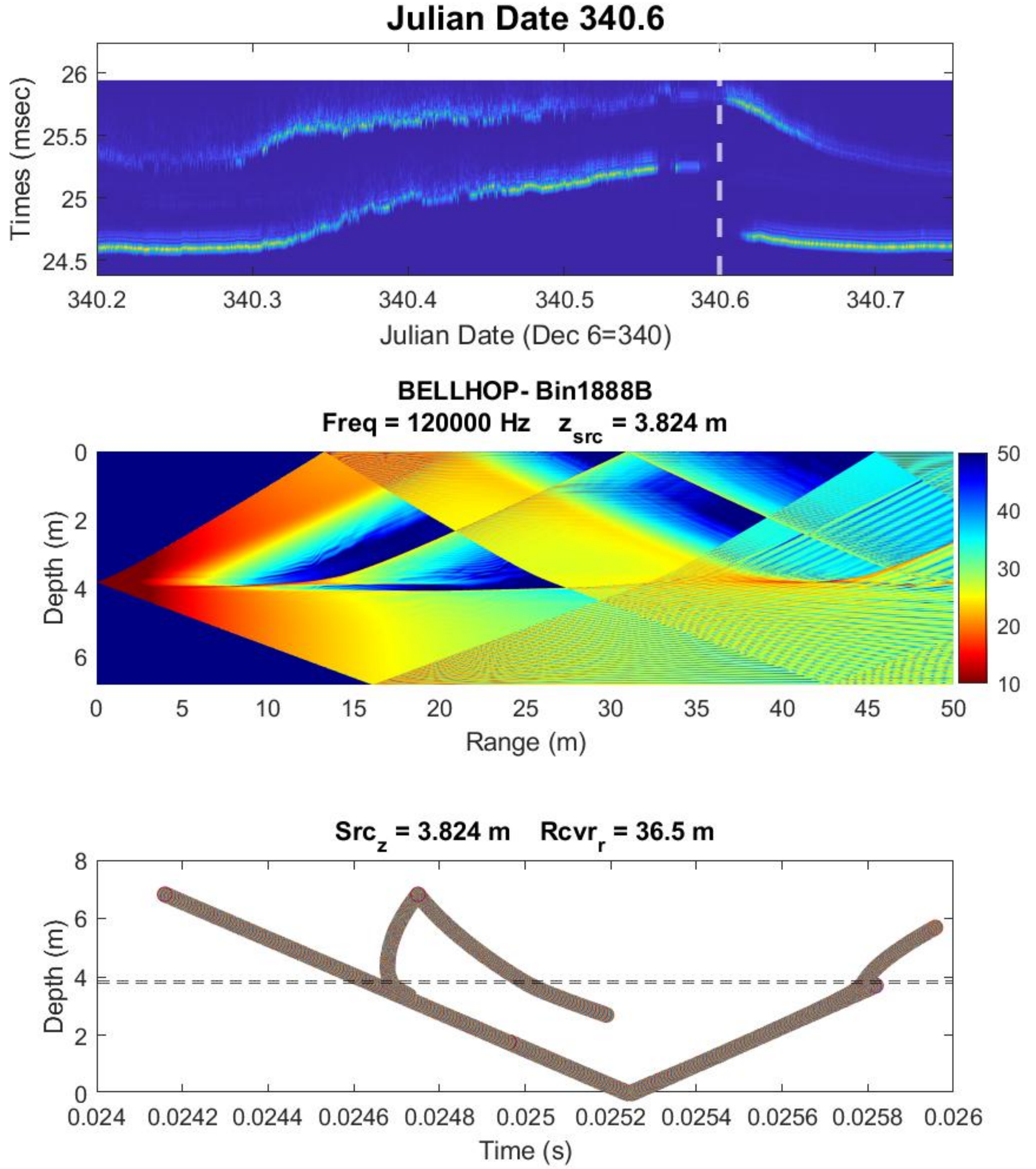

Figure A.34: Plots for Julian date 340.6. Top: Recorded arrival time data from scintillation system. Middle: Transmission loss for main beam with of ±11°. Bottom: Modeled arrival times from BELLHOP.

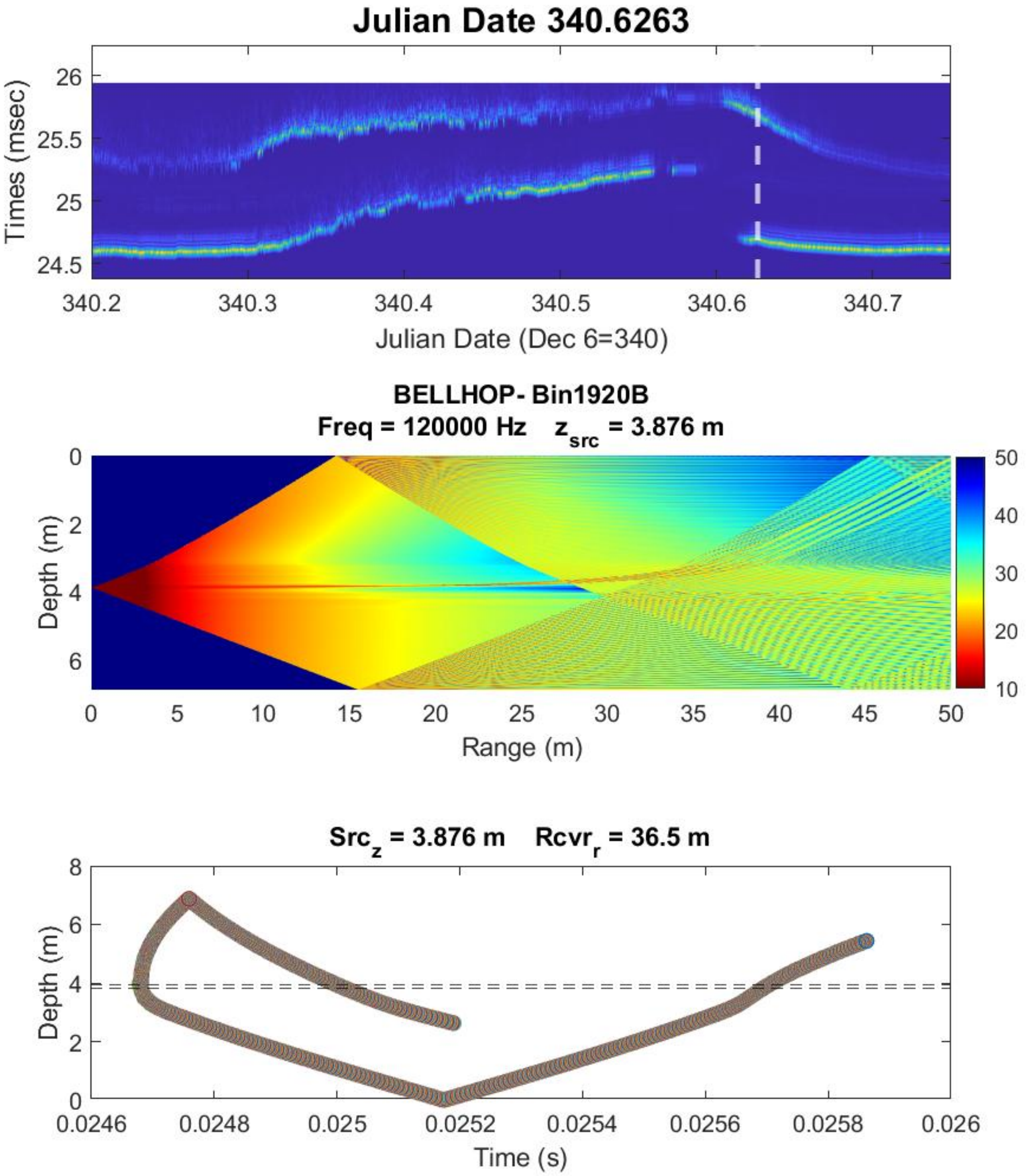

Figure A.35: Plots for Julian date 340.6263. Top: Recorded arrival time data from scintillation system. Middle: Transmission loss for main beam with of ±11°. Bottom: Modeled arrival times from BELLHOP.

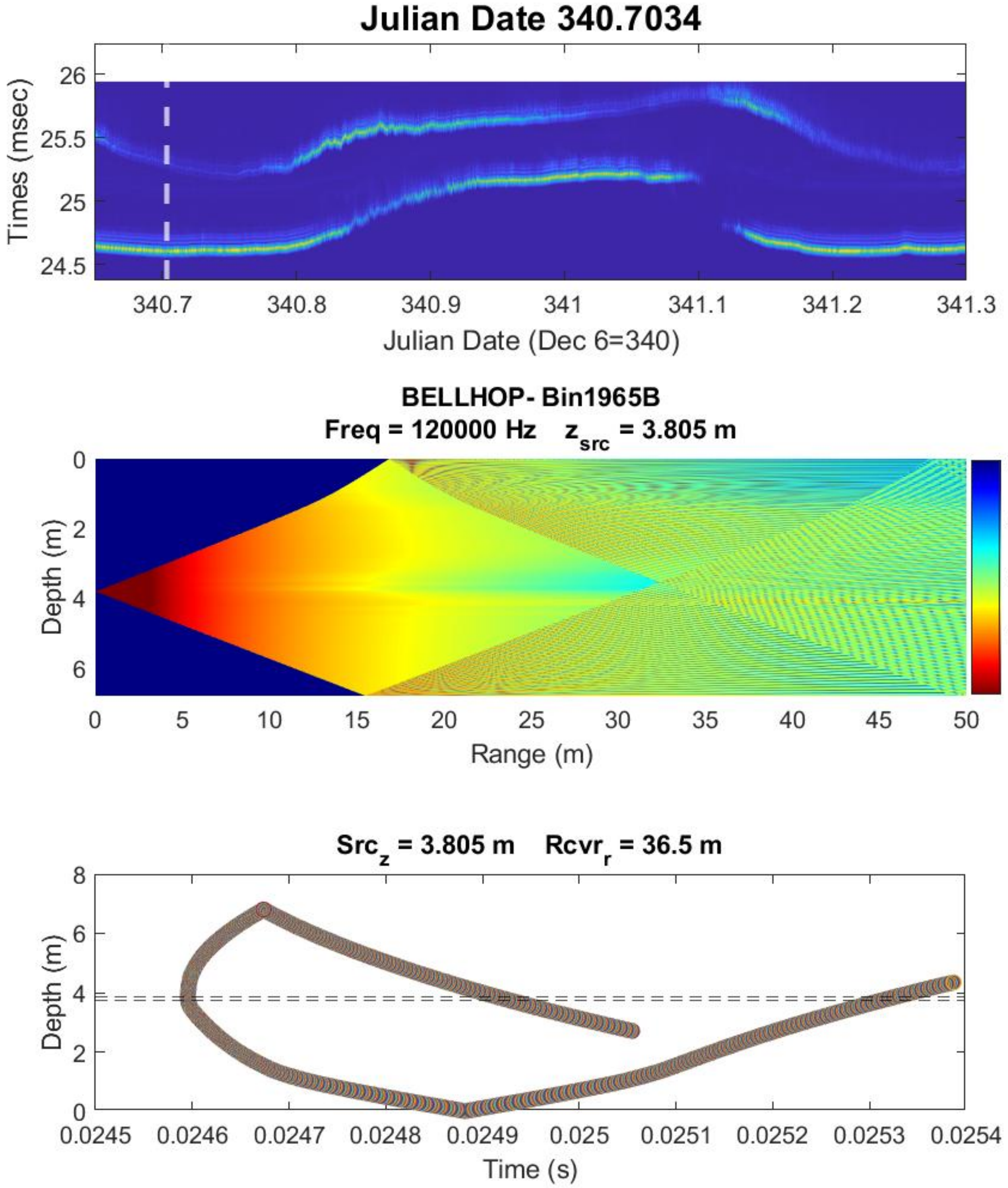

Figure A.36: Plots for Julian date 340.7037. Top: Recorded arrival time data from scintillation system. Middle: Transmission loss for main beam with of ±11°. Bottom: Modeled arrival times from BELLHOP.

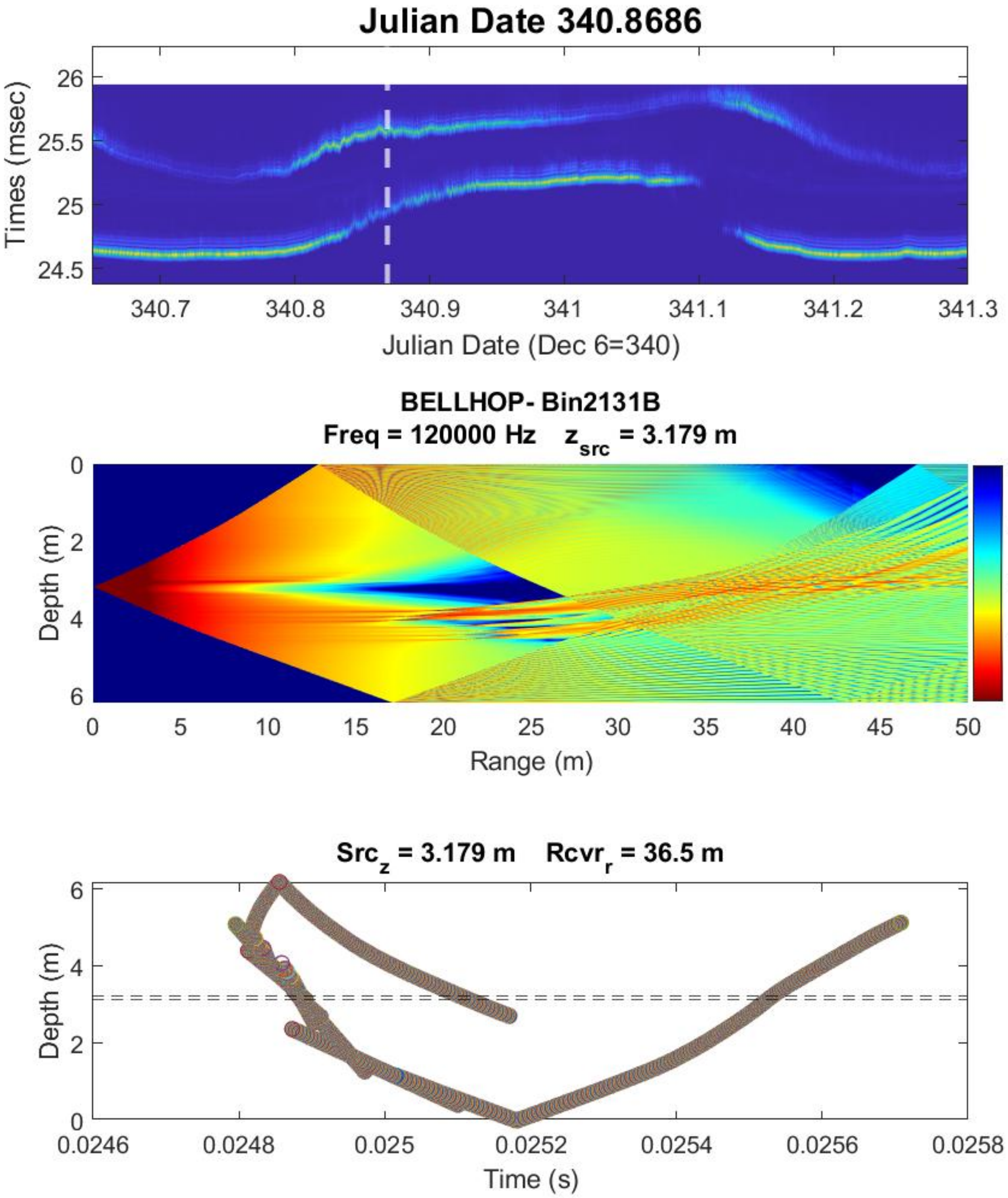

Figure A.37: Plots for Julian date 340.8686. Top: Recorded arrival time data from scintillation system. Middle: Transmission loss for main beam with of ±11°. Bottom: Modeled arrival times from BELLHOP.

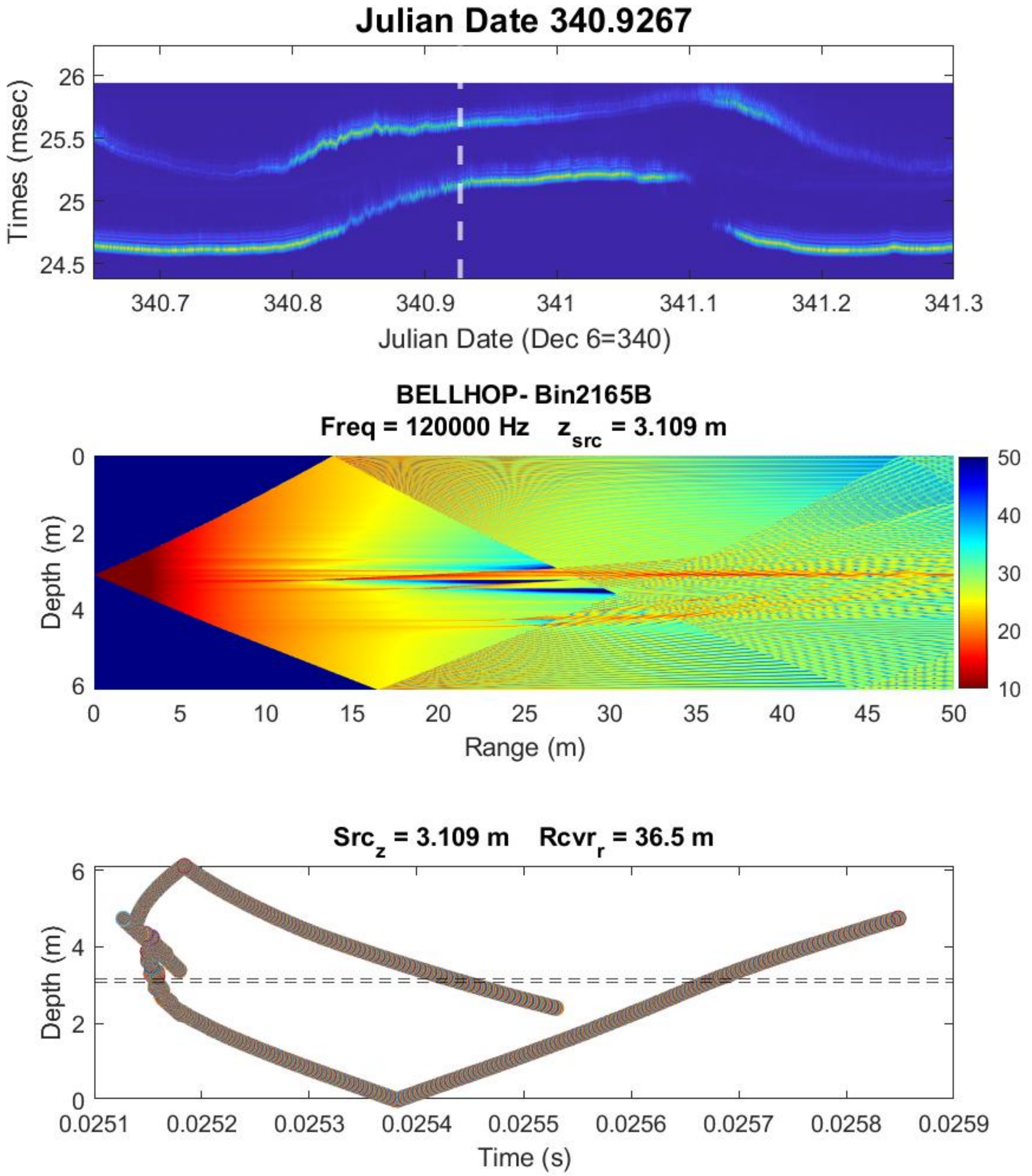

Figure A.38: Plots for Julian date 340.9267. Top: Recorded arrival time data from scintillation system. Middle: Transmission loss for main beam with of ±11°. Bottom: Modeled arrival times from BELLHOP.

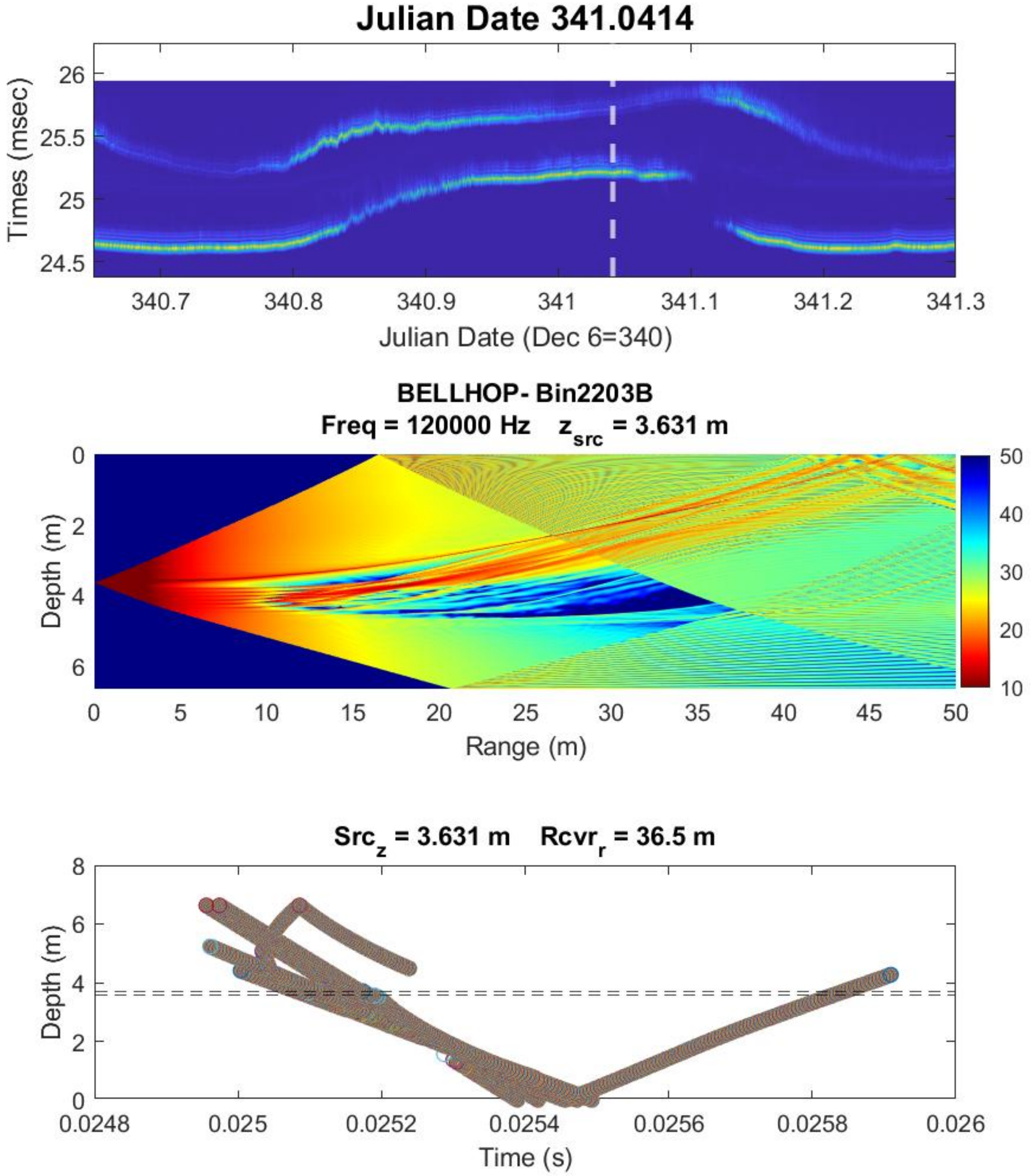

Figure A.39: Plots for Julian date 341.0414. Top: Recorded arrival time data from scintillation system. Middle: Transmission loss for main beam with of ±11°. Bottom: Modeled arrival times from BELLHOP.

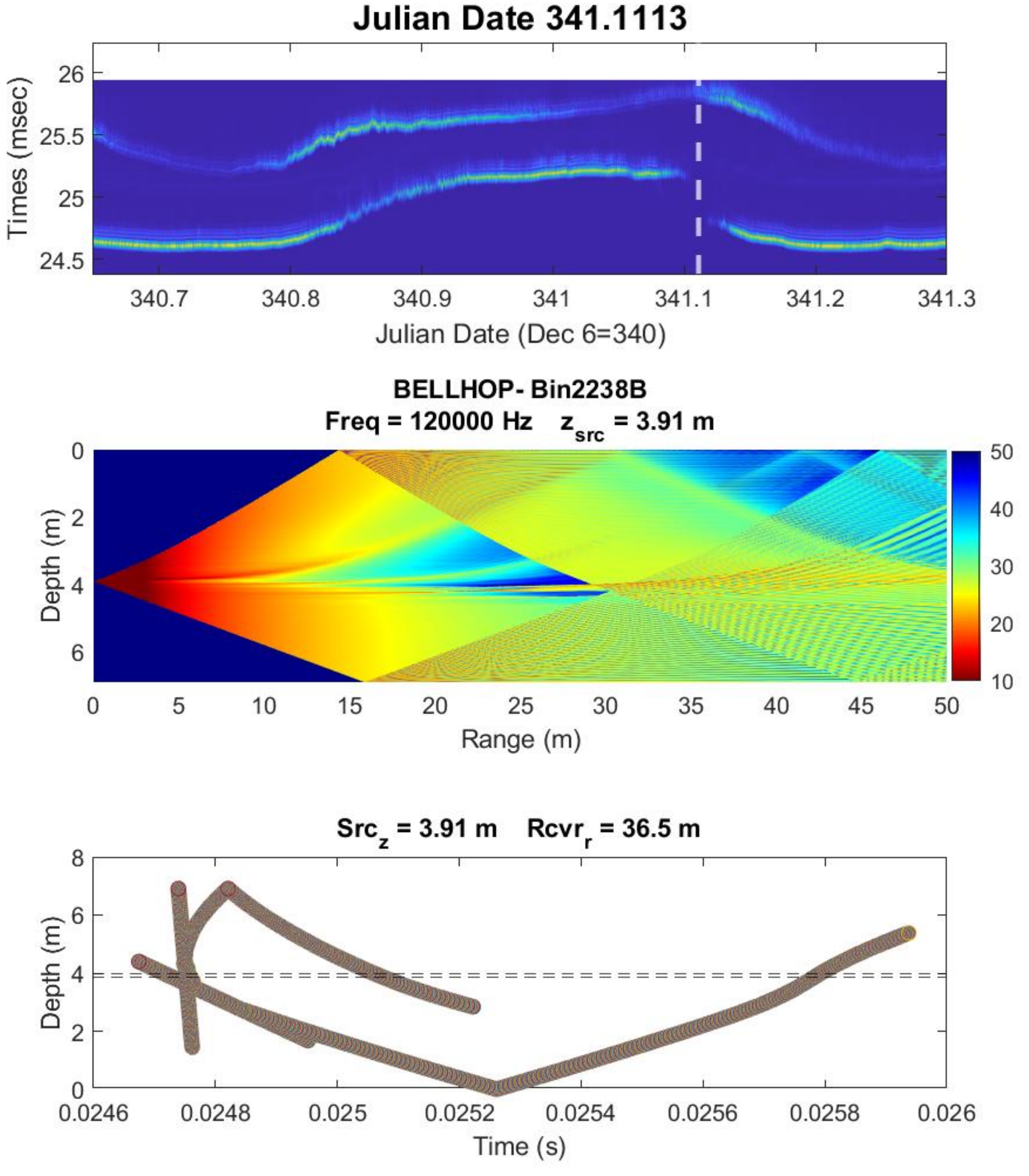

Figure A.40: Plots for Julian date 341.1113. Top: Recorded arrival time data from scintillation system. Middle: Transmission loss for main beam with of ±11°. Bottom: Modeled arrival times from BELLHOP.

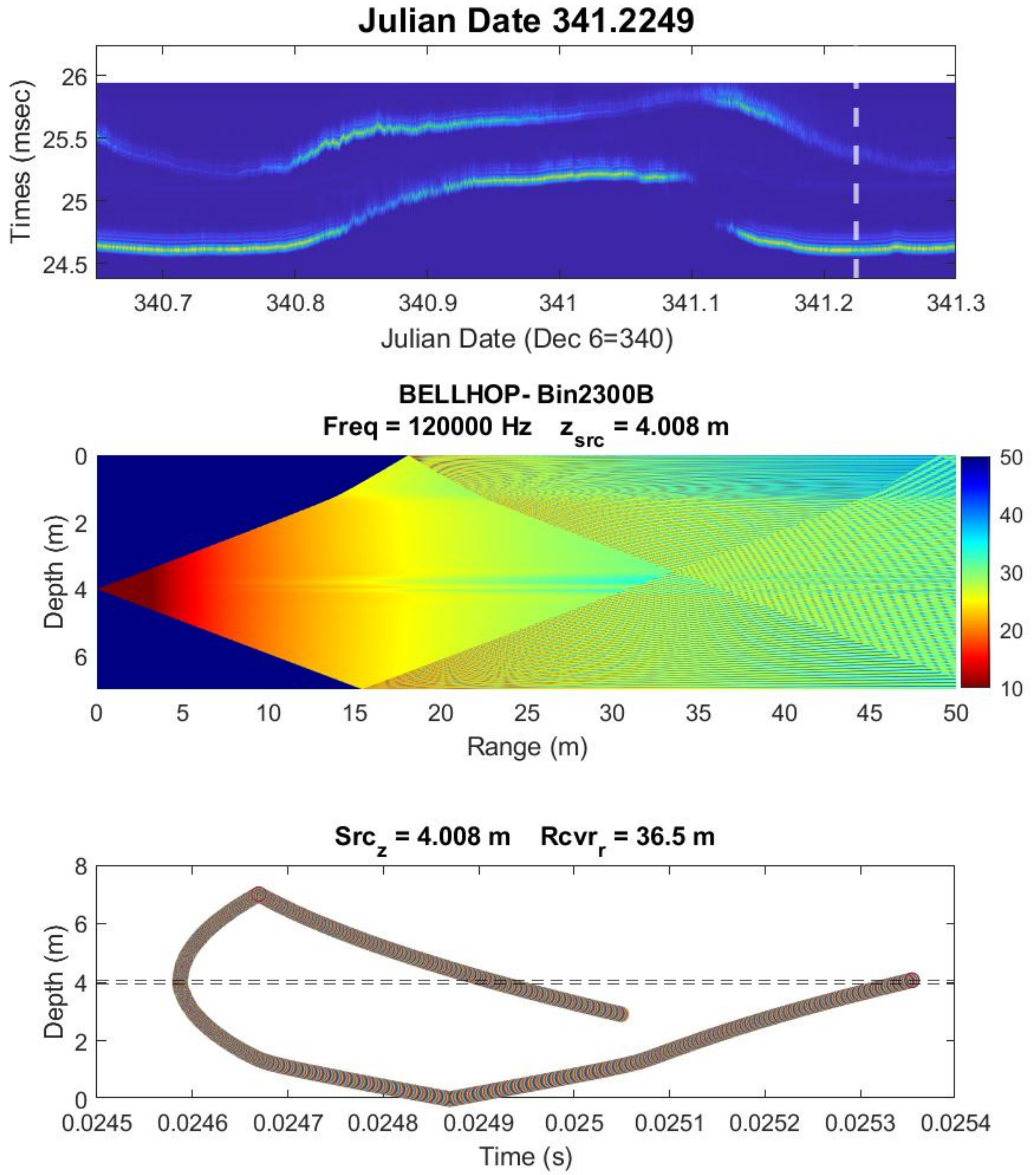

Figure A.41: Plots for Julian date 341.2249. Top: Recorded arrival time data from scintillation system. Middle: Transmission loss for main beam with of ±11°. Bottom: Modeled arrival times from BELLHOP.

B Matlab Code

This section contains some of the Matlab code used in this thesis. Other portions of code are not listed such as calculating bottom depth, SSP, or other more straightforward implementation of BELLHOP and the acoustic toolbox.[1] Note that some numbers and values are specific to the cases of this study.

B.1 Edited BELLHOP *plotarr* function

```
function [h] = plotarrnew( ARRFIL, irr, ird, isd )
% Edited version of plotarr. Original credit to M. Porter.
% This version only has the single 2-D arrival times over depth at a specific
% range.

% plot the arrivals calculated by BELLHOP
% usage:
% plotarr( filename, irr, ird, isd )
% where:
% irr = index of receiver range
% ird = index of receiver depth
% isd = index of source   depth
%
% mbp, April 2009

% read
narginchk( 4, 4 )

% Narrmx = 5000;
[ Arr, Pos ] = read_arrivals_asc( ARRFIL );
```

---

[1] *Acoustic Toolbox*.

```
figure
for ird1 = 1 : size( Arr, 2 )
   Narr = Arr( irr, ird1, isd ).Narr;
   h = plot( real( Arr( irr, ird1, isd ).delay(1 : Narr ) ),...
     Pos.r.z( ird1 ) * ones( length( Arr(irr, ird1, isd ).delay( 1 : Narr)), 1), 'o');
hold on
end

xlabel( 'Time (s)' )
ylabel( 'Depth (m)' )
title( [ 'Src_z = ', num2str( Pos.s.z( isd ) ), ' m...
     Rcvr_r = ', num2str( Pos.r.r( irr ) ), ' m' ] )
```

B.2 Script to write .ENV files

```
% Script to generate env files for BELLHOP
clear all;
close all;
clc;

% Load previous data of specifically time array to matching bin number
load("ssp.mat"); %SSP values for mxn matrix m = depth bin, n x time bin.

% loads bottomdepth and time array for each time bin
load("bottomdepth.mat");
start = 1400;
stop= 2600;

TOTAL_BINS = size(ssp,2);

%%%%%% GENERATE TEXT FILES %%%%%%

DEPTH_VALUES = size(ssp,1); % total number of depth values
NANS = isnan(ssp); % creates a logical matrix identifying positions of NaN entries in ssp
format_row = "%3.3f %f 0 1 / \n"; % format string for the table inputs
startflag = false;
makefiles =1;
```

```
for binnum = 1:TOTAL_BINS
    if makefiles== 1;

    % For each bin of SSPs, create a separate .txt file.
    % open text file by name and overwrite current contents.
    fid = fopen( ['Bin' num2str(binnum + start -1) 'B.env'], 'w' );

    % Create the Header information
    fprintf(fid,"'Bin%dB'",(binnum + start -1));
    fprintf(fid,'\n120000.0 ! FREQ (Hz)');
    fprintf(fid,'\n1 ! NMEDIA');
    fprintf(fid,"\n'SVF'   ! SSPOPT (Analytic or C-linear");

    fprintf(fid,'\n51  0.0  %3.3f,! DEPTH of bottom (m)\n',bottomdepth(binnum));

    startflag = false;
    for i = 1:(DEPTH_VALUES-1)
      if isnan(ssp(i,binnum)) && startflag % checks for end of useable data
          break
      elseif ~isnan(ssp(i,binnum)) && (bottomdepth(binnum) - d(i)) > .045
          startflag = true;
          fprintf( fid, format_row, d(i), ssp(i,binnum)); % ith row, first column
      else
%         fprintf( fid, format_row, d(i), ssp(i,binnum)); % ith row, first column
      end
    end

    % Create the end of file information
    fprintf( fid, format_row, bottomdepth(binnum), ssp(i-1,binnum));
    fprintf(fid,"'A' 0.0");  %Change to A~ or A* if you want bty files used
    fprintf(fid,"\n%3.3f  1600.00 0.0 1.8/   ",bottomdepth(binnum));
    fprintf(fid,"\n1 ! NSD");
    fprintf(fid,"\n%3.3f /         ! SD(1:NSD)",bottomdepth(binnum)-3);
    fprintf(fid,"\n1001 ! NRD");
    fprintf(fid,"\n0  %3.3f /      ! RD(1:NRD)",bottomdepth(binnum));
    fprintf(fid,"\n2001 ! NR");
    fprintf(fid,"\n0.0  0.05 / ! R(1:NR ) (km)");
```

```
    %%%%%%%%%% Important %%%%%%%%%%%%%%%%%%
    % Make this ’C’ for .shd, ’A’ for .arr, and ’R’ for .ray
    fprintf(fid,"\n’A’! Run type: ’Ray/Coh/Inc/Sem’");
    %%%%%%%%%%%%%%%%%%%%%%%%%%%%%%%%
    fprintf(fid,"\n1001  ! NBEAMS");
    fprintf(fid,"\n-11 11/         ! ALPHA1,2 (degrees)");
    % need two % signs to print one %
    fprintf(fid,"\n0.003  %3.3f  .05 ! STEP(m) Box%%z(m) Box%%r(km)",...
    bottomdepth(binnum));

    fclose(fid); % closes the text file
    end

end
%%%%%% FINISHED GENERATING TEXT FILES %%%%%%
```

B.3 Script to read and save data from ’arr’ Plots

```
% Run Bellhop
clear all
close all

%%%%%%%
% Init bellhop stuff: MODIFY THIS FOR YOUR MACHINE

% modify based on the correct path on your machine
addpath((’E:/Project/at/at/bin’));% AT binaries (wherever installed)
    Matdir = ’E:/Project/at/at/Matlab’;
addpath( (Matdir));% AT Matlab routines

% addpath for all extra folders/routines in Matlab
dir_list = dir( Matdir );

for j = 1 : length( dir_list )
   if ( dir_list( j ).isdir )
       % ignore CWD . and parent dir ..
       if ~strcmp( dir_list( j ).name, ’.’ ) && ~strcmp( dir_list( j ).name, ’..’ )
```

```
            addpath( fullfile( Matdir, dir_list( j ).name ) );
        end
    end
end
%% Run Bellhop
start =1400;
stop=2400;
bins_wanted = start:1:stop;

load("bottomdepth.mat"); %loads bottom depth created in other file

for ii=1:length(bins_wanted)
    bellhop(['Bin' num2str(bins_wanted(ii)) 'B']);
end

%% Plot Arrival Times
% Need .arr files from running bellhop with 'A'
range_bin = 1461; %36.5m
depth_bin = 1001;
eps = 0.05; % tolerance to identify a reading as equal to max_depth
arr_times = []; % stores arrival times corresponding to max_depth
savearr = true; %saves figures to separate folder.

load("times_data.mat"); %load old times data comment out if initial run

for ii=1:length(bins_wanted)
%   figure
% GENERATE NEW FIGURE HERE
     h = plotarrnew( ['Bin' num2str(bins_wanted(ii)) 'B.arr'], range_bin, depth_bin, 1);
%     openfig(['ARRfigs/11SL/ARR' num2str(bins_wanted(ii))])
    ax = gca;
    % UPDATE SENSOR DEPTH VALUE
    R_depth = bottomdepth(bins_wanted(ii)-start+1) - 3;

    % This code finds the points at the rcr depth and saves them to
    % times_data.
    for obj = 1:length(ax.Children)
```

```
        x = ax.Children(obj).XData;
        y = ax.Children(obj).YData;
        if ~isempty(x)
            for dp = 1:length(x)
                if y(dp) < R_depth+eps && y(dp) > R_depth-eps
                    arr_times = [arr_times x(dp)];
                end
            end
        end
        clear x y % clear them to avoid bad overwriting
    end
    times_data(bins_wanted(ii)).times = arr_times;
    arr_times = [];

    if savearr
        fig_handle =gcf; %gets the current figure
        %can add additional arguement , 'compact'
        savefig(fig_handle, ['ARRfigs/ARR' num2str(bins_wanted(ii))])
        clear fig_handle

    end
    close all
end
save(['times_data.mat'], 'times_data')
```

B.4 Script to plot saved arr data from multiple 'arr' Plots

```
% Plots previously saved data of arrival times, over time
clear all
close all

%enter range of bins of data wanted
start =1400;
stop=2400;
bins_wanted = start:1:stop;

% Load previous data of specifically time array to matching bin number
```

```
load("bottomdepth.mat");

%% Loads figure of collected data from scintilation system
%comment out this part if not plotting ontop of an existing figure
openfig('scinitllation_TA_RA','visible')
ax = gca;
grid on
ax.Layer = 'top';
ax.GridAlpha =.6;
title(['Arrival times'], 'FontSize', 14)
xlabel ('Julian Date (Dec 6=340)', 'FontSize', 13)
ylabel ('Times (msec)','FontSize', 13)

hold on

%% Plot Arrival Times Matrix overtime
load("times_data.mat");
times_array = [];
for jj = 1:(length(bins_wanted))

    for i =1:length(times_data(bins_wanted(jj)).times)
        times_array(bins_wanted(jj), i) = time(bins_wanted(jj));
    end
    hold on

    %avoids problems where first bin of data is empty due to no returns
    if size(times_array, 2) > 0
        %334 was for julian time conversion
        plot(times_array(bins_wanted(jj), :)+334,...
            times_data(bins_wanted(jj)).times.*1000,...
            'ro', 'MarkerSize', 3 )
    end
    times_array = [];
end
```

Acronyms

ADCP	acoustic Doppler velocity current profiler
CTD	Conductivity temperature, and depth
NOAA	National Oceanic and Atmospheric Administration
SSP	Sound speed profile
TL	Transmission loss
WHOI	Woods Hole Oceanographic Institution